

Piping in sandy tidal deposits

2020



Design of field experiments on piping through sandy tidal deposits in the *Hertogin Hedwigepolder*

A.J. Methorst
Master thesis

Piping in sandy tidal deposits

Design of field experiments on piping through sandy tidal deposits in
the *Hertogin Hedwigepolder*

Master thesis

by

A.J. Methorst

as finalisation to obtain the degree
Master of Science in Hydraulic Engineering
at Delft University of Technology,
faculty of Civil Engineering and Geosciences.
To be defended publicly on Wednesday March 25, 2020 at 3:30 PM

September 2019 – March 2020

Chairman thesis committee:
Thesis committee:

Prof. dr. ir. M. Kok
Dr. ir. B.C. van Prooijen
Dr. M.P. Hijma
Ir. J.C. Pol

TU Delft
TU Delft
Deltares
TU Delft

Cover picture
Salt marshes near the *Hertogin Hedwigepolder* (Deen, 2015)

Preface

This thesis finalises my Master Hydraulic Engineering at Delft University of Technology. The thesis project is carried out in collaboration with Deltares. The reason for this collaboration is that Deltares had an interest in gaining more knowledge on piping in sandy tidal deposits in advance of a large-scale experiment on piping in tidal sands in the *Hertogin Hedwigepolder* in 2021.

I would like to thank my thesis committee, Matthijs Kok, Marc Hijma, Joost Pol and Bram van Prooijen for their feedback and helpful advice along the project. Matthijs, thank you for leading my thesis committee and your optimism about the project. Marc, thank you for the endless support and motivation in all the aspects of this thesis, especially in the structure and writing. Your help was essential to the completion of this thesis. Joost, thank you for your help in understanding the piping process, your valuable feedback and the open conversations that we had. Bram, thank you for the fresh view on the project.

I also want to thank my other colleagues at Deltares for their help. Especially Vera van Beek and Esther Rosenbrand for guiding me in modelling and understanding the piping process and Stefan Janssen and Bas van der Zaan for their help with the biochemical aspects.

Also, a special thanks to my friend Peter van de Stroet. I could always count on you, thank you for the support, motivation and fun we had during our study time. Finally, I want to thank my family, especially my girlfriend, for always supporting and believing in me.

Summary

Backward erosion piping (BEP), in Dutch literature often referred to as ‘piping’, is an internal erosion mechanism and can cause failure of dikes, dams and constructions. It can occur during high water situations, when the groundwater pressure in sand layers below the dike becomes high, that on the inner side of the dike the clayey cover layer cracks and water seeps out. Under specific circumstances also sand gets transported, forming a pipe. When the water level in the river keeps rising, the water level will reach a height at which the pipe progresses underneath the dike, coming in contact with the outside water, after which the pipe widens and deepens, followed by the settlement and failure of the dike. Sellmeijer’s model to assess the water level difference at which the pipe progresses is based and calibrated on a standard subsoil geometry: a permeable, homogeneous, fluvial aquifer covered by an impermeable cohesive layer. The shallow subsurface in tidal areas is, however, influenced by biochemical effects and is strongly heterogenous. This is caused by a large difference in sedimentation environment, salinity and presence of organisms. It is expected that Sellmeijer’s model does not predict critical hydraulic gradients well in this tidal sediment. This thesis is aimed to improve the piping assessment of dikes situated on tidal sediments and is sparked by the first findings from small-scale experiments on this topic. A large-scale experiment on piping in the *Hedwigepolder* is planned by Deltares, Fugro and Waterschap Hollandse Delta for 2021. The *Hedwigepolder* will be returned to the *Westerschelde* and before the dike is removed, it is used to conduct flood safety experiments.

The main question of this thesis is: “What is the most suitable design of the field experiments on flow and piping through sandy tidal deposits in the *Hertogin Hedwigepolder*?”. To quantify and explain the expected additional erosion resistance in tidal sediments, this thesis supplies a design which is substantiated by an in-depth literature study and modelling of small-scale experiments in the piping erosion model D-Geo Flow.

The additional erosion resistance in tidal deposits is thought to arise from a combination of aspects: 1) stacking of layers with different hydrological properties, 2) anisotropy in permeability, 3) cohesion (both physical and biological), 4) embedding of sand grains in the fine grain size fraction and 5) labyrinth structures. The first two aspects can already be accounted for in software (D-Geo Flow), while the last three are hard to quantify at present. This study therefore focused on the influence of the presence of the fine fraction on cohesion and on sediment transport. From literature, an explanation is given on where suspected cohesion in tidal sediments comes from and an advice on how to measure it and incorporate it in the current piping assessment. Physical cohesion is caused by: 1) electrostatic forces which bind clay particles, which increases with salinity and 2) evaporation-driven aggregate formation, which means that when fines $<5 \mu\text{m}$ are present, dried fines form solid bridges which increase the strength of the soil 10-100 times when wetted again. The presence of iron precipitates in these more oxygen rich environments causes a reduction of the permeability. Biological cohesion also influences the process. Marine sediments contain bacteria, algae and benthic fauna which influence the EPS content that causes biological cohesion. Aggregates are formed consisting of fines, plant roots, larger sand grains and binding substance EPS (extracellular polymeric substance, a viscous substance, secreted by diatoms, benthic fauna and bacteria). The presence of these aggregates enhances erosion resistance and reduces permeability. Since EPS is also bonded to clay particles by electrostatic forces, increased salinity causes additional cohesion when the EPS content is higher. Indicative parameters for the increased erosion resistance in tidal sediments are thus fines content, organic content and chlorophyll-a concentration (component of EPS) which degrades in measurable components and is the best-preserved marker of EPS over time.

To quantify the additional piping resistance in tidal sediments, small-scale experiments are modelled in D-Geo Flow and the results are used to find a relation between the Strength Factor (SF, measured critical head difference divided by the calculated critical head difference with Sellmeijer’s model) and suspected influences, as found in literature. This factor indicates by what factor the model outcome (calibrated on fluvial sands) differs from the values measured in the experiments, thereby indicating the effects which are not yet considered in the piping assessment. The modelling and analysis of small-scale

experiments resulted in the following findings. The total SF in the experiments on tidal sand is 2.5. The used 3D factor (factor that explains the difference between 3D reality and a 2D piping model) is 1.5, based on the same type of experiments (same scale and same outflow configuration) on fluvial sand by Van Beek in 2015. The best relation between a soil parameter and the SF in the small-scale experiments is the fines content. The reason why this is so different compared to fluvial sand is that EPS, salinity and more often drying of the soil in tidal sand cause the fines to be more cohesive. The fines content can be represented in the uniformity coefficient, but the uniformity coefficient is only affected when the fines content is sufficiently high (approximately 10 w% or higher). In this way, the fines content can be incorporated in the refined Sellmeijer model (see Annex V .a). An advice is to recalibrate the Sellmeijer formula with uniformity values where d_5 is used instead of d_{10} to better represent the fines content.

A large part of the SF of 2.5 can be attributed to cohesion ($SF_c=1.8$). Cohesion causes the critical shear stress to be higher, which could be incorporated in Sellmeijer's formula by increasing the bedding angle (θ). For the used data set this meant changing the angle from 37° to 46° . To use this in the field, the Sellmeijer model needs to be recalibrated.

The main research question is answered by supplying a substantiated design of the large-scale experiment on piping in tidal sediment in the *Hedwigepolder*, which is planned for 2021, hereby using the results from this research. This experiment will be performed by inserting sheet-pile walls (25 m wide) into the dike, directing the flow towards the constructed outflow hole. The water level needed to force piping is calculated with D-Geo Flow and lies just above the crest level of the dike at NAP+10 m. The result from D-Geo Flow is adapted for the 3D-effect and the tidal strength indication found in small-scale experiments. The water is infiltrated into the aquifer by infiltration pipes. Five infiltration pipes are installed to secure the homogeneity of the inflow head over the width. The water flows from the infiltration pipes towards the exit through the tidal sand aquifer. A 2D finite difference model is used to quantify the head distribution in the aquifer. The outflow hole is one meter wide. When the outflow width is larger, the chance of the pipe growing towards the walls increases, which must be prevented. Also, the 3D-effect will be less when the outflow width is larger.

Finally it can be said that the research objective: "Improve piping assessment in tidal areas and to design the large-scale piping experiment in the *Hedwigepolder* with gained knowledge in small-scale experiments on tidal sand." is met, as more knowledge is gained on the influence of tidal sand on the piping process. This can be applied in the current safety analysis and the design of the experiment on large-scale will lead to validation of the findings in this thesis.

Contents

PREFACE	I
SUMMARY.....	III
LIST OF FIGURES	VIII
LIST OF TABLES	XI
LIST OF SYMBOLS	XII
1. INTRODUCTION	1
1.1. LOCATION	3
1.2. STRUCTURE OF THE THESIS.....	3
2. RESEARCH DESCRIPTION.....	5
2.1. PROBLEM STATEMENT.....	5
2.2. RESEARCH OBJECTIVE	6
2.3. RESEARCH QUESTIONS.....	6
2.4. APPROACH	6
3. LITERATURE AND BACKGROUND.....	7
3.1. PIPING	7
3.1.1. The failure mechanism piping.....	7
3.1.2. Research on piping.....	8
3.1.2.a. Sellmeijer	8
3.1.2.b. Numerical model to simulate pipe progression.....	11
3.1.2.c. Shields-Darcy	11
3.1.3. Recent developments.....	12
3.1.3.a. Permeability	12
3.1.3.b. Grain size and uniformity coefficient	12
3.1.3.c. Phases in piping.....	14
3.1.3.d. Pipe erosion.....	14
3.1.3.e. Pipe dimensions	15
3.1.3.f. Spatial variability of the subsoil	16
3.1.3.g. 3D-effects.....	18
3.1.3.h. Foreshore.....	19
3.2. TIDAL SANDS	19
3.2.1. Dutch subsoil	19
3.2.2. Field observations	20
3.2.3. Origin of tidal deposits	20
3.2.4. Consistency	21
3.2.4.a. Grainsize.....	21
3.2.4.b. Biological content	22
3.2.4.c. Location in the tidal basin.....	22
3.2.4.d. Permeability	26
3.2.5. Strength.....	26
3.2.5.a. Heterogeneity & anisotropy.....	27
3.2.5.b. Fine grain size fraction.....	27
3.2.5.c. Biological cohesion.....	32
3.2.5.d. Predicting	36
3.2.6. Lab experiments on tidal sand.....	40
4. MODELLING AND ANALYSIS SSE	41
4.1. EXPERIMENTS ON TIDAL SAND.....	41

4.1.1.	Experiment set-up	41
4.1.2.	Material from the field	42
4.1.3.	Results	43
4.2.	2D MODELLING.....	43
4.2.1.	D-Geo Flow	43
4.2.1.a.	Limitations	44
4.2.2.	Input parameters D-Geo Flow	44
4.2.2.a.	Permeability	45
4.2.3.	Model configuration	47
4.2.4.	Sensitivity	48
4.2.5.	Results	48
4.3.	ANALYSIS	50
4.3.1.	3D-effect.....	50
4.3.2.	Tidal sand strength.....	50
4.3.2.a.	Weight percentage of fines.....	51
4.3.2.b.	Obstacles to flow	53
4.3.2.c.	Cohesion.....	53
4.3.2.d.	Scale effect	54
5.	PIPING EXPERIMENT HEDWIGEPOLDER.....	57
5.1.	GOALS AND REQUIREMENTS	57
5.2.	PROJECT LOCATION	58
5.3.	(SUB)SURFACE ANALYSIS	58
5.3.1.	Soil drillings and CPT's	58
5.3.2.	Soil parameters	59
5.3.3.	Geometry	61
5.3.4.	Safety.....	61
5.4.	HYDRAULIC BOUNDARY CONDITIONS.....	63
5.5.	DESIGN CHOICES	64
5.5.1.	Length	66
5.5.2.	Number of inflow pipes	70
5.5.3.	Outflow width	71
5.5.4.	Width	71
5.5.5.	Sensitivity head and wall permeability	72
5.6.	OPTIMAL DESIGN.....	73
5.7.	EXPERIMENT COMPARTMENTS	73
5.8.	MEASUREMENTS.....	74
6.	DISCUSSION	75
6.1.	OVERALL DISCUSSION	75
6.2.	DISCUSSION FINDINGS	76
6.2.1.	Tidal sand cohesion.....	76
6.2.2.	Tidal sand strength from SSE	77
6.2.3.	Piping experiment <i>Hedwigepolder</i>	78
6.3.	FUTURE RESEARCH RECOMMENDATIONS	79
7.	CONCLUSION	81
7.1.	INTRODUCTION	81
7.2.	MAIN RESEARCH QUESTION	81
7.2.1.	Sub-question 1.....	82
7.2.2.	Sub-question 2.....	83
7.2.3.	Sub-question 3.....	84
	LITERATURE LIST.....	85
	ANNEXES	89

ANNEX I. SOIL CHARACTERISTICS SSE.....	90
ANNEX II. PHOTOS SSE.....	91
ANNEX III. PERMEABILITY SSE.....	93
ANNEX IV. PIPE DEVELOPMENT SSE.....	97
ANNEX V. PIPING MODELS	100
ANNEX VI. SCHEMATIC OF THE PIPING PROCESS	105
ANNEX VII. SOS PROBABILITY TIDAL SAND.....	106
ANNEX VIII. 3D MODELLING SSE.....	107

List of Figures

Figure 1 - High water level at the Rijn near Rhenen (Vergouwe, 2014).....	1
Figure 2 - Hedwigepolder (3)(Meetjesland, 2018) , aerial view maps (1 and 2) (Microsoft Corporation Earthstar Geographics, 2019; Van der Meulen et al., 2003) and the initial design plan from 2016 (4) (Smitskamp & Koks, 2013).....	3
Figure 3 - Flow chart of the approach and structure of this thesis.....	6
Figure 4 - Lifting of the cover layer. The seepage force exceeds the weight of the cover layer ('t Hart et al., 2016) (top) Fault tree of a levee with a cover layer by lifting and cracking of the cover layer, heave and piping (Jonkman, 2018) (bottom).....	7
Figure 5 - Piping and well locations (based on incomplete data, 75% covering and delivered by the separate waterboards) (Förster et al., 2012).....	7
Figure 6 - Relative influence of d_{70} , permeability (k), aquifer thickness (D) and seepage length (L) to the critical head difference from Sellmeijer's equation.....	10
Figure 7 - Permeability (k) values per soil type and drainage indication (Sidik et al., 2014).....	12
Figure 8 - Critical gradient of historical failures for different types of soil (hard material being pan) (Kanning, 2012).....	12
Figure 9 - Relation between grain size and the permeability for uniform sands (L) and effect of grain size on the hydraulic gradient (R) (Van Beek, 2015).....	13
Figure 10 - Sand boil Netherlands 2011 (Van Beek, 2015).....	14
Figure 11 - Indication of pipe depth (in mm) over distance (Vandenboer et al., 2017).....	15
Figure 12 - Example of pipe formation in the medium scale experiments by Van Beek in 2015 (Van Beek, 2015).....	16
Figure 13 - Classification of uncertainties (Kanning, 2012).....	16
Figure 14 - Typical cross-section of a dike in length direction (Kanning, 2012).....	16
Figure 15 - An illustration of heterogeneity and anisotropy.....	17
Figure 16 - Simulated 3D seepage patterns in piping experiments (Negrinelli et al., 2016).....	18
Figure 17 - Locations where tidal deposits (blue) are found underneath the cover layer (top sand layer) in the Netherlands (Van Asselen et al., 2018).....	19
Figure 18 - Field observations of sand boils in areas with tidal deposits in the Netherlands (12 sand boils, red dots and one breach, red square) (Hijma & Oost, 2019).....	20
Figure 19 - Indication on the formation of a sandy clay tidal deposit (MIM, 2017).....	20
Figure 20 - Classification of gap-graded soils: (a) with fines contents less than 10%; (b) with fines contents between 10% and 35%; (c) with fines contents more than 35% (Chang & Zhang, 2013).....	21
Figure 21 - In the left figure: cumulative sieve analysis of the typical Dutch formations, the orange line is tidal channel sand and the other lines are fluvial sand (blue and purple) and cover sand (pink). In the right figure: NEN5104 clay (lutum) -silt-sand triangle; in which the grey part in the small triangle can be found in the Netherlands. The top blue x is the unsieved material of F213 from Friesland, the two other blue x's are Baskarp with Kaolinite, the orange x is the material from the Grevelingen and the green x is the sieved material of F214 and F215 from Friesland (R) (Wiersma & Hijma, 2018).....	22
Figure 22 - Drilling H_Mg_zm, 1 m long.....	23
Figure 23 - Drilling H_Mg_zf, 1 m long.....	23
Figure 24 - Formation of double mud drapes in case of a dominant tide (Hijma & Oost, 2019).....	24
Figure 25 - Priel in the Dollard, Netherlands (Kwant, 2015) and low intertidal flat sediment structure (Hijma & Oost, 2019).....	25
Figure 26 - High intertidal sediment structure with bioturbation (Hijma & Oost, 2019).....	25
Figure 27 - Salt marsh sediment structure(Hijma & Oost, 2019).....	26
Figure 28 - Permeability with changing iron-sludge (containing 33 w% Fe) percentage (Koopmans et al., 2010).....	26
Figure 29 - Heterogeneity on a micro scale (Wiersma & Hijma, 2018) (herein referring to Cheel, 2002).....	27
Figure 31 - Proposed geometric criteria for different types of soil by Chang et al. (Chang & Zhang, 2013).....	28

Figure 31 - Classification of gap-graded soils: (a) with fines contents less than 10%; (b) with fines contents between 10% and 35%; (c) with fines contents more than 35%(Chang & Zhang, 2013)	28
Figure 32 - Experiment soil from Grevelingen (L) and Friesland (R) through a microscope. The fines are clearly visible in between the larger sand particles	29
Figure 33 - Percentage clay coating with varying: (A) mean grain size, (B) clay fraction, (C) grain size sorting and (D) sample depth (Wooldridge et al., 2018).....	30
Figure 34 - Clay coat coverage for different concentrations of chlorophyll-a (Wooldridge et al., 2018)	30
Figure 35 - Clay cohesion on molecule scale (Shehata, 2015).....	31
Figure 36 - Sediment stability over salinity for lightly disturbed soils when salinity is increased (10%) and more heavily disturbed soil when salinity is increased (30%) (Spears et al., 2008).....	31
Figure 37 - Aggregate stability of Illite clay particles when dried (A) and rewetted (C), formed solid bridges (Seiphoori et al., 2020).....	31
Figure 38 - Interparticle bonding (Friend, 2001) (L) and Scanning electron microscopy (SEM) images of surface clay-coated sand grains. Arrows indicate regions and key textural characteristics of clay coats (Wooldridge et al., 2018) (R)	32
Figure 39 - Soil transport over time for different percentages of EPS content (Malarkey et al., 2015) ...	33
Figure 40 - Soil aggregate classification when EPS is present (Costa et al., 2018)	33
Figure 41 - Benthic diatom (◊) embedded in EPS (about 20 μm) (Black et al., 2002).....	34
Figure 42 - Critical shear stress and chlorophyll-a on a more landward station in March and April (L) and on a more seaward measuring station in March, April and May (R) (Friend, 2001)	34
Figure 43 - Lugworm, feeding shaft and fecal mound (Clipground, 2019).....	35
Figure 44 - Chemical structure of chlorophyll-a (Reuss, 2005)	36
Figure 45 - Molenplaat in the Westerschelde (Widdows et al., 2004)	38
Figure 46 - Shields diagram (Hoffmans & Van Rijn, 2018).....	39
Figure 47 - Results of the CSM field measurements by Friend plotted on a Shields diagram with an indication of the Shields curve (Friend, 2001)	39
Figure 48 - Pictures of the experiment, measuring discharge and writing down the rise heights (L), schematic of the flow and riser tube measurements (T) and placement of the riser tubes (R) (Hijma & Oost, 2019; Negrinelli et al., 2016).....	41
Figure 49 - Location of the Springersdiep on a map from 1960, the sand sample was retrieved at the red circle on the map (Hijma & Oost, 2019).....	42
Figure 50 - Example of a cross section with an infiltration pipe in D-Geo Flow; pipe (yellow), mesh (black) and boundaries (blue = river water level, red = no flow boundary, pink = polder water level and green = seepage boundary).....	44
Figure 51 - Permeability of the experiment on Baskarp with 3 w% Kaolinite. The error bands are shown in light red and the discharge in blue. The green line indicates the applied head at which the pipe started growing visibly	46
Figure 52 - Gap-graded soils with a low fines content and medium fines content (Chang & Zhang, 2013)	46
Figure 53 - Permeability over head difference for the small-scale experiments on tidal sands. Green=Grevelingen sand, Brown=Grevelingen sand with clay layers, Orange=Friesland sand and Grey=Baskarp sand with Kaolinite clay	47
Figure 54 - Model set-up D-Geo Flow for the experiments with and without vertical clay layers.....	48
Figure 55 - Results SSE, measured and calculated with Sellmeijer's formula and D-Geo Flow	49
Figure 56 - Results of small- and medium scale experiments with a hole type of outflow (3D) calculated with Sellmeijer's model (2D, original and adjusted form) (Van Beek, 2015).....	50
Figure 57 - SF (strength) over w% of fines (left Sellmeijer and right D-Geo Flow). The black bars represent the bound when the minimum and maximum permeability, measured in the experiments, is used to calculate the strength	51
Figure 58 - SF (strength) over w% of fines of the experiments with Baskarp sand and Kaolinite clay (left Sellmeijer and right D-Geo Flow). The black bars represent the bound when the minimum and maximum permeability, measured in the experiments, is used to calculate the strength	52
Figure 59 - Permeability over percentage of fines	52
Figure 60 - Uniformity over fines percentage (<63 μm).....	52

Figure 61 – SF (strength) over uniformity coefficient (Van Beek, 2015) (L) and strength factor varying over uniformity (middle Sellmeijer and right D-Geo Flow) (R)	53
Figure 62 – SF (strength) in relation to number of layers, width of the layers and seepage length (G210 and G211)	53
Figure 63 - Location overview at the Lingestraat in the Hedwigepolder, retrieved from Google maps Street View	58
Figure 64 – Soil profile along the dike constructed from soil drillings on the orange dots in the overview figure. NAWA being the Naaldwijk formation, BX the Boxtel formation and OO the Oosterhout formation (see 3.2.3). The green dot is the location of the soil drilling of which the photo is made and the yellow rectangle in the picture is the soil on which the experiment will be performed .	59
Figure 65 - Geotechnical length profile, from left to right in Figure 66.	60
Figure 66 - Project area with CPT's, 50 m from each other. The underlined numbers are the depth of the underside of the peat layer (0 if not present) in the rectangle in the middle there is no peat layer present	60
Figure 67 - Cross sections based on AHN3 and CPT interpretation for two types of subsoil.....	61
Figure 68 - Polder water level Hedwigepolder from 1964 until 2000 at the green dot on the map (TNO, 2009)	63
Figure 69 - Tidal record at Schaar van de Noord September 2018 - March 2019 (RWS, 2020)	63
Figure 70 - Top view of the piping experiment.....	64
Figure 71 - Finite difference model.....	65
Figure 72 - Top view of the project area (with 5 inflow points, a length of 22.5 m, a width of 25 m and an outflow width of 3 m) in the finite difference model in Excel. The 3D graphs on the right are indications of the head (top) and the discharge in x-direction (bottom)	65
Figure 73 - D-Geo Flow model of profile 1	66
Figure 74 - Pressure on the surface between the cover layer and the aquifer for cross section 1 (top) and 2 (bottom). The pressures are water pressure caused by the critical head differences and soil pressure. As mentioned in Table 9, the permeability of the cover layer is assumed to be lower. When this is considered, the critical head difference is approximately 5% lower	68
Figure 75 - Head adjustment over time for different lengths when the head is increased with 0.5 or 0.3 m per hour.....	69
Figure 76 - Final design impression of the experiment in a cross section (bottom) and from the crest of the dike (top).....	73
Figure 77 - Placing pattern pressure transducers	74
Figure 78 - Strength factor over weight percentage of fines <16 μm	77
Figure 79 - Experiment set-up Hedwigepolder	82
Figure 80 – Head drop during pipe progression (Förster et al., 2012)	101
Figure 81 - Simplification of the head difference in the sand layer during pipe formation (Hoffmans, 2014)	101
Figure 82 - Schematisation of the subsurface, head and pipe formation in the SD model (Van Beek & Hoffmans, 2017).....	102
Figure 83 - SOS probability of occurrence of tidal sand in the top 5 m of subsoil in the Netherlands (Hijma & Oost, 2019).....	106
Figure 84 - Visualisation of the difference in flow lines for models (a) 30 cm wide and (b) 10 cm wide (Vandenboer et al., 2014)	107
Figure 85 - Visualisation of the results from DgFlow with a hole-type outflow, presenting the head and water velocity at the final calculation step visualized with Paraview	108

List of Tables

Table 1 - Gravitational and drag force in the Sellmeijer formula	15
Table 2 - Grain size distribution of the Naaldwijk formation (member Walcheren) (Hijma, pers. comm.)	21
Table 3 - Correlation chlorophyll-a and critical shear stress (Friend, 2001)	34
Table 4 - Influence and consequences of and on chlorophyll-a preservation and concentration	36
Table 5 - Chlorophyll-a levels Blackwater Estuary, Essex (Underwood et al., 1995)	37
Table 6 - Chlorophyll-a levels Molenplaat (Widdows et al., 2004)	38
Table 7 - Results critical head difference SSE	43
Table 8 - Results SSE on tidal sand and fluvial sand (3D) compared to 2D calculations with Sellmeijer's formula and D-Geo Flow	48
Table 9 - Soil characteristics Hedwigepolder	62
Table 10 - Characteristic soil properties values	62
Table 11 - Sensitivity in permeability	62
Table 12 - Variations in input parameters FD-model	66
Table 13 - Adaptation of the head near the outflow with the head increasing by 0.5 m per hour	69
Table 14 - Head lag near the outflow with sensitivity of the head development to permeability and head increase steps	70
Table 15 - Ratios w/a tidal sand experiments	107
Table 16 - Results SSE on tidal sand and fluvial sand, calculations with 3D DgFlow	109

List of Symbols

$\partial\varphi/\partial x$	head gradient over the pipe	[m/m]
A	cross-sectional surface area / anisotropy factor	[m ²], [-]
a	pipe depth	[m]
B	width dike base	[m]
c	cover layer resistance (= d/k_d),	[s]
C_3	erosion coefficient aquifer (= 0.3)	[-]
$C_{G,v}$	vertical transmissivity aquifer	[-]
C_ℓ	pipe geometry factor	[-]
d	grain diameter / thickness cover layer	[m]
D	sand sample thickness / aquifer thickness	[m]
$d_\%$	grain diameter for which % of the sample (by weight) is finer	[m]
D^*	dimensionless particle number	[-]
d_{70m}	reference d_{70} -value (= $2,08 \cdot 10^{-4}$)	[m]
d_{min} ; d_{max}	minimal and maximal grainsize which identify the gap in the grains size distribution	[m]
D_{ref}	effective thickness aquifer SD-model	[m]
E	coefficient describing the geometry and soil parameters	[-]
F	mass fraction of particles finer than grain size d	[-]
F_r	resistance factor	[-]
F_s	seepage force / scale factor	[N], [-]
g	gravitational acceleration (= 9.81)	[m/s ²]
G_r	gap-ratio in grain size distribution	[-]
h	hydraulic head	[m]
H	head drop across the sand sample or embankment / mass fraction of particles ranging from d to 4d	[m] / [-]
H_c	critical head drop across the sand sample or embankment at which progressive erosion occurs	[m]
H_i	minimum head drop across the sand sample or embankment at which the pipe is initiated	[m]
h_p	polder head	[m]
h_{pipe}	pipe head	[m]
i	vertical exit gradient	[m/m]
i_c	critical heave gradient	[m/m]
$k(x, y)$	hydraulic conductivity in direction x or y	[m/s]
KAS	roundness of particles 0 (round) to 100 (angular) ($\approx 40 - 60$)	[-]
L	length of seepage	[m]
l	pipe length	[m]
l_{Re}	length scale coefficient SD-model (= $18E-6$)	[-]
n	porosity / number of particles	[-], [#]
P	weight percentage of fines	[%]
P_f	percentage sand weight that has to erode from the skeleton of the sand before piping can occur (= 70 (Wang, 2014))	[%]
Q	(groundwater or pipe) discharge	[m ³ /s]
$Q_{p,m}$	discharge through the pipe SD-model	[m ³ /s]
$q_{p,m,c}$	specific discharge (=discharge per unit of width) SD-model	[m ² /s]
RD	relative density (also known as packing density)	[-]
Re	Reynolds number	[-]
Re^*	particle or grain Reynolds number	[-]
$Re_{m,c}$	Reynolds number downstream of the pipe SD-model	[-]
S	aquifer storage coefficient	[-]

S_B	bio stabilization index cohesive sediments	[-]
$S_{\text{pipe},c}$	critical head gradient in the pipe	[m/m]
$S_{\text{sand},c}$	critical head gradient in the aquifer	[m/m]
T	transmissivity	[m ²]
t	time	[s]
U	uniformity coefficient (= d_{60}/d_{10})	[-]
u	seepage velocity at the pipe tip	[m/s]
u^*	shear velocity	[m/s]
V	coefficient of variation	[-]
w	pipe width	[m]
x	x-coordinate	[-]
y	y-coordinate	[-]
Z	limit state function	[-]
α_f	groundwater coefficient SD-model (= 5)	[-]
$\alpha_{\text{Re},l}$	Reynolds coefficient SD-model (= 6)	[-]
β	compressibility	[m ² /N]
Δ	(γ'_p / γ_w) / difference	[-], [-]
η	White's constant	[-]
θ	bedding angle	[°]
κ	intrinsic permeability	[m ²]
μ	dynamic viscosity / friction coefficient / mean	[Pa s], [-], [-]
ρ_s	particle density	[kg/m ³]
ρ_w	water density	[kg/m ³]
σ	standard deviation	[-]
τ	shear stress	[N/m ²]
φ	groundwater head	[m]
Ψ	Shields parameter	[-]
$\Omega_{p,c}$	critical horizontal in the pipe	[s/m ³]
Ω_s	horizontal groundwater flow resistance of the aquifer	[s/m ³]
γ_p	unit weight of particles	[kN/m ³]
γ'_p	submerged unit weight of particles	[kN/m ³]
γ_w	unit weight of water	[kN/m ³]
ν	kinematic viscosity (water at 20 °C = $1,33 \cdot 10^{-6}$)	[m ² /s]

Subscripts

0	starting value
C	cohesion
c , crit	critical
calc	calculated
d	cover layer
exp	experimental
F	finer
i	initiation
in	situated near the inflow
lam	laminar
m	mean value from selected small-scale experiments
max	maximum
out	situated at the outflow
p	polder / pipe / particle / piping
r	ratio
s	specific / sand / soil
w	wall / water
wall	situated near the wall

Definitions

Chl	chlorophyll-a concentration	[$\mu\text{g/g}$], [$\mu\text{g/gDW}$]
DW	dry weight	[-]
Fe	iron	[-]
Fine fraction / Fines / Fine material	weight percentage of fines of which the grain diameter is smaller than 63 μm , so smaller than sand	[w% fines <63 μm]
Lutum fraction	weight percentage of fines of which the grain diameter is smaller than 2 μm and soil is called clay when more than 25% of the soil consist of lutum particles	[w% fines <2 μm]
NaCl	salinity	[g/kg], [g/L]
SF	strength factor	[-]
Silt	very fine sand particles which grain diameter lies between 2 and 63 μm	[-]
Sludge (Dutch: slib) fraction	weight percentage of fines of which the grain diameter is smaller than 16 μm	[w% fines <16 μm]
w%	weight percentage	[%]

1. Introduction

The name ‘Netherlands’ tells us a lot; large parts of the Netherlands are located below sea level. Not only the threat from the sea, but also the presence of large rivers like the *Rijn* (Figure 1) and *Maas* make the Netherlands vulnerable to flooding. To take appropriate measures against flooding, the regulations concerning flood protections are included in the law (Knops, 2018; MIM, 2010).

The flood protection system that is in accordance with these regulations is quite extensive. Primary defenses protect the land against floods from the *North Sea*, the *Waddenzee* and the main rivers (*Rijn* and *Maas*). The total length of these primary defenses is around 3500 km. Regional dikes protect the land from floods from inland water.

Dikes are constructed along rivers, artificial waterways, lakes and coasts. In the Netherlands they are constructed across the country, crossing different subsoils, often depending on the geological history. In most cases, these dikes consist of earthen structure composed of a sandy body with a water impermeable cover layer, based on soft soils with a sandy aquifer underneath.



Figure 1 – High water level at the *Rijn* near *Rhenen* (Vergouwe, 2014)

The safety philosophy in the Netherlands is based on the risk of flooding. The risk of flooding is a combination of the probability that it occurs and the consequences if it would occur (Jonkman & Cappendijk, 2006). Flooding only occurs when the flood protection fails to fulfill its task, called failure (Knops, 2018). Flood defenses can fail due to several different failure mechanisms, which are listed below (Van Baars & Van Kempen, 2009):”

- A. Run-over (dike too low for water level);
- B. Wave overflow (waves too high or too much run up);
- C. Instability of outer slope protection or erosion (damage to masonry pitching or rock fill);
- D. Erosion of inner slope protection (or dike crest, often by wave overflow infiltration);
- E. Micro-instability (washing out of the dike core sediment, such as piping below the dike);
- F. Piping (local groundwater flow, sediment transport and erosion below dike);**
- G. Heave (lifting of and liquefaction of inner sand layer by vertical groundwater up-flow);
- H. Bursting (forcing up of polder top clay layer by high pore water pressure in sand layer below);
- I. Liquefaction of shoreline (loose sand layer in front of dike becomes unstable by steepening of the slope);
- J. Sliding outer slope (macro instability of steep outer slope);
- K. Sliding inner slope (macro instability of steep inner slope);
- L. Horizontal sliding (complete dike pushed aside by water pressure);
- M. Ice drift (both thrusting water load and direct ice load through current or wind);
- N. External factors (Human: piercing, bombing, ship collision. Animals: worms, rats).”

The research questions in this thesis are aimed to gain knowledge on the failure mechanism piping in tidal areas, where sandy cohesive sediment is found. A short introduction on piping and tidal sediment is given below.

Piping

Backward erosion piping (BEP), in Dutch literature often referred to as ‘piping’, is an internal erosion mechanism and can cause failure of levees, dams and constructions. Internal erosion occurs when soil particles in an embankment dam or its foundations are carried downstream by seepage flow. Due to seepage flow underneath the low permeable cover layer, when high water occurs on the river side of the dike, the potential in the permeable aquifer rises on the inner side of the dike (polder side). Due to

the low permeable cover layer on top of the aquifer, the water pressure rises and causes lifting and cracking of the cover layer, when the water pressure exceeds the weight of the cover layer. Water starts to flow upward out of these cracks, the exit point, this process is called heave or initiation of the pipe (Van Beek, 2015). In this stadium, the sand is in equilibrium in the vertical outflow, i.e. the seepage force equals the weight of the sand-water mixture. When the water level in the river keeps rising, the pipe progresses to the upstream side (river side), after which the pipe widens and deepens, followed by the settlement and failure of the dike (Van Beek, 2015). A schematic of the process is included in Annex VI.

Flood defenses in the Netherlands are assessed, to check if they are sensitive to piping, with rules initially developed by J.B. Sellmeijer in 1988, but substantially adjusted in 2011. A lot of research has been conducted on piping in the last century. Because the process takes place underneath a dike and the location where it will happen is not known in advance, still a lot is unknown about the process on field scale. The largest uncertainties rise from the schematization of the subsoil and the onset of particle motion in the pipe. Also, the limitations of the current design model like the 2D-3D-effects play a significant role in the uncertainties.

Sellmeijer's model is based on a standard geometry: a permeable homogeneous aquifer covered by an impermeable cohesive layer. The shallow subsurface in tidal areas is, however, influenced by biochemical effects and is strongly heterogenous. It is expected that Sellmeijer's model does not predict critical hydraulic gradients well in this tidal sediment. More on this topic in the problem statement in Chapter 2.

Tidal sediment

Offshore, currents generated by the tides interact with an array of processes, including waves, storm/wind-generated currents and geostrophic currents that are part of the global-ocean circulation, giving the potential for the creation of a variety of sedimentary deposits closer to shore (Reynaud & Dalrymple, 2012). These tidal deposits are formed in areas where sedimentation is dominated by tidal action and where the influence of wave action on the composition of the deposit is limited.

Tidal areas are characterized by a regular alternation of periods of more and less flow and supply of sediment. In intertidal areas, this leads to periodic drying out and a regular variation in the intensity of wave action. The flow velocity decreases sharply around slack water and the finer particles from the water column are deposited (MIM, 2017). The size and consistency of the forms are strongly depending on flow velocity and wave action. In comparison with fluvial deposits, the tidal deposits have lower average grains sizes, higher percentages lutum and silt (fines), more thin, discrete clay layers, more labyrinth structured layer formations, different organisms, are more saline and have a much faster dry-wet alternation. More on this topic in 3.2.5.

1.1. Location

The location where the above-mentioned experiment will take place is the *Hertogin Hedwigepolder*. This polder is situated in *Zeeuws-Vlaanderen*, in the southwestern part of the Netherlands (Figure 2). The *Hedwigepolder* was reclaimed from the *Westerschelde* in 1907. It is surrounded by the *Drowned land of Saeftinghe*, *Prosperpolder* and *Westerschelde*. The *Hedwigepolder* measures 316 ha; 304 ha on Dutch and 12 ha on Belgian (*Vlaanderen*) soil (Kole, 2013).

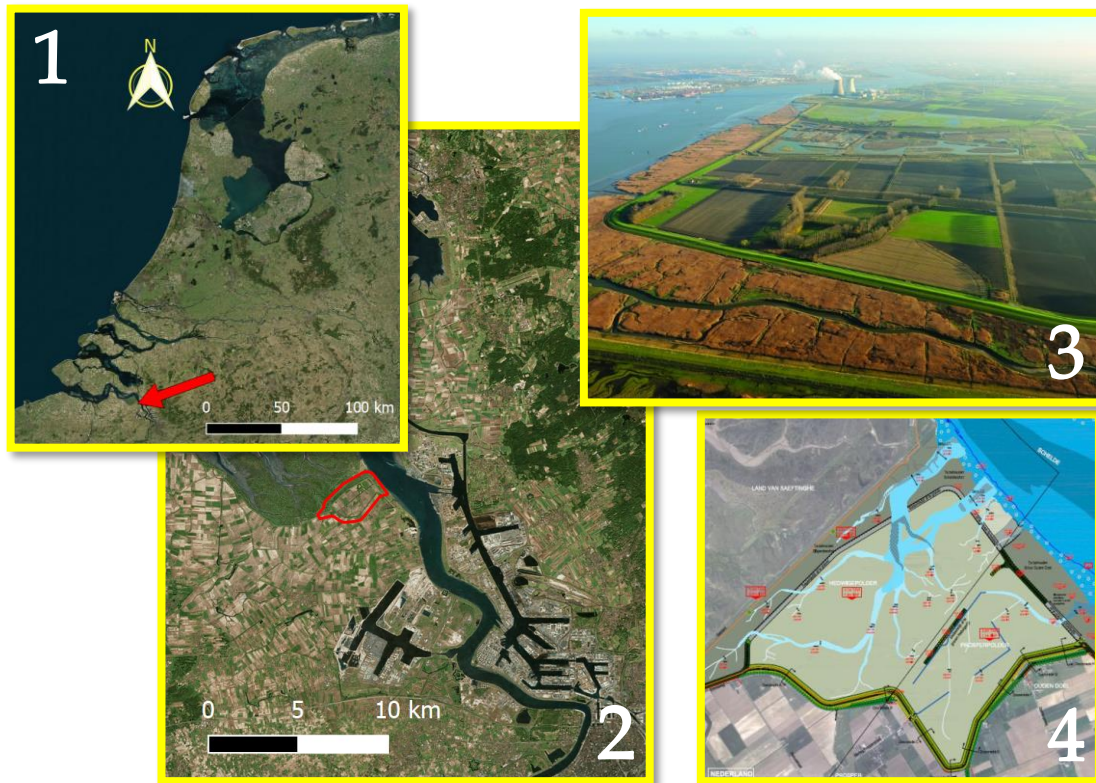


Figure 2 – *Hedwigepolder* (3)(Meetjesland, 2018) , aerial view maps (1 and 2) (Microsoft Corporation Earthstar Geographics, 2019; Van der Meulen et al., 2003) and the initial design plan from 2016 (4) (Smitskamp & Koks, 2013)

Because the *Westerschelde* will get deepened to allow for bigger and more ship, a nature-compensation measure was needed. After agreements with *Vlaanderen*, the Dutch government decided in 2012 to return the polder to the *Westerschelde*. Residents and landowners showed a lot of resistance against these plans. A member of the resistance group even called the new plans “a creation of a desolate bin of sludge, which they call nature”, pointing out the sedimentary nature that would arise (Oldenbeuving & De Jong, 2019). In January 2018, the Supreme Court definitively put an end to a struggle that lasted more than ten years, the *Hedwigepolder* had to be depoldered. At the end of 2018, the trees and houses were removed from the polder and the construction of a new sea dike will start soon. The current *Scheldedijk* around the polder will be excavated and the seawater will reach the *Hedwigepolder* (OmroepZeeland, 2019). The initial design plan by Oranjewoud in 2016 is presented in Figure 2.4.

1.2. Structure of the thesis

This thesis is structured in the following manner. It first gives an introduction on the main topics in this thesis (Chapter 1). Chapter 2 declares the problem, questions and approach in a research description. Chapter 3 contains a literature study to provide background theory. Chapter 4 presents the modelling and analysis of small-scale experiments conducted by Deltares. Chapter 5 holds the design of a large-scale piping experiment in the *Hedwigepolder*, which is planned for 2021. The discussion of the results and method is presented in Chapter 6, although this is also done interim because in some cases discussion is needed to move on to other sections. Chapter 7 holds the conclusion of the thesis, giving answers to the research questions.

2. Research description

2.1. Problem statement

Sellmeijer's formula (Eq.5) is based on a standard geometry: a permeable homogeneous aquifer covered by an impermeable cohesive layer. The shallow subsurface in the Netherlands is, however, strongly heterogeneous (Kanning, 2012). These heterogeneities are present on different scales; 1) micro-scale where soil parameters in a layer may vary. Kanning (2012) found that the parameters that have the most influence on piping are the hydraulic conductivity (k) and the grain size (d_{70}). Due to placement of the grains and settlement, the horizontal and vertical hydraulic conductivity may vary from each other. The inequality of hydraulic conductivity between the horizontal and vertical direction is called anisotropy. 2) On a macro-scale, heterogeneities are present where the aquifer may consist of multiple layers like gravel or clay. Also the presence of old riverbeds and tidal deposits, which are often highly anisotropic, cause heterogeneities on macro-scale (Kanning, 2012; Knops, 2018).

Sellmeijer's model was developed with analytical equations for 2D groundwater flow towards the pipe (Sellmeijer, 1988) for an infinitely deep aquifer. The limited application of such a model was soon realized, resulting in a mathematical formulation of groundwater flow towards the pipe in homogeneous and isotropic aquifers with a finite depth (Van Beek & Hoffmans, 2017). In addition to the homogeneity and isotropy, important aspects like 3D flow and time dependency are currently not included in the assessment rules (Van Beek & Hoffmans, 2017). The flow concentrates in 3D towards the outflow leading to higher gradients near the outflow. The time dependency of the process is important in two ways: 1) the aquifer does not respond instantly to changes in water level and 2) the duration of a flood has influence on the length over which the pipe can develop.

Notwithstanding the mentioned limitations of Sellmeijer's model, it is the prevailing assessment rule for piping in the Netherlands. To use Sellmeijer's model, sufficient data of the soil characteristics is needed and the geometry of the cross-section of the dike (Deltares, 2017). In practice, not enough and precise data is available to perform realistic calculations in a certain cross-section. Because of this lack in knowledge, the aquifer is schematized homogenous with conservative soil parameters.

Several research projects have shown that tidal deposits under our primary and regional flood defenses offer much more resistance to piping than the current piping models show. This was found to be due to three aspects: 1) a physical barrier against flow, 2) the Sellmeijer model is calibrated on experiments without the fine clay and silt fraction (different grain size-permeability relation) and 3) additional strength due to anisotropy, heterogeneity, physical and biological cohesion (Hijma & Oost, 2019). This suggests that the erosion mechanism in tidal deposits is different than in the homogenous soil experiments, which Sellmeijer conducted.

Further development after these conclusions remains limited to theoretical models and small-scale laboratory tests. This means that flood defenses are unnecessarily deemed insufficient and being reinforced: a waste of tax money (Van Goor et al., 2019). Deltares, Fugro and Waterschap Hollandse Delta intend to conduct a large-scale field trial into the resistance of tidal deposits against piping in the *Hertogin Hedwigepolder*. This offers a unique opportunity to validate and advance the knowledge already gained on piping in the tidal area (Van Goor et al., 2019).

To make this field experiment useful, a suitable design is needed. This design needs to be substantiated theoretically and by the knowledge gained by analysing scale experiments on tidal sands.

2.2. Research objective

The main goal of this thesis is to improve piping assessment in tidal areas and to design the large-scale piping experiment in the *Hedwigepolder* with gained knowledge in small-scale experiments on tidal sand. The knowledge of the piping process in tidal deposits, gained in this thesis, contributes to the available knowledge in the field of flood risk because the evaluated physical and biochemical influences are undiscovered terrain and it is estimated that 1000 km of flood defenses in the Netherlands are situated on top of tidal deposits.

2.3. Research questions

The main research question is:

“What is the most suitable design of the field experiments on flow and piping through sandy tidal deposits in the *Hertogin Hedwigepolder*?”

This main research question is supported by the following sub-questions:

- I. What are the differences between the piping erosion process in tidal sands and fluvial sands?
- II. What is the influence of tidal sands on the differences between the data from the small-scale experiments on tidal sands and the outcomes of the modelled scale-experiments in D-Geo flow?
- III. How can the piping experiment in the *Hertogin Hedwigepolder* be designed?

2.4. Approach

This thesis is a modelling study and design to investigate the influence of tidal deposits on groundwater flow and piping. In the research method, the steps of the sub-questions are followed. Before modelling the scale experiments, knowledge needs to be gathered from literature. The literature study provides insight into tidal deposits and the mechanism of piping. To answer sub-question one, especially the aspects that are likely to have much influence on tidal sand strength; percentage of fines and cohesion (Hijma & Oost, 2019) are described. The percentage of fines is expected to have a profound influence on both permeability and cohesion. Literature is gathered to learn about the cohesion process in tidal sediments, markers to measure cohesion and options to consider cohesion in piping assessment.

The second sub-question is answered by the modelling and analysis of the small-scale experiments conducted by Deltares on tidal sands. The experiments with tidal sands are modelled in D-Geo Flow and by comparing the results with the measured data, an explanation is sought for the difference. This difference is expected since Sellmeijer’s model is calibrated on experiments on fluvial sand.

With the knowledge about the influence of the fines and cohesion in the small-scale experiments, a substantiated design is made for the large-scale experiment in the *Hertogin Hedwigepolder*. The subsurface is evaluated and the effects of large-scale layering, 3D-effect and anisotropy in permeability are incorporated. The requirements for this design followed from the validations that Deltares wants to do with the results from the large-scale test. The base requirements for the design are:

- I. Sand boils must appear, and backward erosion piping must occur;
- II. The dike may not fail due to other failure mechanisms than piping;
- III. The data obtained from the experiments is must be valuable to study the effects of tidal deposits on piping. This means that measurements of the influential parameters must be performed beforehand and the pipe development must be tracked during the experiment.

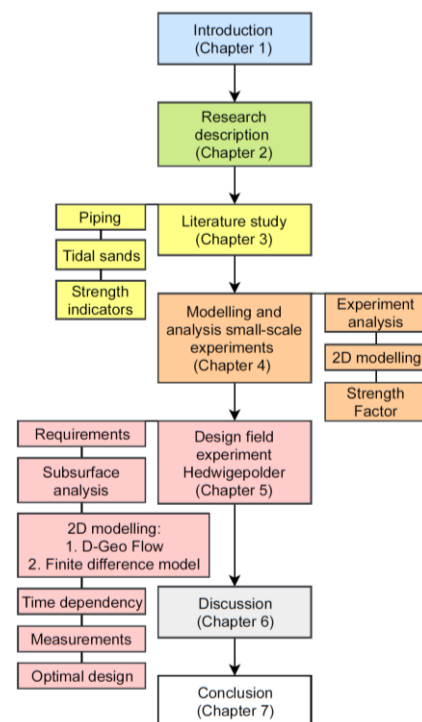


Figure 3 - Flow chart of the approach and structure of this thesis

Sand boils are observed regularly, around 120 were observed during the 1993 flood, of which 40 along the *Rijn*, 40 along the *Waal*, 30 along the *IJssel* and 10 along the *Maas*. Around 180 sand boils were observed during the 1995 high water, many of which had already been seen in 1993 (Vergouwe, 2014). In 2009, Deltares, Royal Haskoning and Fugro made an overview of the locations of the observed sand boils in the Netherlands (Figure 5).

3.1.2. Research on piping

Over the past century, a lot of research is conducted on seepage erosion under dikes. In this paragraph, an overview of the most important past research is given. Conclusions and how they were drawn by different researchers based on different data sets are very important to this thesis.

Clibborn and Beresford developed an empirical rule that relates the hydraulic head across the structure (H), a coefficient that depends on the geometry and soil parameters (E) and the seepage length (L) (Sellmeijer, 1988):

$$L = E \cdot H \quad \text{Eq.1}$$

Bligh (1910) and Griffith (1913) followed the same concept. In 1922, Terzaghi developed the early heave gradient. He presented the concept of a vertical critical gradient. In this concept; heave occurs when the upward seepage forces exceed the downward gravitational forces, a sand boil.

Lane (1935) found that the vertical seepage length contributes more to the safety than horizontal length. He adjusted the empirical rule to the so called 'weighted seepage method', based on a total of 200 test in the U.S. (Sellmeijer, 1988; Van Beek et al., 2011). Harza (1935) proposed the electric analogy method, where electric currents are used to simulate groundwater flow (Sellmeijer, 1988; Zee, 2011).

After the flood disaster in 1953 there was a need to change the safety philosophy of dikes in the Netherlands (Van Beek et al., 2011). A few years later, in 1965 the Technical Advisory Committee for Water-retaining Structures (TAW in Dutch) was founded to investigate the state of the Dutch dikes. The alarming finding that during high water periods many sand boils were observed along the river levees, even at levels far below the design level, resulted in new research on piping (Van Beek et al., 2011). At the same time, a German research group investigated the piping phenomenon (Müller-Kirchenbauer, 1978 and Hanses, 1985). They looked in detail into the erosion process, which included both fluidization at the head of the pipe and bed erosion, by which the pipe widened and deepened (Van Beek et al., 2011). De Wit (1981 and 1984) investigated the influence of several soil characteristics, such as dimensions of the sand bed, grain size, porosity and the type of exit through the cover layer (Kramer, 2014). Besides that, he reported experiments in partly covered sand layers (Sellmeijer, 1988).

The conducted experiments led to a better understanding of the process and in 1988 J.B. Sellmeijer came with a theoretical model (Eq.2) in which the equilibrium of grains on the bed of the pipe was used as criterium for development of the pipe (Sellmeijer, 1988).

Large-scale tests, performed in the Delta flume in the Netherlands, allowed for validation of the model at different scales. Based on values from literature and these experiments, the model was calibrated by adjusting the bedding angle and the formula (Eq.2) was included in the technical report on sand boils, TAW1999 (Van Beek et al., 2011).

The three most recent and advanced methods are the empirical model of Sellmeijer (started in 1988), the erosion rate model of Wang et al. from 2014 and the Shields-Darcy (SD) by Hoffmans in 2014 (Van Beek & Hoffmans, 2017). Sellmeijer's model is incorporated in the finite element calculation platform D-Geo Flow. In the sub-paragraphs below, the models are described.

3.1.2.a. Sellmeijer

Sellmeijer described the relation between the hydraulic head across the structure (H), seepage length (L) and soil properties in 1988 with four classical theories: groundwater flow, boundary balance, hydraulics and mechanics at particle level. These theories led to three sub-models: A groundwater model

describes the seepage in the sand layer; the pipe model predicts the flow in the erosion channel and the transport model computes the incipient motion of the particles at the bed of the channel (Hoffmans, 2014). The groundwater flow is solved with the Laplace equation. The flow in the channel is modelled by the Hagen–Poiseuille equation for parallel plates (2D). The incipient motion condition is reached when the hydraulic forces in the pipe exceed the resisting forces. Sellmeijer (1988) used White’s theory for describing erosion in the channel (Hoffmans, 2014).

In contrast to the empirical comparisons of Bligh (1910) and Lane (1935), Sellmeijer developed a more theoretical design formula. The first formulation of Sellmeijer consisted of analytical formulas describing the groundwater flow through the aquifer to the pipe in 2D with an infinite thickness of the aquifer. It was soon realized that the application was very limited, and the thickness of the aquifer was implemented. In this new approach, the pipe represents a boundary condition and the head at that boundary depends on: pipe flow and limit state equilibrium of the particles in the pipe (Sellmeijer, 2006).

The three differential equations were implemented in MSeep, a 2D numerical groundwater flow model. By performing calculations for a wide range of values for the influencing parameters (described below Figure 6, except KAS, U and RD) of soil characteristics and dike configuration, Eq.2 was derived (TAW, 1999). Therein the critical head difference (ΔH_c), the bedding angle of the sand (θ), the seepage length (L), the aquifer thickness (D), White’s constant (η), representing the exposure of a group of grains to the pipe flow, the grain size (d_{70}) and the intrinsic aquifer permeability (κ).

$$\Delta H_c = \alpha c \frac{\gamma_p}{\gamma_w} \tan(\theta) (0.68 - 0.10 \cdot \ln(c)) L \quad \text{Eq.2}$$

$$\alpha = \left(\frac{D}{L}\right)^{\left(\frac{0.28}{\left(\frac{D}{L}\right)^{2.8} - 1}\right)} \quad \text{Eq.3}$$

$$c = \eta d_{70} \left(\frac{1}{\kappa L}\right)^{1/3} \quad \text{Eq.4}$$

This equation is based on a balance between 4 forces: 1) weight of a single grain, 2) vertical seepage force, 3) horizontal drag force due to channel flow and 4) horizontal seepage force due to the horizontal seepage gradient (Sellmeijer, 2006).

Eq.2 was changed to a two-force equilibrium after new insights in 2006. It was found that the vertical and horizontal seepage force had no direct influence on the grain that will flow out to develop a pipe. This form of the equation is called the adjusted Sellmeijer rule: Eq.5 (Förster et al., 2012). Therein new, compared to Eq.2, is the relative density of the grains (RD).

$$\frac{H_c}{L} = F_{resistance} F_{scale} F_{geometry} \quad \text{Eq.5}$$

$$F_{resistance} = \frac{\gamma_p}{\gamma_w} \{ \eta \tan(\theta) \} \left(\frac{RD}{RD_m} \right)^{0.35} \quad \text{Eq.6}$$

$$F_{scale} = \frac{d_{70m}}{\sqrt[3]{\kappa L}} \left(\frac{d_{70}}{d_{70m}} \right)^{0.4} \quad \text{Eq.7}$$

$$F_{geometry} = 0.91 \cdot \left(\frac{D}{L}\right)^{\left(\frac{0.28}{\left(\frac{D}{L}\right)^{2.8} - 1}\right) + 0.04} \quad \text{Eq.8}$$

This (Eq.5) is the current standard in the Netherlands for design and assessment of dikes. The Sellmeijer formula was refined in a next step, but these refinements are not yet in use for assessment and design of dikes in the Netherlands. These refinements include: 1) multiple layered aquifer, 2) shape of the grains, 3) relative weight of a grain and 4) width of the grainsize distribution (Kramer, 2014). This refined formula can be found in Annex V .a.

The relative influence of the main parameters of the Sellmeijer equation are depicted in Figure 6. The figure shows what happens to the critical head difference when the most important parameters in Sellmeijer's formula change. The limits of the parameters for which the adjusted rule of Sellmeijer is calibrated are given below. The assumptions for the Sellmeijer model are included in Annex V .a.

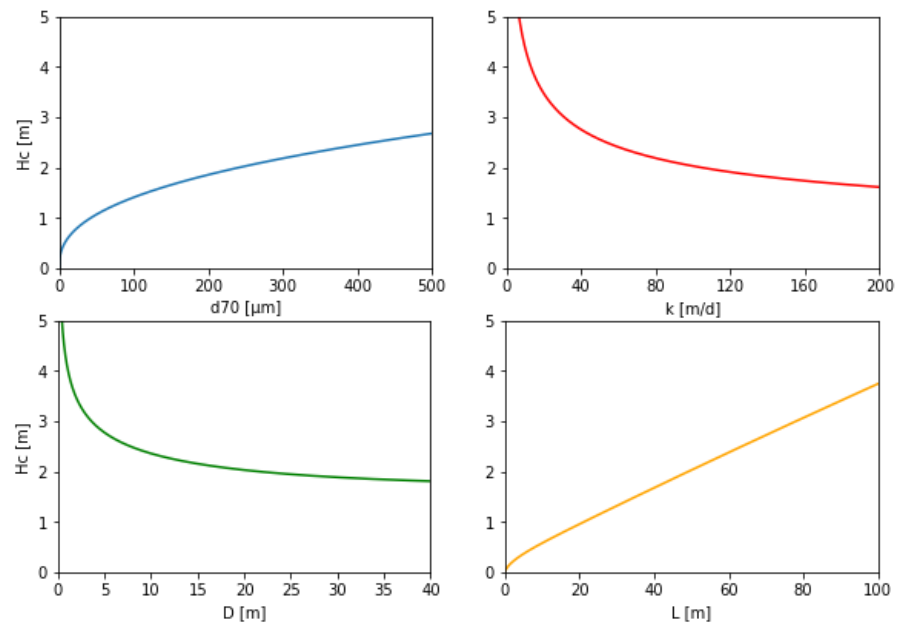


Figure 6 - Relative influence of d_{70} , permeability (k), aquifer thickness (D) and seepage length (L) to the critical head difference from Sellmeijer's equation

	Description	Mean value
L	length of seepage	d.n.a
k	hydraulic conductivity	d.n.a
d_{70}	grain diameter for which 70% of the sample (by weight) is finer (min 150 and max 430)	208 μm
D	aquifer thickness	d.n.a
η	White's constant	0.25
θ	bedding angle of sand	37°
γ'_p	submerged unit weight of particles	1650 N/m ³
γ_w	unit weight of water	1000 N/m ³
RD	packing density (also known as Relative Density) (min 0.5 and max 1)	0.725
KAS	roundness of particles 0 (round) to 100 (angular) ($\approx 40 - 60$)(min 35 and max 70)	49.80%
U	uniformity coefficient (d_{60}/d_{10}) (min 1.3 and max 2.6)	1.81

Model uncertainty

Now that the model is explained, it is important to know how well it performs. Since the approach contains a lot of calculations with Sellmeijer's model, it is good to know how reliable the model is and thus how reliable the answer is to how large the influence of tidal sand on the piping process is. The model uncertainty of Sellmeijer's model has not been determined. To be able to give some indication on the model uncertainty, a description of how the theoretical model has evolved and which steps are taken to reduce model uncertainty is given.

Three steps in particular are important to the model uncertainty: 1) The bedding angle (θ) has been determined based on expert judgement and large-scale experiments in the *Deltagoot*. 2) The model was

deemed unsafe in small-scale experiments (2D, ditch type outflow) for coarse material. A multi variate analysis (MVA) is used to adapt the influence of d_{70} in such a way that the model was more accurate for coarse grains. This adaptation was found to be tolerable in medium- and large scale (*Ijkdijk*) experiments. 3) In small-scale experiments with a ditch type outflow, no equilibrium was found (Van Beek, pers. comm.). This means that at a certain water level, the pipe started to grow and progressed directly. Sellmeijer's model assumes that a pipe is present and gives an answer to what gradient is needed to progress. This means that when the pipe has started to grow, an equilibrium is expected after which another head increase is needed to cause progression. This was not the case in these experiments and it raised questions on how reliable Sellmeijer's model is. In most piping cases, the outflow is not ditch type but hole type and this causes the flow to be 3D. Experiments were conducted with this hole type of outflow, introducing the 3D-effects. Small- and medium-scale experiments on concentration of the flow led to the conclusion that piping occurred at approximately $\frac{1}{2}$ the gradients calculated with a 2D model. This gives enormous differences and it is not known what the effect of 3D flow is on dike-scale.

3.1.2.b. Numerical model to simulate pipe progression

In 2014, Wang et al. produced a numerical model in which the erosion length can be calculated over a certain time. The assumption here is that due to the groundwater flow the small sand particles first erode, so that the porosity increases, and the soil becomes less strong. This progresses to a certain extent ($n_c \approx 0.7$) in which the small particles are transported, which has an influence on the flow (Wang, 2014). The basic assumptions and the formula are included in Annex V .c.

3.1.2.c. Shields-Darcy

Like Sellmeijer's model, the Shields-Darcy (SD) model describes the critical head difference over the flood defense by analysing: groundwater flow to the pipe, flow through the pipe and erosion criteria for the start of movement of particles in the pipe (Van Beek & Hoffmans, 2017). The subsoil is schematized with resistances against flow per layer depending on the progression of the pipe. The model approximates the flow towards the pipe in 2D in a homogeneous isotropic sand layer. The pipe consists of a semicircle and the Shields approach for laminar flow is used to indicate the initiation of erosion. The reason why the SD model is not widely used is that the flow is highly simplified and that is not what is needed in the future. It is likely that future models incorporate the subsurface and the flow more precisely. The schematization of and the basic assumptions for the Shields-Darcy model are included in Annex V .b.

3.1.3. Recent developments

In this paragraph, the recent developments in knowledge about smaller processes and parameters in piping are described.

3.1.3.a. Permeability

The permeability of the aquifer highly influences the critical head gradient. A permeable aquifer allows more water to be conveyed to the (exit of the) pipe. This leads to a lower allowable head difference over the dike, as shown in Figure 6. An indication for permeability values of different types of soil is given in Figure 7.

		Coefficient of permeability k (cm/s) (log scale)											
		10 ²	10 ¹	1.0	10 ⁻¹	10 ⁻²	10 ⁻³	10 ⁻⁴	10 ⁻⁵	10 ⁻⁶	10 ⁻⁷	10 ⁻⁸	10 ⁻⁹
Drainage		Good					Poor			Practically Impervious			
Soil types	Clean gravel	Clean sands, clean sand and gravel mixtures			Very fine sands, organic and inorganic silts, mixtures of sand silt and clay, glacial till, stratified clay deposits, etc.			“Impervious” soils, e.g., homogeneous clays below zone of weathering					
							“Impervious” soils modified by effects of vegetation and weathering						

Figure 7 - Permeability (k) values per soil type and drainage indication (Sidik et al., 2014)

The permeability is positively correlated to several other soil characteristics like, grain size, uniformity and porosity (Stoop, 2018). The separate influences on permeability are described in the sections below.

3.1.3.b. Grain size and uniformity coefficient

In 2012, Kanning showed for some historical failures that there is a dependency on the type of soil, having as a distinguishing factor mainly the grain size (Figure 8). The trend he observed was that the coarser the material, the more resistant it is to piping. The higher erosion resistance of a coarser grain is thus more important than the higher permeability that comes with coarser grains (Kanning, 2012).

In Sellmeijer’s model, the d_{70} (grain diameter for which 70 w% of the sample is finer) is used to define the grain size. This 70% value is chosen because it is assumed that for pipe development, both larger and smaller grains have to move (Sellmeijer, 1988; Van Beek, 2015). Depending on the sorting of a sample, the d_{70} can deviate from the sand median. In a well sorted sample, the d_{50} and d_{70} will be close together, in a poorly sorted sample they are further apart. The degree of sorting influences the properties of a sample: a poorly sorted sample, for example, is less permeable than a well-sorted sample with a similar d_{50} . This means that depending on the degree of sorting, samples with the same d_{70} can have different hydraulic properties (Wiersma & Hijma, 2018). Also; pre-treatment, sample size, measurement techniques and interpolation can have a major influence on the calculated d_{70} . Parameters such as the sand median or the modal grain size are less sensitive to these effects (Wiersma & Hijma, 2018).

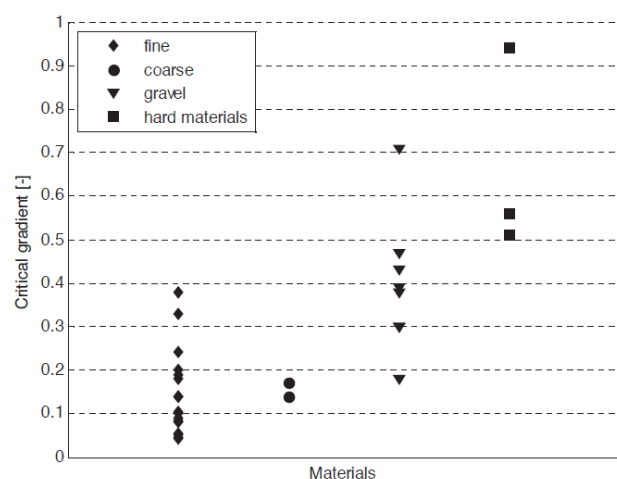


Figure 8 - Critical gradient of historical failures for different types of soil (hard material being pan) (Kanning, 2012)

In 2015, Van Beek concluded that in small and medium-scale experiments and in the *IJkdijk* experiments, grain size had a relatively minor effect on the critical gradient in uniform sands (Figure 9) (Van Beek, 2015). The grainsize does have an influence on the permeability, implicitly influencing the critical gradient.

That research also delivered the conclusion that sand samples with a large uniformity coefficient have critical gradients that are higher than those in the samples consisting of more uniform sand. Soils with a higher uniformity coefficient have a wider grain size distribution. In general, this means that there are more fine and coarse particles present than in uniform soil with a small uniformity coefficient. The critical gradient goes up because the permeability is lower when the soil is less well-sorted, which is the case when the uniformity is high.

Another consequence of poorly sorted soil is that washout of the fine materials, from the larger grain skeleton towards the outflow, may change the conditions. When water starts to flow towards the exit hole (no pipe development yet), the fines clog the pores around the exit, leading to a lower permeability. In the washed-out area, the porosity is higher, i.e. the permeability is higher. Clogging around the exit may lead to higher critical gradients and a higher permeability in the washed out area to lower critical gradients (Robbins & Van Beek, 2015).

In 2014, a report was published in the context of WBI-2017, which looked at the influence of heterogeneity on the piping process. Besides other influences, the uniformity coefficient was evaluated. Here, contrary to the tests on which the Sellmeijer model is based, 15 tests were performed with the entire grain size distribution of the sand. The critical head drops resulting from the tests were then compared with the critical head drops following from the Sellmeijer model. It follows, after correction for the fact that Sellmeijer was set up for a 2D configuration and the tests were carried out in a 3D configuration (suspected factor 2 (Van Beek, 2015)), that the measured critical head drop is on average 20% higher than calculated with the Sellmeijer model (with a range of 27% lower to 150% higher). Please note: quartz sand without lutum is used in these tests (Hijma & Oost, 2019).

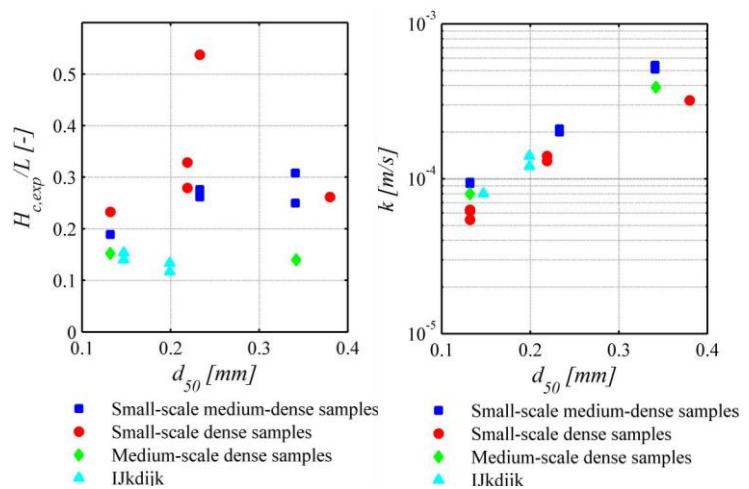


Figure 9 - Relation between grain size and the permeability for uniform sands (L) and effect of grain size on the hydraulic gradient (R) (Van Beek, 2015)

3.1.3.c. Phases in piping

In 2011, Van Beek conducted small-, medium and full-scale experiments to examine the failure mechanism piping. The observations of all the small-scale tests yielded a good description of the different phases in the piping process (phase 1: seepage, phase 2: backward erosion initiation, phase 3: backward erosion progression, phase 4: widening, phase 5: failure of the dike and phase 6: break-through (Van Beek et al., 2014).

Once there is seepage and an exit through the cover layer, the hydraulic gradient near the exit determines whether erosion will begin. The initiation of backward erosion requires the fluidization of sand near the exit point, which occurs when the seepage pressure in the sand matches the submerged weight of the sand, resulting in the expansion of the sand, which then turns into a fluid sand-water mixture. This equilibrium situation can be disturbed when the fluid flow is enough to carry soil particles outside the fluidized zone and deposit these particles in a ring outside the sand boil center and build up (Van Beek, 2015). Sand deposition often stops in the field when the ring of sand reaches a certain height. This means that the development of the pipe can cease after some time. Apparently, there is a critical value for the head drop that needs to be exceeded before the pipe can progress in the upstream direction and connect the upstream and downstream sides (Van Beek, 2015).

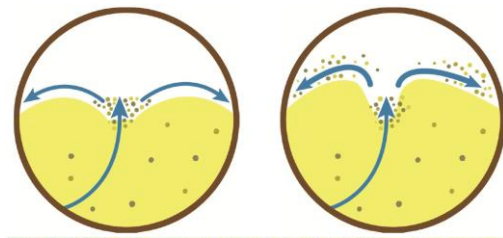


Figure 10 - Sand boil Netherlands 2011 (Van Beek, 2015)

3.1.3.d. Pipe erosion

Primary and secondary erosion criteria control the progression of the pipe. Hanses (1985) was the first to distinguish between primary and secondary erosion. The first is defined as erosion at the tip of the pipe resulting in pipe lengthening, and the latter as the erosion of the walls of the pipe resulting in pipe widening or deepening. The widening of the pipe has more effect on the flow than lengthening (Van Beek, 2015).

The Sellmeijer model only relies on secondary erosion, using a particle equilibrium based on the approach by White (1940), with a constant value for the bedding angle calibrated in large-scale experiments, whereas in the SD-model the more widely accepted (in the field of bed sediment transport) Shields approach for laminar flow is applied (Van Beek & Hoffmans, 2017). The flow being laminar (as assumed by Sellmeijer) leads to much higher critical flow velocities for start of erosion. This is caused by the absence of turbulence in laminar flow. The absence of turbulence leads to much lower lift forces on a grain.

Hydraulic regime

The hydraulic regime in the pipe depends on the relative roughness. A comparison of the critical Reynolds number and the actual Reynolds number from experiment conducted by Van Beek in 2015 proved that, in certain experiments, the flow through the pipe was laminar. At present, it is assumed that this will also be the case for pipes at other scales and other fine to medium-grained sands (Van Beek, 2015). The experiments to derive the Shields parameter were conducted in flumes with a much larger depth than the erosion channels underneath a dike, which implies that the Shields approach is much more applicable in turbulent flow. In turbulent flow, the grains are loosened by viscous drag- and lift forces that fluctuate due to the turbulence. In laminar flow the grains are subjected to a steadier flow and are loosened in an instant and not because of large fluctuations in the flow.

Shear stress

The erosion of particles under the action of horizontal flow is governed by the shear stress exerted by the water. Once this shear stress has exceeded a critical value – the critical shear stress (τ_c) – particles are transported. Although a lot of research has been conducted on this topic and how to incorporate it in the erosion model for piping, the uncertainties are large. The grains have different sizes, shapes and orientations, which all influence the start of motion. Especially in non-uniform sands the critical shear stress is hard to define, even in laminar flow.

White

In Sellmeijer’s formula (Eq.6), the resistance factor almost equals the critical shear stress defined by White in 1940 (Eq.9 and Eq.18).

$$\tau_c = \eta \frac{\pi}{6} \gamma'_p d \tan(\theta) \quad \text{Eq.9}$$

In which θ is the bedding angle, which was used as a calibration parameter in the Delta Flume experiments (Van Beek, 2015). The packing coefficient η was set at a safe value of 0.25 based on the $\alpha\eta$ values derived from the experiments by Sellmeijer in 1988. The cohesion in tidal sands might influence the critical shear stress in Sellmeijer’s formula. The forces involved in the resistance factor are: 1) gravitational force, 2) drag force and 3) horizontal seepage force.

Table 1 - Gravitational and drag force in the Sellmeijer formula

$F_g = \gamma'_p \frac{\pi}{6} d^3$	In which d is the mean grain size and γ'_p is the specific weight of the submerged particles.
$F_d = \tau_w \cdot \frac{d^2}{\eta}$	With White’s constant $\eta = \frac{nd^2}{A}$, in which n is the number of particles, d is the mean grainsize and A represents the unit area (Van Beek, 2015; White, 1940).

The lift forces on the grains by inflowing water from the boundaries of the pipe is neglected in this approach because Martin (1970) found that the vertical seepage gradient disappears when the grain is lifted (Van Beek, 2015).

Grouping

In 2011, Zee found that particles erode from the pipe like slurry flow, by hundreds at the same time. The grains are dislodged from the granular matrix by the pressure difference and are pushed through the channel (Zee, 2011). Van Beek (2014) assumed that the heave of a group of particles initiates the backward erosion process (Van Beek et al., 2014).

3.1.3.e. Pipe dimensions

At laboratory scale, Van Beek et al. (2008, 2011) demonstrated that, at the beginning of the erosion process, the pipe formation is similar to that of braided rivers (Figure 12). It was shown that the pipe meanders through the soil. In Annex II, photos of the experiments after pipe growth are included. Van Beek (2015) deduced a relation between the width and the depth of the pipe. The width to average depth ratio of sand with a d_{50} of 0.38 mm is 11-13 and for a d_{50} of 0.13 mm 7-8. The average depth is used because the depth of the pipe varies fast and often is sine-shaped. The depth, researched by Vandenboer (2017), is a few grain diameters in small-scale experiments. The maximum depth that was found in this experiment, where the seepage length (L) was 0.3 m, was 1 mm. Sand transported through such a shallow pipe can easily clog the pipe, after which pressure builds up until a group of grains is pushed out (Van Beek, 2015; Vandenboer et al., 2017).

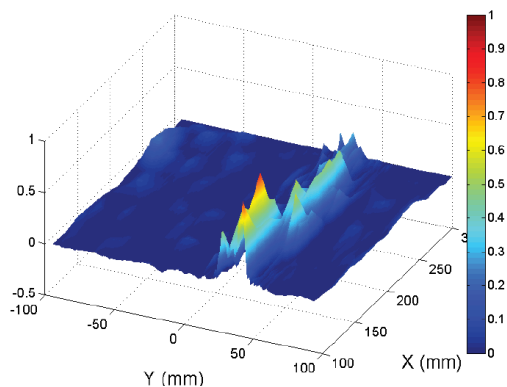


Figure 11 - Indication of pipe depth (in mm) over distance (Vandenboer et al., 2017)

It is known that when the pipe starts to deepen and widen (secondary erosion, see also 3.1.3.d), the flow capacity increases with a chance of large sand boils. Description of the enormous sand boil at a dike failure by piping in the Netherlands at Zalk in 1926 (Van Dam & Beijersbergen, 1981) (translated from Dutch): “When we turned around, we saw a man-sized fountain of mud where the boil had been. It soon became clear that no steps would avail and so the fire bell was sounded in all haste and bicycle relays were dispatched to warn the populace in the hinterland.”

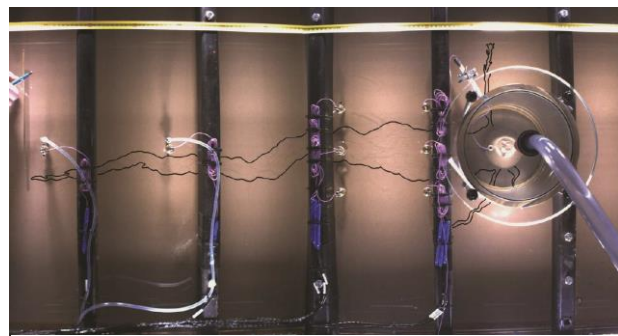


Figure 12 - Example of pipe formation in the medium scale experiments by Van Beek in 2015 (Van Beek, 2015)

3.1.3.f. Spatial variability of the subsoil

The subsoil parameters and layer dimensions vary in space, these variations have an influence on the uncertainties that affect the piping mechanism. These uncertainties can be divided in two groups: 1) inherent uncertainties, that stem from natural variability of the subsoil and 2) modelling uncertainties, that stem from the translation of reality into a model. Both these uncertainties contribute to measured variability (Kanning, 2012). Most of the uncertainties in structural performance with respect to piping are the permeability (k), the grain size (d_{70}) and the presence of old riverbeds and tidal deposits, which are often highly anisotropic. Since the focus of this research is on tidal deposits and the modelling of them, the focus in uncertainty lies on inherent uncertainties in space and modelling uncertainties in D-Geo Flow (Figure 13). Tidal deposits have much more spatial variation in layering compared to fluvial deposits (see also 3.2.3).

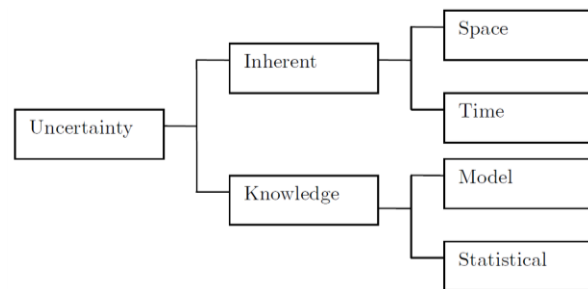


Figure 13 - Classification of uncertainties (Kanning, 2012)

The subsoil parameters influence the outcome of the critical head a lot. With modern methods to gain knowledge about the subsoil, an estimation of these parameters in 2D is made in practice, to assess the possibilities of the occurrence of piping. Sampling intervals are often not sufficiently small to get a good view of the horizontal variability in permeability, grain size and layering of the subsoil. Kanning (2012) found that due to rapid fluctuation of soil uncertainties in space, the probability of piping failure increases with the length of the dike as a weak spot might be encountered, the so-called length-effect (Kanning, 2012) (Figure 14).

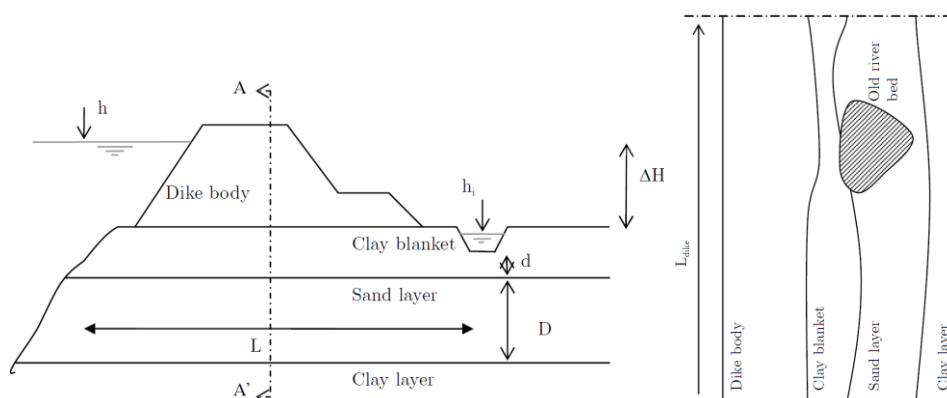


Figure 14 - Typical cross-section of a dike in length direction (Kanning, 2012)

Van Beek et al. (2012), concluded that schematizing the subsurface with one homogeneous layer does not result in an optimized prediction, but may serve as a first approximation if the value of certain parameters is conservatively chosen (Van Beek et al., 2018). These differences within layers and from layer to layer in the subsoil are often referred to as anisotropy and heterogeneity respectively (Figure 15).

Heterogeneity

In this thesis, heterogeneity describes variations of physical properties between two or more elements or layers (Ikelle & Amundsen, 2018). Hence, a heterogeneous subsoil consists of at least two elements or layers with different physical properties (Stoop, 2018) (Figure 15).

The most important parameters that influence the degree of heterogeneity are permeability and grain size. The grain size typically varies between the layers and these (often) sudden changes form a barrier to the flow, thereby influencing the permeability (Huysmans et al., 2008). Besides the differences in permeability, also the differences in consistency of the layers make it harder to form a continuous path or cause the path to be longer, thereby increasing the resistance against piping. Layers are formed on different scales:

- micro (millimeters to centimeters);
- meso (decimeters up to 10 meters);
- macro (tens of meters to hundreds of meters);
- meta (tens of kilometers).

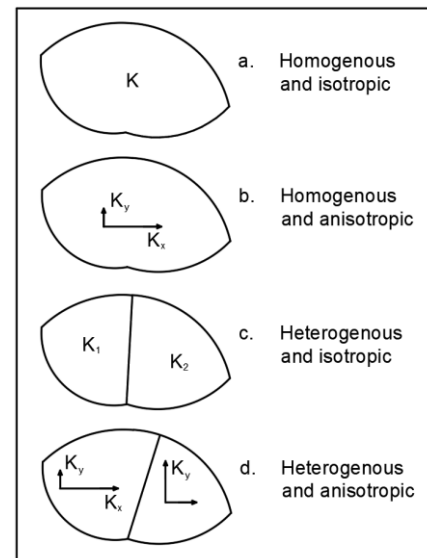


Figure 15 - An illustration of heterogeneity and anisotropy

Van Beek et al. (2018) conducted research on the influence of micro-scale laminae on the piping process and found that for laminae with a thickness of 2 cm, with varying permeability, the increase in strength was 20-80% (Van Beek et al., 2018). In 2018, Stoop conducted research on heterogeneity and piping in his master thesis. He found that isotropic heterogeneity on dike scale (macro scale) leads to an increase in critical head difference of 5%.

Anisotropy

A material, element or body is anisotropic when the physical properties are directional dependent, which implies different physical properties with direction (Figure 15). The physical properties should therefore differ with direction at a given point (note that a point can represent a particle, element or body) (Ikelle & Amundsen, 2018). The parameters that have the highest directional dependency are permeability and grain size. If the permeability is the same in all directions, the soil is called isotropic. However, a lot of soils have different permeabilities in vertical and horizontal direction. In most cases, the vertical permeability (k_y) is smaller than the horizontal permeability (k_x). These soils are called anisotropic. The differences in vertical and horizontal permeability are due to different causes: 1) conditions during deposition and 2) biological activities (digging by animals and iron oxidation).

In 2018, Stoop conducted research on anisotropy in his master thesis. He found that the varying of the vertical and horizontal hydraulic conductivity leads to an increase in critical hydraulic head of 12-18%. In 2018, Van Asselen et al. did research on anisotropy and found that for $k_x=3*k_y$, the critical gradient was 22% higher and for $k_x=5*k_y$ it was 34% higher. In that report, an indication of vertical and horizontal permeability is given for a wide range of soil types (Van Asselen et al., 2018). The point measurements of the permeability in a certain type of soil need to be scaled to the right scale that is used in the modeling of groundwater flow. This means blocks with a certain permeability, depending on a length-scale and different point measurements, are implemented in the groundwater flow model.

The ranges of the anisotropy ratios ($A = k_x/k_y$) that were found by Bierkens in 1994 are (Van Asselen et al., 2018): 1) fluvial moderately coarse to coarse sand: 1.07, 2) aeolian moderately coarse to coarse sand: 1.03, 3) fine (loamy) sand: 3.71, 4) sandy and silky clay: 10.4. The expected anisotropy ratio for tidal deposits and mudflats is 3.5 in a bandwidth of 1-6.

SOS

In the Netherlands, the Wettelijk Beoordelingsinstrumentarium (WBI, a dike assessment instrument) is used for evaluating whether primary flood defenses meet the required standards. A part of the WBI is the Stochastic Subsoil Schematization (Stochastische Ondergrond Schematisatie, SOS). WBI-SOS provides information about the global (schematic) construction of the subsurface under a dike based on scenarios, each with a certain chance of finding. The scenarios consist of stacked subsurface units (SOS-units), each describing a certain type of deposit. To these units, basic parameters can be assigned, after which an estimate can be made of the failure risks of the dike. Along with insight into failure mechanisms, SOS can lead to responsible local schematization of the subsurface (Hijma & Lam, 2015). In Figure 17, an indication is given of the chance of finding tidal deposits in the first 5 m of subsoil in the Netherlands (Hijma & Oost, 2019).

3.1.3.g. 3D-effects

Piping is a three-dimensional process, which should be considered when analysing the mechanism. Usually, only the cross section is evaluated, while the variabilities in length direction of the dike can be quite large (Figure 14). These uncertainties are normally considered by selecting a representative cross section but it is suspected that the flow pattern is 3D, which causes the 2D models to be inaccurate.

When the cover layer is lifted and cracked, the water starts to flow through the cracks, to the exit hole. When the permeability of the cover layer is lower than the permeability of the sand (which is normally the case) there will be concentration of the flowlines near the exit point, leading to local higher water flow velocities and therefore making backward erosion piping more likely (Van Beek, 2015). This concentration of the flowlines is a 3D process (Figure 16).

Vandenboer et al. (2014) and Van Beek et al. (2015) conducted research on the 3D-effect and found that the deviation (in critical head difference) between 2D and 3D is approximately a factor of 2 for both small- and medium-scale experiments with fine uniform sands, indicating that the Sellmeijer model over-predicts the critical gradient in a 3D configuration. They found that the critical hydraulic head is strongly depending on the width of the model. This suggests that the Sellmeijer model is not yet suitable for 3D situations. Van Beek finally concluded that certain parameters or processes, which are currently not taken into account, have a major impact because some strange outliers were found (Van Beek, 2015; Van Beek & Hoffmans, 2017; Vandenboer et al., 2014).

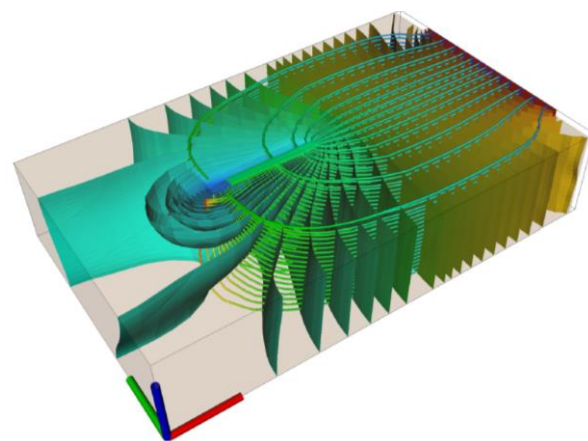


Figure 16 - Simulated 3D seepage patterns in piping experiments (Negrinelli et al., 2016)

The scale experiments are conducted in a small box with an outflow on the top. This is a 3D situation and the flowlines will converge to the outflow, also from the sides. The main influence on the amount of 3D-effect is the ability of the water to flow elsewhere than the outflow. It is expected that, in reality, less water is attracted by the outflow because it can flow to the sides and to the polder. Also ditches parallel to the dike relieve some pressure because water flows upward through the thin cover (depending on the thickness and permeability). This leads to less 3D-effect than observed in experiments where the water can only flow from the aquifer through the exit hole.

Since the model that is used in this thesis is a 2D model (D-Geo Flow), the findings on the differences between a 2D and a 3D situation, especially for these different types of sand, are evaluated by a comparison with experiments on fluvial sand and the gained knowledge from literature.

3.1.3.h. Foreshore

In 2018, Knops conducted a case study on the influence of the foreshore (Dutch: *voorland*) on piping. He performed calculations in D-Geo Flow for ranges of the involved parameters. The goal was to see if the seepage length could be increased when the cover layer of clay on the foreshore gives enough resistance against flow. The conclusion of this research was that the uncertainty of holes being present on the foreshore, i.e. the water is in direct contact with the aquifer, is in most cases too high and must be assessed closely (Knops, 2018). This also suggests that lifting and cracking of the cover layer will most likely occur at these holes. These holes or weak spots being often present suggests that the criterium that lifting of the cover layer must have occurred before initiation can take place, is overrated.

3.2. Tidal sands

Tidal deposits are characterized by the frequent occurrence of clay layers that will influence piping sensitivity (MIM, 2017). In this part of the literature study: 1) Dutch subsoil 2) field observations on piping in tidal sands 3) origin of tidal deposits, 4) consistency of tidal deposits, 5) strength in tidal deposits and 6) lab experiments on similar subjects are evaluated.

3.2.1. Dutch subsoil

Flood defenses in the Netherlands are present near the coast, rivers and lakes. The subsoils in these areas are different due to their different depositional history. To make a distinction between the different areas in the Netherlands, a classification can be made based on the geology, here meaning the type of sediments in the upper 5-20 m. Figure 17 show division of the Netherlands in areas with different geology.

Fluvial deposits

This deposition type consists of clay and sand and is deposited by the rivers *Rijn*, *Maas* and their tributaries during the Holocene. In the fluvial sediment district, the top aquifer consists of sandy sediment. Locally also deposits of peat and loam can be present but in general it can be assumed that the top aquifer consist of Pleistocene coarse sand (Knops, 2018; Veer, 2006). In the *Maasvallei*, the subsoil mainly consists of sand, coarsening downwards, also containing gravel. The sandy *Rijnland* subsoil is governed by fine to medium sand deposits with (locally) thin layers of clay (Veer, 2006).

Tidal deposits

The tidal sediment material consists of deposits formed in the tidal basin. The deposits often contain shell fragments and their texture ranges mainly from fine sand to heavy clay (Veer, 2006). Within the tidal *Naaldwijk* formation (situated along the entire coast of the Netherlands), various members are discerned. The *Wormer* member generally shows a fining upward sequence from fine sand to heavy clay. Especially in the Southwestern parts of the Netherlands, this layer is covered by the younger *Walcheren* member, which consists of fine sand and sandy to silty clay. In the West of the Netherlands, the tidal deposits often overly the peat of the *Nieuwkoop* formation as well as fluvial deposits of the *Rijn* and *Maas* (*Echteld* formation). Large areas in the tidal district (blue in Figure 17) consist either of lakes or coastal areas that were reclaimed, thereby uncovering the underlying tidal deposits of the *Wormer* member (Veer, 2006). The *Hedwigepolder* is situated in area where tidal deposits are present, consisting of



Figure 17 - Locations where tidal deposits (blue) are found underneath the cover layer (top sand layer) in the Netherlands (Van Asselen et al., 2018)

tidal sand (silty, with clay lenses) sandwiched in between tidal-clay units. In Annex VII, the probability of finding tidal sand in Dutch subsoil is visualized on a map.

3.2.2. Field observations

A finding that underlines the additional piping resistance in tidal sand, compared to fluvial sand is the amount of observed sand boils. Very few sand boils are known in the West of the Netherlands. This can have several reasons but since tidal deposits are present in the West, it is likely that it has an influence. Figure 18 gives an overview of the well-known sand boils in the west of the Netherlands. No cases are known from the northern part of Netherlands, apart from some rising water in ditches. A few cases are known from *Zeeland* and the *Hoeksche Waard* that are not yet in the online database (Hijma & Oost, 2019). The relative amount of sand boils in areas with tidal deposits in the first 5 m of subsoil is a lot lower than the relative amount of sand boils in areas with fluvial subsoil (Figure 5).

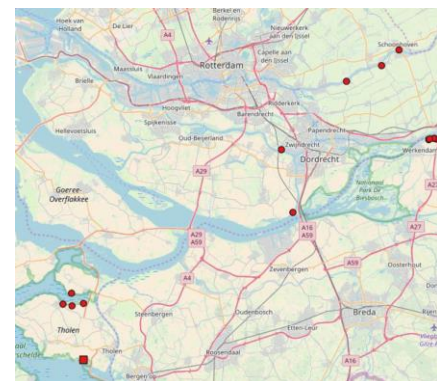


Figure 18 - Field observations of sand boils in areas with tidal deposits in the Netherlands (12 sand boils, red dots and one breach, red square) (Hijma & Oost, 2019)

3.2.3. Origin of tidal deposits

Offshore, currents generated by the tides interact with an array of processes, including waves, storm/wind-generated currents and geostrophic currents that are part of the global-ocean circulation, giving the potential for the creation of a variety of sedimentary deposits closer to shore (Reynaud & Dalrymple, 2012). These tidal deposits are formed in areas where sedimentation is dominated by tidal action and where the influence of wave action on the composition of the deposit is limited. Estuaries with low wave action are sensitive to the occurrence of tidal deposits.

Tidal areas are characterized by a regular alternation of periods of more and less flow and supply of sediment. In intertidal areas, this leads to periodic drying out and a regular variation in the intensity of wave action. The flow velocity decreases sharply around slack water and the finer particles from the water column are deposited (MIM, 2017). The size and consistency of the forms are strongly depending on flow velocity and wave action (Figure 19). From this, a separation can be made on location in the tidal area. These locations are also used in the SOS (3.1.3.f) and a distinction is made between channel deposits and tidal flats.

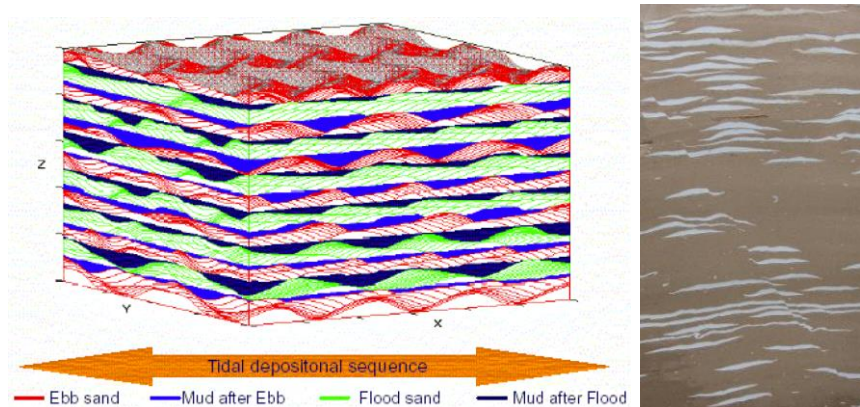


Figure 19 - Indication on the formation of a sandy clay tidal deposit (MIM, 2017)

Both the tidal and wave energy and thus the grain sizes decrease in inland direction in the coastal area. This implies that the mud and clay content increase in landward direction. This is due to the fact that sediment in motion can be categorized by the way that they are transported: 1) fine-grained sediments (<160 μm) that will be transported almost completely suspended, 2) soil load population, the grains of which are partly transported rolling over the soil and are only transported floating at higher speeds (>0.4 m/s) and 3) the coarse sand which is only transported at high flow velocities in the channel close to the sea (Hijma & Oost, 2019).

3.2.4. Consistency

Tidal deposits consist of closely spaced sand, silt and clay with a small percentage of organic material (see Figure 20c). Usually this organic material consists of benthic biological communities and shows a lot of variety in both biological as well as chemical composition. Natural sandy deposits often consist of a sand matrix with fines in between. This corresponds with Figure 20b, containing less than 35% of fines. Tidal deposits can roughly be divided in 3 categories based on grain size and matrix. Sand (>90% sand), mixed sand and mud (50-90% sand) and mud (15-50% sand). Tidal deposits are a mix of sand and mud, the small-scale experiments are drawn in the lutum, silt, sand triangle in Figure 21. They are situated at the turning point between sand and a mix of sand and mud.

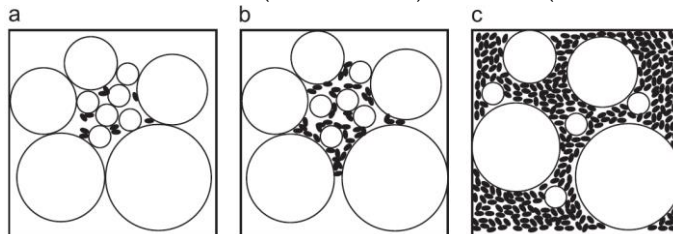


Figure 20 - Classification of gap-graded soils: (a) with fines contents less than 10%; (b) with fines contents between 10% and 35%; (c) with fines contents more than 35% (Chang & Zhang, 2013)

In this paragraph, the consistency of the tidal sand is evaluated in 1) grain size, 2) permeability, 3) biological content, 4) the influence of the location in the estuary and 5) chemical composition.

3.2.4.a. Grainsize

The main cause of the difference in grain size between fluvial and tidal deposits is the flow velocity at which the sediment is deposited. At the turning of the tide, the flow velocities are lower than the flow velocities at which sand layers in a river are formed. At the lower flow velocities, the fine particles can settle more easily. This variation in flow velocity creates a layered pattern of different grainsizes.

When looking at piping, the coarser grains are less easily removed at the bottom of the pipe due to their weight. Finer sands have a lower resistance, such that they are more easily removed from the bed, although they are sheltered behind the larger grains. Also, finer particles often have a different chemical nature and different tendency to clog. The grainsize and grainsize distribution are thus very important in the piping process. For the *Naaldwijk* formation, member *Walcheren*, (often recalled as tidal sediment) the fines percentages, grain diameter (d_{70}) and uniformity are determined (Table 2) to give an indication of what is meant when tidal sand is mentioned. A disadvantage of Sellmeijer's rule is that it is calibrated on a minimum d_{70} of 150 μm , lower values are found in tidal sands.

Table 2 - Grain size distribution of the *Naaldwijk* formation (member *Walcheren*) (Hijma, pers. comm.)

	Tidal flat sand				Tidal channel sand			
	Mean	Min.	Max.	Standard dev.	Mean	Min.	Max.	Standard dev.
w% fines <63 μm [%]	25.9	8.8	42.4	11.6	7.2	1.4	24.1	5.2
w% fines <16 μm [%]	7.2	3.9	9.8	1.9	3.2	0.9	10	2.1
w% fines <2 μm [%]	2.4	1.5	3.1	0.5	1.2	0.5	3.3	0.6
d_{70} [μm]	128	105	162	22	208	126	526	101
U [-]	1.6	1.4	1.7	0.1	1.7	1.6	2.8	0.3

Not all combinations of grainsizes (lutum, silt and sand; in different w%) can be formed naturally. Figure 21 shows the possible mixing ratios. These ratios give an indication of the total soil type. The mixing ratios which are used in the small-scale experiment are placed in this diagram (x's). In this document, by fine fraction, the mass fraction with a diameter <63 μm is meant. This is the smallest sieve diameter in the Dutch sieve classification by NEN2560 (Wiersma & Hijma, 2018). Friend (2001) used the rule of thumb that when sediments contain more than 5-10% lutum by weight, cohesion (due to the presence of clay minerals) becomes significant (Friend, 2001).

For the tidal deposits, it can be clearly seen in Figure 21 that, the percentage of the fine fraction is a lot higher (orange line) than in the fluvial sands. This means that in general the porosity (n) is lower, the permeability (k) is lower and the uniformity coefficient (U) is higher.

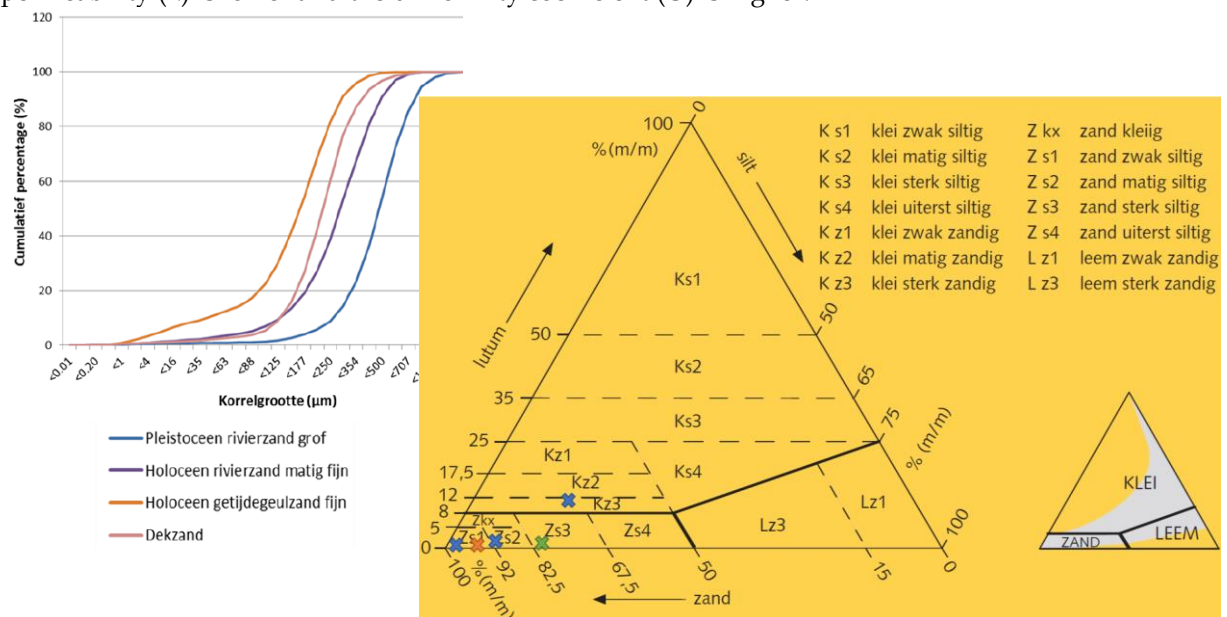


Figure 21 – In the left figure: cumulative sieve analysis of the typical Dutch formations, the orange line is tidal channel sand and the other lines are fluvial sand (blue and purple) and cover sand (pink). In the right figure: NEN5104 clay (lutum) -silt-sand triangle; in which the grey part in the small triangle can be found in the Netherlands. The top blue x is the unsieved material of F213 from Friesland, the two other blue x’s are Baskarp with Kaolinite, the orange x is the material from the Grevelingen and the green x is the sieved material of F214 and F215 from Friesland (R) (Wiersma & Hijma, 2018)

3.2.4.b. Biological content

There is no natural sediment deposit that is not inhabited by biota. Even sediments more than 500 m beneath the ocean floor support a biota of bacteria (Black et al., 2002). The biggest challenge in understanding and quantifying the influence of these biota is the activity, causing variability in effects both in time and space.

By the time grain fragments, carried downstream by the river, come into contact with an estuarine environment, they are physically associated with organic matter as well as suspended bacteria (Black et al., 2002). Van Leussen (1988) notes that virtually all sediments in estuaries have a surface coating existing of organic material and metal hydroxides. Once deposited, the sediments form a combination of biologically active and chemically reactive material (Black et al., 2002; El Ganaoui et al., 2004). This material consists of several types of algae, brush worms, crustaceans, shells, sand, clay and chemical and biological compounds. The more precise consistency of the most important groups and what effects they have on soil strength is described in 3.2.5.

3.2.4.c. Location in the tidal basin

As mentioned before, a large difference in sediment consistency in the tidal basin can be made between the tidal channels and tidal flats due the difference in sedimentational environment.

Tidal channel deposits

The semi-diurnal rise and fall of the water level creates the so-called intertidal zone that is exposed during low water and submerged during high water. In the absence of high waves (tide dominated or sheltered in a basin), wide and low gradient tidal flats develop with channels transporting the tidal prism (Bosboom & Stive, 2015). As described, the channel velocities are relatively high due to their relatively small size compared to the tidal flats. The higher velocities cause the grains in the channel to be relatively coarse with the coarsest grains in the deepest parts of the channel. The types of channel

deposits are described from coarse to fine. Hijma, Lam and Oost studied tidal deposits. A lot of information in this paragraph is retrieved from their work (Hijma & Lam, 2015; Hijma & Oost, 2019).

Moderately fine to very coarse tidal channel sand

In a quick scan by Hijma (2019), the following SOS-units are linked to this type of deposit:

SOS-code	Formation	Consistency
H_Mg_zm /P_Mg_zm	Naaldwijk/Eem	Sand, fine and medium, clayey, with mm-cm thin and narrow clay/silt layers, fluctuating occurrence of the small clayey layers.



Figure 22 - Drilling H_Mg_zm, 1 m long

In general, the clay/silt layers of the larger channels will be thin (mm to cm, Figure 22). These small layers are formed during slack water. Due to the many ridges and internal erosion planes (due to turbulence and high flow velocities), the lateral continuity of these thin sludge layers on the bottom will generally be limited. The thicker sludge layers are formed due to two causes: 1) amalgamation of the successive sludge deposits in those places where sand cannot settle during tides. The thickness of such sludge layers is usually up to a few dm and they can laterally be present over distances of tens of meters. And 2) Inside bend deposits where the conditions are so calm that sand deposits only during periods of higher dynamics. The inner bend deposits often form an inclined surface. Unfortunately, these inside bend deposits have not been studied extensively so that there is little information about their lateral extent and continuity, but closed packages over a few hundred meters occur with thicknesses up to about 2 meters.

Extremely fine to moderately fine tidal channel sand

In a quick scan by Hijma (2019), the following SOS-unit is linked to this type of deposit:

SOS-code	Formation	Consistency
H_Mg_zf	Naaldwijk	Tidal channel sand, fine, clayey, mm-cm thin and narrow clay/silt layers, fluctuating occurrence of the small clayey layers.



Figure 23 - Drilling H_Mg_zf, 1 m long

The extremely fine to moderately fine tidal channel sand is characteristic for the sediments deposited in places where the flow velocities are relatively lower than in the previous group. In general, maximum flow rates from a few dm/s to around 60 cm/s should be considered. This mainly concerns small tidal channels. Due to the lower flow rates, the clay content is often somewhat larger (Figure 23). Because erosion is somewhat less strong, packages of thin sludge layers (each mm-cm) can form. Just like the larger channels, these deposits also have inner bend deposits that can consist of 0.5-2 m thick sub-layers of more silt-rich sediment, interspersed with sand layers. The lateral extent of the deposits will often be less than 30 m.

Extremely fine to moderately fine tidal channel sand with thin clay and silt layers

In a quick scan by Hijma (2019), the following SOS-units are linked to this type of deposit:

SOS-code	Formation	Consistency
H_Mg_zk / P_Mg_zk	Naaldwijk/Eem	Tidal channel sand, fine, clayey, mm-cm and thin, narrow clay/silt layers, large variation in occurrence of clayey layers and less clean pieces of sand.

The extremely fine to moderately fine tidal channel sand with thin clay and silt layers is characteristic of the sediments deposited in those places where the flow velocities are relatively slightly lower than in the previous group. In general, maximum flow rates of a few dm/s to around 40 cm/s should be considered. This mainly concerns small to very small tidal channels. Due to the lower flow rates, the clay content is relatively large in these deposits. They are located in the gullies far from the trench where the sludge content in the water is high. Just like the larger channels, these deposits also have inner bend

deposits which can deposit 0.5-2 m thick sub-layers of more silt-rich sediment that consist of cm-dm thick layers. The lateral extent of these deposits is often less than 30 m.

Moderately fine to very coarse estuary tidal channel sand

In a quick scan by Hijma (2019), the following SOS-unit is linked to this type of deposit:

SOS-code	Formation	Consistency
H_Eg_zm	Naalddwijk	Similar to Mg_zm but formed in an estuary. Particularly present in the Rotterdam area. Consists of alternating sand and clay layers.

Estuaries such as the *Eems* and the *Westerschelde* are characterized by large channels where flood and ebb flow, flow through different channels. As a result, often the flood or ebb is dominant in a trench. As a result, a thicker layer of sand will deposit during the dominant tide and a thinner layer during the opposite tide. During the changes, sludge deposits in a mm to cm thick layer. These "drapes" can often laterally extend to meters. Because there is a daily inequality of the tide, two layers of sand are always formed during the successive dominant tides, one of which is thicker than the other. A schematization of the formation of double mud drapes is given in Figure 24. Due to the many differences in tidal strength, the thin clay/silt layers are easily affected by erosion. Either because the sludge is eroded by the following tide, either by shifting the orientation of bottom shapes, or by new bottom shapes that affect older ones. In general, these deposits are of limited lateral continuity over distances of tens of meters (Hijma & Oost, 2019).

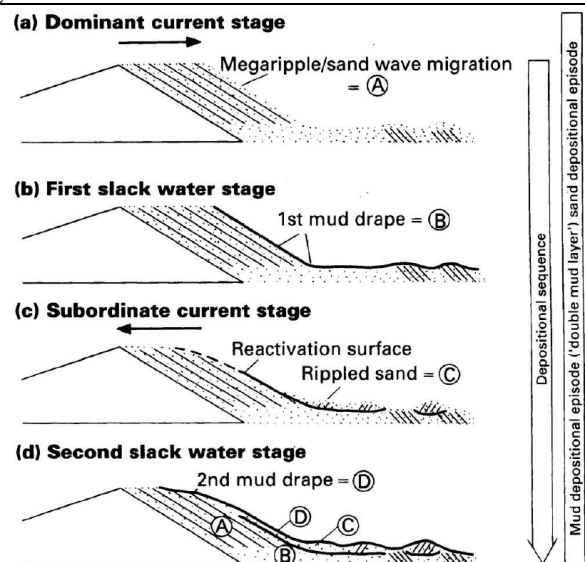


Figure 24 - Formation of double mud drapes in case of a dominant tide (Hijma & Oost, 2019)

Extremely fine to moderately fine estuarine tidal channel sand

In a quick scan by Hijma (2019), the following SOS-unit is linked to this type of deposit:

SOS-code	Formation	Consistency
H_Eg_k&z	Naalddwijk	This unit also mainly occurs around <i>Rotterdam</i> . Consists of thicker, up to 20 m thick, packages with alternating layers of sand and clay. The layers itself are mm-dm thick.

In the estuaries, certainly near the *Rijn* and *Maas* river mouths, there is always a lot of sludge and organic material present in the water. In quieter places in estuarine channels, these can settle, together with extremely fine to moderate estuarine tidal channel sand. Sand and sludge both settle easily, indicating fluctuations in flow speed, with peak velocities being relatively low. This often involves secondary channels that often have a very low discharge. Therefore, finer material and organic material can settle. This fine material is often present in thin layers, sometimes as laminae. Bioturbation by organisms can completely disrupt and fine-tune this finely layered structure, leaving a homogenous sludge-sand mixture. Thereby clay layers of cm to 0.5 m can be formed. Local organic material can also settle. Vertically, large variations occur in the amount of clay layers and layers of clay within 1-2 m and over distances of 2-20 m. In the *Rotterdam* area there are packages of 15-20 m thick that consist entirely of these kinds of layered deposits.

Intertidal flats

The tides fill and empty a basin via channels that cut through lower and higher sand and mud flats. These intertidal flats (Dutch: *wadplaten* or *slikken*) fall dry at low water and are submerged at high water. In between channels and the intertidal flats lies a part of the flats that is exposed very infrequently (at very low water levels), called the subtidal zone. Only the higher, most landward, parts stay dry at high

water; these vegetated parts are supra-tidal flats or salt marshes (Dutch: *kwelders*) (Bosboom & Stive, 2015).

In a quick scan by Hijma (2019), the following SOS-unit is linked to this type of deposit; being sandy tidal flat deposits:

SOS-code	Formation	Consistency
H_Mp_zf	<i>Naaldwijk</i>	Sand, fine with a few thin clay/silt layers, can consist of relatively clean sand.

The types of flats that form in the inter- and subtidal areas based on their location are: 1) subtidal flats, 2) low intertidal flats, 3) high intertidal flats and 4) salt marshes.

Subtidal flats

The subtidal flats mainly consist of filled up abandoned gullies that fill up to a subtidal flat. The filling is usually built of layers with a thickness of one dm to one meter per year. This is often sludge in the summer half year and sandy deposits in the winter half year. Bioturbation occurs but is often not predominant. Due to the build-up of sludge and sand layers that are relatively horizontal, such a channel filling doesn't have many thick sand layers of more than one meter (Hijma & Oost, 2019).

Low intertidal flats

The moment the tidal water enters the banks of the channels, the flow velocities decrease rapidly. The coarser grains are mainly deposited directly near the channels, where they form banks. During the ebb phase, the highest velocities occur around the time that the tidal plates almost fall dry. The waves reach to the bottom and stir the sediment.

Prielen (Figure 25) are intertidal trenches that drain the plates and where velocities up to more than 1 m/s can occur. During meandering, these *prielen* form inner bend deposits that consist of alternating sand and sludge layers.



Figure 25 - Priel in the Dollard, Netherlands (Kwant, 2015) and low intertidal flat sediment structure (Hijma & Oost, 2019)

The lower flats are, due to the flow and wave action in lower water, mainly characterized by physical structures such as ridges. Sand and sludge behave hydrodynamically in such a way that they are deposited as separate layers. The space in between the ridges is, depending on the velocities and sludge concentrations, filled with sand or sludge.

High intertidal flats

As the flats are higher and more sheltered, organisms will dominate. Through their digging and feeding movements, they ensure that the sediment is completely mixed: sludge and sand are mixed in this way (Figure 26). If the sludge content does not exceed 15 w%, it can be expected that the sludge will be in the pores between the sand grains. This reduces the permeability of the sand. Above 15 w%, the sludge starts to take up so much volume that the grains of sand touch each other less and less and they increasingly "float" in a matrix of sludge (Hijma & Oost, 2019).

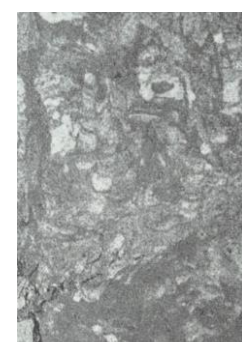
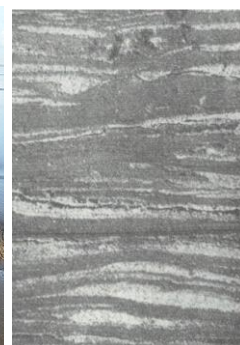


Figure 26 - High intertidal sediment structure with bio-turbation (Hijma & Oost, 2019)

Salt marshes

The vegetation on salt marshes often starts with *Salicornia* (Dutch: *Zeekraal*) that can already live on a few dm under MSL (means sea level). The plants influence the flow patterns and promote slurring. As the salt marsh gets higher, other pioneer plants will dominate the vegetation. Due to their arranging effect, preferential channels are created on the salt marsh. Practically no animals live above mean high water: for saltwater species it is not covered frequently enough; for freshwater species too often. As a result, the layering of the sediments is hardly or not at all disrupted by animals. Disruption does occur due to plant roots in the soil. However, this is a much smaller effect than caused by bottom animals on the mud flats. The interfaces in the sediment of the salt marshes are very irregular. This is not only due to the plant roots but also due to the irregularity of the thickness because the sediment is deposited on an uneven, always drying surface and is bound to the space between the plant stems (De Groot & van Straaten, 1964; Hijma & Oost, 2019). Because sedimentation occurs during floods, the mm to cm thick layers will usually each decrease in grain size upwards: from sandy to clayey. As a result, a fairly impenetrable package of sediments forms that are non-piping sensitive (part of the SOS-units which are deemed non-piping sensitive, Kruse et al., 2015) (Hijma & Oost, 2019). An important notion regarding piping sensitivity is that from time to time extreme storm tides can deposit very thick layers of sand (up to approx. 1 m thick and 1 km inland). This increases the sensitivity to piping strongly.

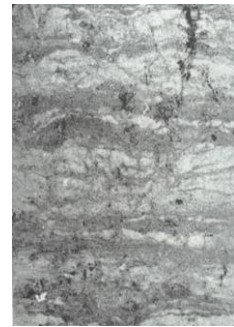


Figure 27 - Salt marsh sediment structure (Hijma & Oost, 2019)

3.2.4.d. Permeability

The difference in composition compared to fluvial sand is causing a difference in permeability. This has multiple reasons: presence of more fine material, sedimentation environment, cohesion (both physical (3.2.5) and biological (3.2.5.c) and the presence of iron oxide. The fines create more obstacles to the flow in the pores which reduces the flow area. The sedimentation environment, as mentioned in 3.2.3, results in more anisotropy and heterogeneity which both cause the total permeability to be lower. Cohesion causes connections between grains which results in the emergence of very low permeable aggregates (more in 3.2.5.).

It is expected that tidal sediments contain more iron than fluvial sand because the iron concentration in tidal sediments is shown to be positively correlated to the presence of clay particles (Montalvo et al., 2014). More oxygen-rich environments are present in sediments in the coastal area due to rapid changes in water level (due to the tide). In oxygen rich environments, sediment iron is naturally occurring as solid Fe(II) (Monien et al., 2014), which is oxidized to Fe(III), which can easily precipitate in components (rust, ironstone, etc.) which largely reduce the permeability (Jansen, pers. comm.). An indication of the permeability reduction is found in research by Koopmans et al., in which they tried to bind phosphates in 'iron reactive barriers' (Koopmans et al., 2010).

They added Fe-sludge (containing a lot of iron oxide) to sand resulting in the permeability drop shown in Figure 28. Veer found a mean iron concentration in marine sediments in the Netherlands of 2.3 w% (Veer, 2006) (can be reached when 7 w% of Fe-sludge is added to sand, see Figure 28). Since the process is depending largely on the oxygen level, controlled experiments must be performed to support and quantify this theory.

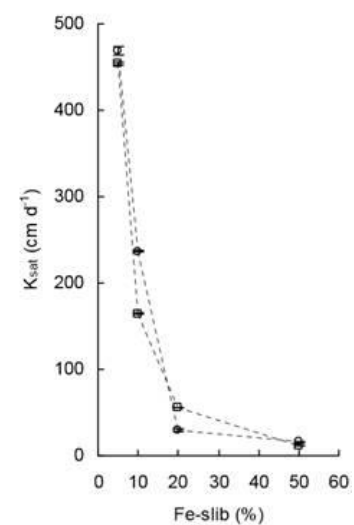


Figure 28 - Permeability with changing iron-sludge (containing 33 w% Fe) percentage (Koopmans et al., 2010)

3.2.5. Strength

The research conducted on piping in case of tidal deposits, in a quick scan by Deltares (Hijma & Oost, 2019), led to the conclusion that tidal deposits are less prone to piping than river sands. This conclusion can be separated in three main contributions against flow and erosion: 1) clay strips which cause heterogeneity and anisotropy, 2) fine fraction and 3) biological cohesion.

The influence of physical and biological cohesion has recently received much attention through a series of articles on the influence of this cohesion on sediment transport. Many sediment transport models are based on empirical relationships derived from tests with "clean" sand without a fine fraction. When doing tests on sand in which this fine fraction is present, sediment transport starts much later (Malarkey et al., 2015; Schindler et al., 2015; Parsons et al., 2016), referred to in (Hijma & Oost, 2019). Studies have shown that sediments which contain extracellular polymeric substances (EPS) are much less sensitive to erosion, even with very small amounts of EPS (Tolhurst et al., 2002).

In 2016, Parsons et al. examined the importance of combined physical and biological cohesion on current generated bed form morphology with experiments. The experimental data reveals that both have significant influence and that biologically produced EPS are by far the most effective of the two components in reducing bed form dimensions and steepness, due to their stronger interparticle bonding. The combined effect of biological and physical cohesion has been shown to alter bed form dimensions by up to an order of magnitude and bed roughness by up to 2 orders of magnitude (Parsons et al., 2016).

In the next paragraphs, the three main contributions to the additional strength are investigated.

3.2.5.a. Heterogeneity & anisotropy

Clay strips and layers in tidal deposits can hinder and prevent the growth of tunnels with possible effects being (MIM, 2017): 1) The vertical and horizontal permeability of the deposits is limited by the clay strips. Lower permeabilities lead, under otherwise unchanged circumstances, to a higher critical head in the approach used for piping. 2) The growth of pipes is hindered by the physical barrier effect of clay layers. 3) The growth of pipes may be influenced by the influence of the clay layers on the local pore water pressure gradients.

Laminae formation declares much of the layering patterns in sedimentary structures. On a micro scale (millimeters), sandy sediments consist of thin layers (laminae). The laminae can be piled up horizontally (planar laminae), but usually they deposit under an angle (cross-laminae). The laminae arise from variation in grain size and mineralogical composition. This is caused by the fact that sand transport over the water bottom takes place in soil forms such as dunes and ridges (Figure 29). By variation in water flow on the downstream side of this streams, the deposition of relatively fine sediment is alternated with coarser sediment pulses (Wiersma & Hijma, 2018). The layering influences the permeability and the porosity, influencing piping. The angle of deposition and the different permeability cross- and parallel to the laminae (cross direction has a lower permeability) cause anisotropy which affects the piping process.

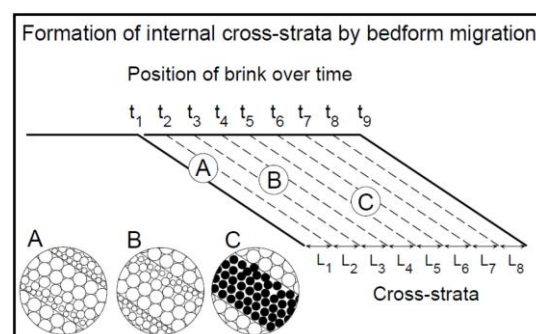


Figure 29 - Heterogeneity on a micro scale (Wiersma & Hijma, 2018) (herein referring to Cheel, 2002)

3.2.5.b. Fine grain size fraction

Fine fraction, this is the mass fraction with a grains size diameter $<63 \mu\text{m}$. This fraction of fine grainsize material being present (not present in the experiments on piping by Sellmeijer, see also 3.1.2) might have the following influences on the piping process: 1) clogging, 2) a lower permeability due to a lower porosity, 3) physical cohesion and 4) larger grains are more embedded between fine grains. These effects are discussed below in sub-paragraphs being the expected causes of the effects.

Internal stability

Transport of fine material towards the exit point might have local blockage as a possible consequence. Plumes of escaping fine material were observed during the small-scale experiments on tidal sand, possibly indicating a breakthrough of such a blockage. Sellmeijer implicitly includes a grain size-

permeability relationship. When the fine fraction is present, this implicit relationship will be different (lower permeability than expected). The relation will be different because the permeability which is supplied to Sellmeijer's is affected by the fines content but the d_{70} is not. This will result in an underestimation of the critical head difference.

Internal stability refers to the ability of the coarse fraction of a soil to prevent the loss of its fine fraction due to seepage flow (suffusion). In the case of tidal sands, where fine particles are mixed with larger sand particles, the washing out of these fines on one location and clogging on another location, is more likely to occur than in fluvial sands.

In 2013, Chang et al. conducted research on internal stability criteria for soils under seepage. The main objective of this paper was to extend internal stability criteria (Figure 31) for well-graded and gap-graded soils based on a physical understanding of the microstructures of the soils (Chang & Zhang, 2013). The classification gradation of gap-graded soils is depicted in Figure 31.

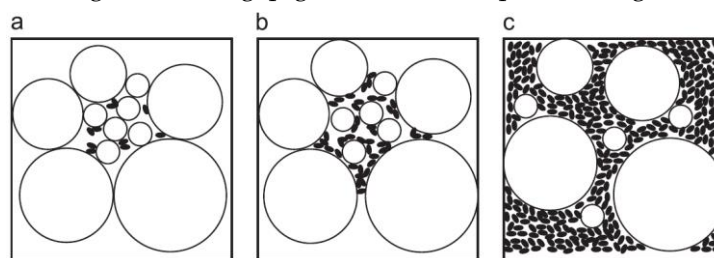


Figure 31 - Classification of gap-graded soils: (a) with fines contents less than 10%; (b) with fines contents between 10% and 35%; (c) with fines contents more than 35% (Chang & Zhang, 2013)

Gradation conditions	Fines content, P (%)	Geometric criteria
Well-graded soils	$P < 5$	$(H/F)_{\min} > 1.0$: internally stable
	$5 \leq P \leq 20$	$(H/F)_{\min} > -(1/15)P + 4/3$: internally stable for low plasticity soils
	$P > 20$	Stable
Gap-graded soils	$P < 10$	$G_r < 3.0$: internally stable
	$10 \leq P \leq 35$	$G_r < 0.3P$: internally stable for medium plasticity soils
	$P > 35$	Stable

Figure 31 - Proposed geometric criteria for different types of soil by Chang et al. (Chang & Zhang, 2013)

Therein, F is the mass fraction of particles finer than grain size d and H is the mass fraction of particles ranging from d to $4d$ and the gap-ratio in Eq.10. In this equation d_{\max} and d_{\min} are defined as the maximal and minimal grainsizes which identify the gap in the grains size distribution.

$$G_r = \frac{d_{\max}}{d_{\min}} \quad \text{Eq.10}$$

Since it is expected that tidal sediments are gap-graded and contain 0-35% fines, the geometric stability criterium is that the gap-ratio must be smaller than $0.3P$ to be stable. If the grain size distribution of tidal sand as given in Figure 21 is evaluated in this way, P is 12%, d_{\max} is 90 μm and d_{\min} is 20 μm . In this situation, the soil is not internally stable due to the large gap.

When the soil is not internally stable, wash out of fines will occur under seepage flow. When this suffusion occurs, the smaller particles are transported downstream through the pores between the larger grains. This wash out has two consequences: 1) due to the outflow of small particles, the permeability upstream goes up and 2) due to the accumulation of small particles downstream, the permeability goes down, clogging the outflow. This effect is not modelled in D-Geo Flow. The tidal sands used in the small-scale experiments by Deltares from the *Grevelingenmeer* and *Friesland* (Figure 32), are gap-graded (when looking at the samples through a microscope).

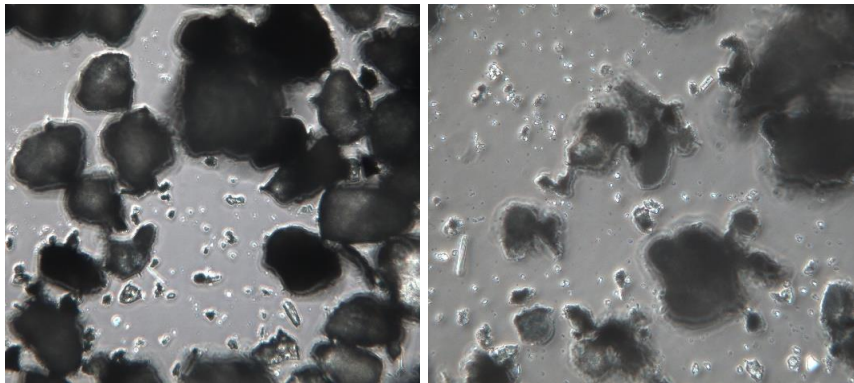


Figure 32 - Experiment soil from *Grevelingen* (L) and *Friesland* (R) through a microscope. The fines are clearly visible in between the larger sand particles

The gap ratio is measured from the grains size distribution. The influence of the grains size distribution on piping is investigated by Van Beek (2019) in terms of the uniformity coefficient (U , Eq.11). It was concluded that with an increasing coefficient of uniformity (less uniform sand), the material becomes less piping sensitive. A disadvantage of this method, when considering tidal sands is that the weight of fines is mostly situated underneath d_{10} , so the gap between larger and smaller grains is not (or badly) represented.

$$U = \frac{d_{60}}{d_{10}} \quad \text{Eq.11}$$

Clay coat coverage

Clay coats are characterized as accumulations of clay minerals, silt-size particles and remains of biota and secreted material (diatoms and EPS) forming coating and bridging structures between sand grains (Wooldridge et al., 2017). The fine particles create the structure and the particles are bonded by physical and biological cohesion.

In 2018, Wooldridge et al. did research on clay-coated sand grains and sediment heterogeneity in tidal flats. They come to the following conclusions: the percentage of the sand grains covered with a coating increases with a decreasing average grain size, an increasing percentage of clay fraction and with an increasing poor sorting (Figure 33). There is no relation with depth, which is used in the report as an argument that processes after sedimentation (bioturbation, irrigation, see 3.2.5) play a limited role (Hijma & Oost, 2019; Wooldridge et al., 2018).

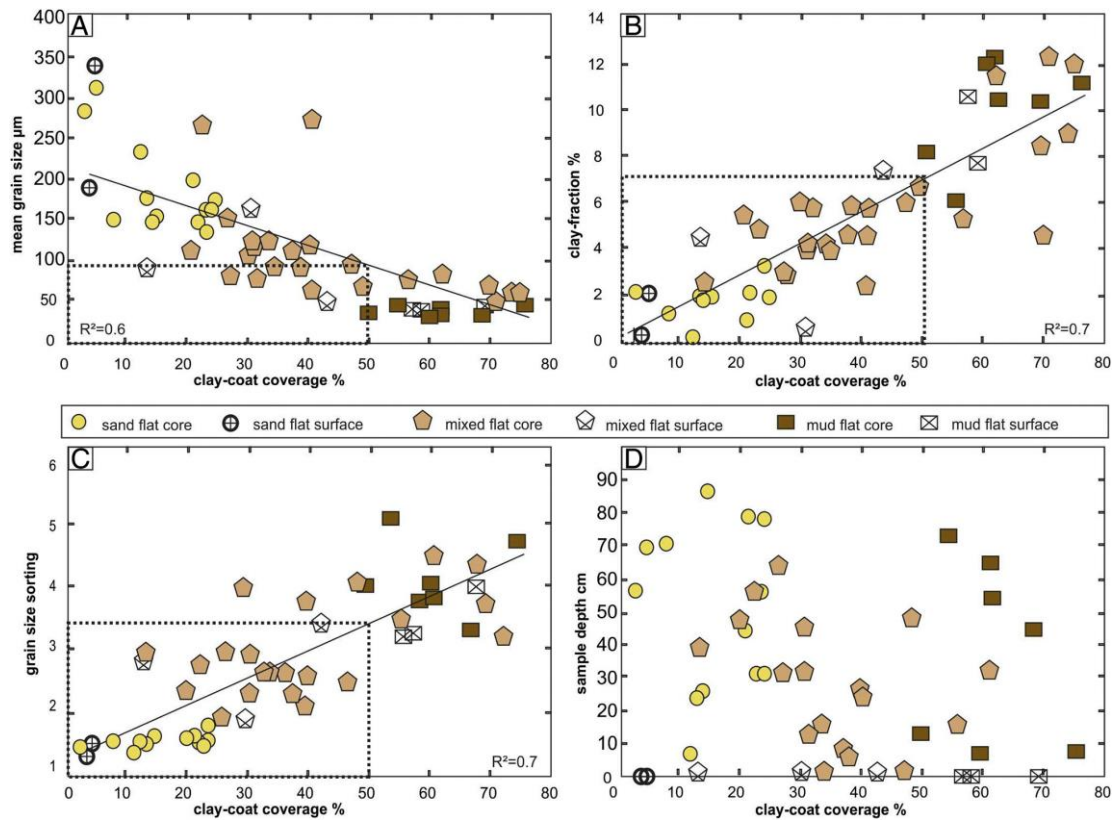


Figure 33 - Percentage clay coating with varying: (A) mean grain size, (B) clay fraction, (C) grain size sorting and (D) sample depth (Wooldridge et al., 2018)

Wooldridge et al. showed that the clay coat coverage is positively correlated with chlorophyll-a (Figure 34) (chlorophyll-a is an algae pigment). As explained in 3.2.5, the amount of EPS is positively correlated with chlorophyll-a.

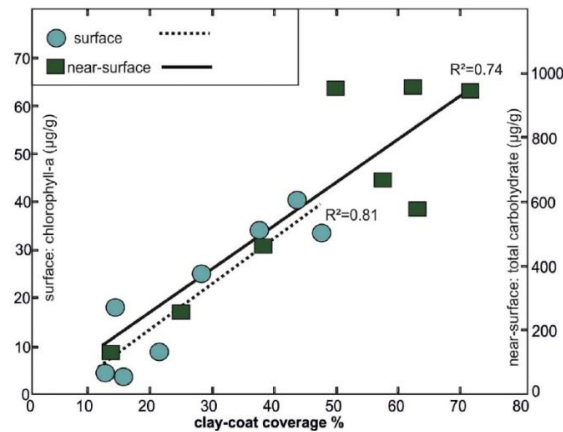


Figure 34 - Clay coat coverage for different concentrations of chlorophyll-a (Wooldridge et al., 2018)

Physical cohesion

In this thesis, cohesion is referred to as the interparticle force which works between adjacent particles (Yokoi, 1968). Two types of cohesion are discussed: 1) physical cohesion caused by the affinity of the clay particles for water and 2) cohesion by biological cementing (i.e. biological cohesion, see 3.2.5.c).

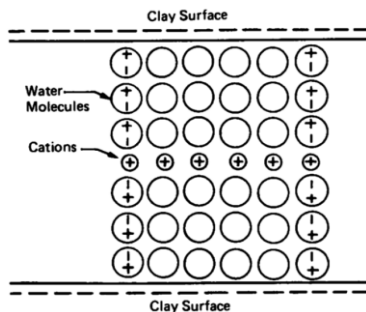


Figure 35 - Clay cohesion on molecule scale (Shehata, 2015)

Cohesion between clay particles in sediments is known to be governed by several interfacial attractions, such as electrostatic attraction and capillary adhesion. Cohesion by electrostatic attraction is mainly governed by the composition of the surrounding water. The cohesion process occurs on molecule scale on the solid-liquid interface. In fresh water, the electrolyte concentration is low. In this situation a 'diffusive double layer' forms between the clay particle surface and water molecules. This double layer buffers the supply of cations (electrically charged ion) to the clay surface, resulting in a net negative surface charge (Figure 35). In saline water, the electrolyte concentration increases, thereby increasing the supply of cations to the clay surface, promoting particle-particle attraction. Also EPS can interact with clay

particles via cation exchange (Spears et al., 2008). This means that with increasing salinity, not only the particle-particle attraction increases but also interaction between EPS and clay particles, resulting in additional cohesion (more on biological cohesion by EPS in 3.2.5.c).

Water in the Netherlands is identified as saline when the salt concentration is higher than 16.5 g/L and fresh when the concentration is lower than 0.1 g/L. In the North sea, the concentration varies between 34 and 35 g/L and the average over the oceans of the world is 35 g/L (Vliz, 2006). Near the Dutch coast, where rivers cause freshening of the water, the salinity roughly varies between 14 and 19 g/L (Rijskwaterstaat, 2019). The increase of physical cohesion, measured as sediment stability, over salinity is presented in Figure 36. A clear difference can be observed between sediment stability in fresh and saline water due to increased cohesion in saline water. The sediment salinity (near the banks of the *Schelde* close to the *Hedwigepolder*) is approximately 5-18 g/L. This was found by Belgian researchers at the opposite bank of the *Westerschelde* in drillings to 1.4 m depth (Van de Broek et al., 2016).

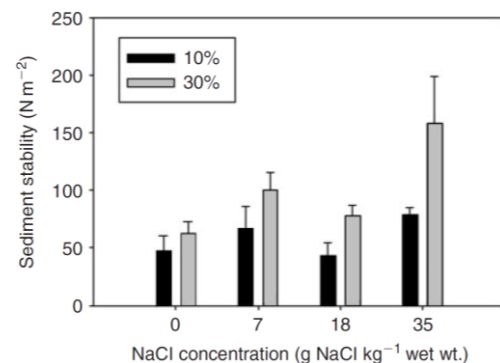


Figure 36 - Sediment stability over salinity for lightly disturbed soils when salinity is increased (10%) and more heavily disturbed soil when salinity is increased (30%) (Spears et al., 2008)

A newly discovered type of fluid-related cohesion in natural cohesive sediment is evaporation-driven aggregation (Seiphoori et al., 2020). This finding can explain the increased clay-coat coverage with increasing fines content, found by Wooldridge in Figure 33. The idea is that when particles <5 μm are present and the water between particles with sizes ranging from 0.1 μm < d < 100 μm evaporates, the particles form bridges (Figure 37) which are purely depending on the size of the particles. These bridges are found to be 10-100 times stronger when rewetted than in a situation where these particles <5 μm are absent.

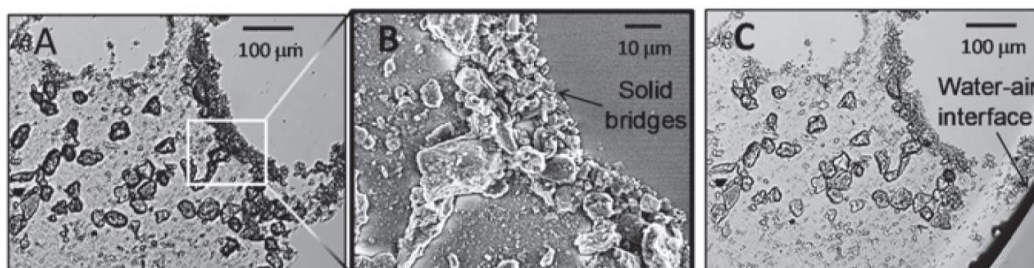


Figure 37 - Aggregate stability of Illite clay particles when dried (A) and rewetted (C), formed solid bridges (Seiphoori et al., 2020)

3.2.5.c. Biological cohesion

The second type of cohesion that is considered to have an influence on the piping process in sandy tidal deposits is biochemical cohesion (i.e. cementing). The treatment of cohesive sediment transport remains a recurrent problem in water-related engineering disciplines, it is an important element that has played a key role in many engineering projects. The important influence that accommodates this cementing is biology. The presence of biomass and activity of sediment-inhabiting organisms change the soil conditions. Although physical forces overwhelm most biological influences during storms and floods, during quiet periods the biotic effects becomes more important. Several researchers tried to find relations between sediment erosion rate and the presence of cohesion. For the process evaluated here, piping, erosion is an important process as well as groundwater flow. The initiation of motion in the pipe is suspected to be at higher gradients when more biotic processes are involved.

Water flowing through sands convert these sands into expansive filter systems. Organic content is transported with the penetrating water into the sediment, where they become trapped in the pores (Boudreau et al., 2001). Organic content has an influence on physical, chemical and biological soil parameters. The presence of organic material enhances the soil particles to stick together and reduce the weight of the soil.

Infaunal and epifaunal benthic organisms can alter the nature of the seabed, enhancing or reducing the resuspension potential of the surface sediments (Friend, 2001). When buried over time, the resuspension potential is important when looking at piping. Besides the altering by organism, also the differences in collective properties of the tidal sands compared to fluvial sand complicate the definition of a general analytical theory to describe erosion resistance of tidal sands (Black et al., 2002).

In the following paragraphs, biological cohesion is explained. The main influences on the resistance against piping are highlighted to guide towards a measuring technique of resistance against piping.

Influences

The biotic effects on bed-stability can broadly be classified as either stabilizing (bio stabilization) or destabilizing (bio destabilization). The two biotic aspects which, in general, have the most influence on resistance against flow and erosion by piping: 1) bio stabilization by cohesion due to EPS and 2) bio destabilization and mixing of surface layers through bioturbation.

Bio stabilization by EPS

In natural sediments, bed stability is a function of many parameters, including the clay mineral (fines) content and extracellular polymeric substances (EPS). The widespread occurrence of EPS has been recognized since at least the last century (Friend, 2001). Cohesion between particles arises from the secretion of extracellular polymeric substances (EPS) by bacteria, which coat grains and bridge pores to form a cohesive network. EPS is a flexible, viscoelastic material when hydrated, and is known as able to absorb turbulent energy far more effectively than clean grains. Frankel and Mead (1973) cited EPS as the main factor in the stabilization of sediments, by microbial mats (often seen on salt marshes). It is

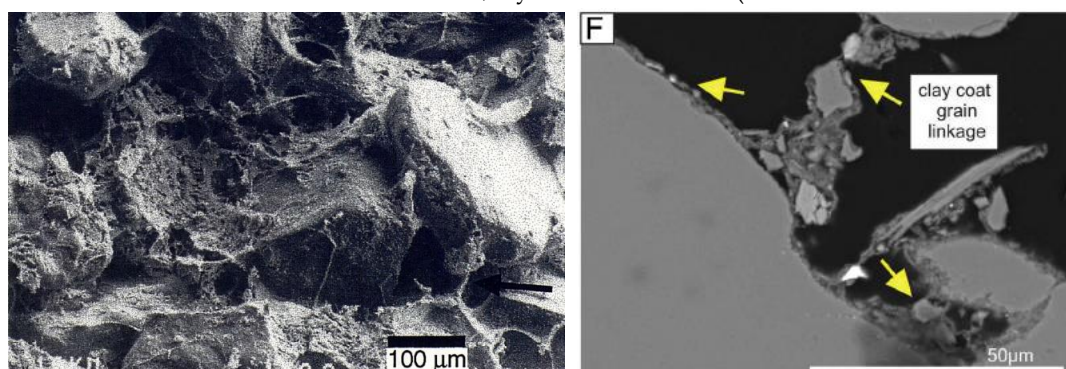


Figure 38 - Interparticle bonding (Friend, 2001) (L) and Scanning electron microscopy (SEM) images of surface clay-coated sand grains. Arrows indicate regions and key textural characteristics of clay coats (Wooldridge et al., 2018) (R)

estimated that a single bacterium can produce enough EPS to coat >500 particles per day (Friend, 2001). Biochemical cohesion is formed by the presence of biofilms, composed of mats and strings of EPS, on the surface of the sand grains. These biofilms form a coating around the sand particles. High resolution microscopes show this coating well (Figure 38). The EPS can physically link the grains of sand to each other and thus provide extra resistance against BEP (Wooldridge et al., 2018).

EPS can consist for >90% of polysaccharides. It is the properties of these polymers (hydrogen bonding and metal-bridging) which determine their capacity to cause adhesion between surfaces (Decho, 1994), see Figure 38. The EPS, situated between 2-20 μm particle aggregates (silt) creates larger aggregates which interfere with plant roots, organisms and larger grains (Figure 40). The formed aggregates create a less permeable and stronger soil.

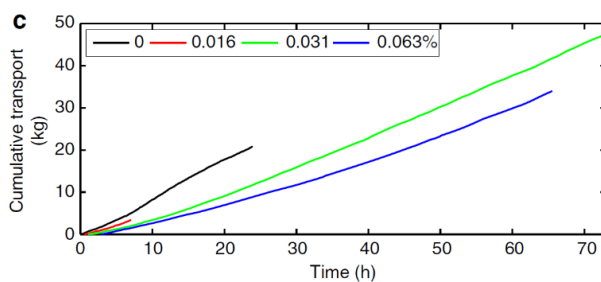


Figure 39 - Soil transport over time for different percentages of EPS content (Malarkey et al., 2015)

The importance of EPS in modifying sediment hydraulic properties has been shown by several studies. Dade et al. (1996) for instance, determined a 60% increase in critical shear stress for marine sediments containing EPS (Black et al., 2002). In a separate study, they showed that the erosion potential of a fine sand was increased four-fold by the presence of either a pure exopolymer alone or EPS generated during in situ growth of the bacteria (Black et al., 2002). Malarkey et al. (2015), conducted research on bedform development in case of biological cohesion by EPS. In the experiments they conducted, the soil transport was monitored for soils with different EPS contents (Figure 39). This shows a clear increase of erosion resistance with increasing EPS content. Not only erosion resistance increases when EPS is present, its hygroscopic (absorbing and adsorbing) properties cause increased water storage and decreased groundwater flow.

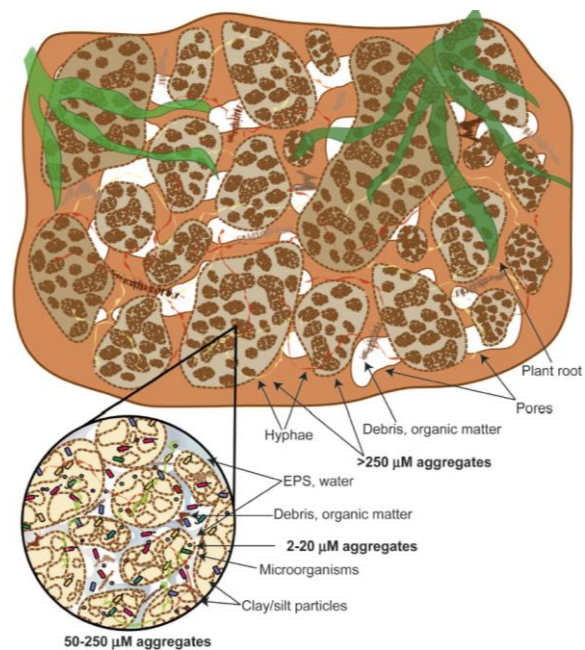


Figure 40 - Soil aggregate classification when EPS is present (Costa et al., 2018)

The importance of EPS in modifying sediment hydraulic properties has been shown by several studies. Dade et al. (1996) for instance, determined a 60% increase in critical shear stress for marine sediments containing EPS (Black et al., 2002). In a separate study, they showed that the erosion potential of a fine sand was increased four-fold by the presence of either a pure exopolymer alone or EPS generated during in situ growth of the bacteria (Black et al., 2002). Malarkey et al. (2015), conducted research on bedform development in case of biological cohesion by EPS. In the experiments they conducted, the soil transport was monitored for soils with different EPS contents (Figure 39). This shows a clear increase of erosion resistance with increasing EPS content. Not only erosion resistance increases when EPS is present, its hygroscopic (absorbing and adsorbing) properties cause increased water storage and decreased groundwater flow.

EPS degradation

The degradation of EPS is a very important aspect. When EPS has been buried for a long time, it is crucial to know if biofilms are preserved. Some EPS components are only slowly biodegradable. The large variety of components means that their complete degradation requires a wide range of enzymes (Flemming & Wingender, 2010). The biofilm is a sponge-like system that provides surfaces for a diverse range of molecules. This leads to several benefits to the biofilm, such as nutrient intake and stabilization. Surface-attached biofilms are not only able to take up nutrients from the water but can also digest biodegradable components from the soil, which – if enough ‘food’ is present – can keep the biofilm alive and stable when buried. Besides the intake, biofilms are also capable of surviving exposure to antimicrobial compounds like toxic metals and small-molecule antibiotics (Flemming et al., 2016).

Extracellular polymeric substances are complex substances and our understanding of their composition, structures and functions, although very broad, is far from complete. When looking at piping, further knowledge on the degradation rate of EPS and the remaining strength over time needs further research. The further investigation involves complex and time-consuming techniques, and thus, the development of knowledge in this area may proceed slowly. Many microorganisms produce EPS and because each

polymer is different, many opportunities remain for investigation and discovery (Cai et al., 2019; Costa et al., 2018).

Benthic microalgae

Bacteria are, in numerical terms, the dominant microbial constituent in mud. A second microbial group, the microphytobenthos, also contribute to microbial binding of grains. Microphytobenthos consist of groups of photoautotrophic (can live from inorganic materials and light energy) algae. The dominant group that secretes EPS is the benthic diatom. Their large size (10–200 μm) in comparison to bacteria (0.2–2.0 μm) affords a greater capacity to modulate particle-particle bonds (Black et al., 2002). Presence of these diatoms gives the sediment a dark brown color.

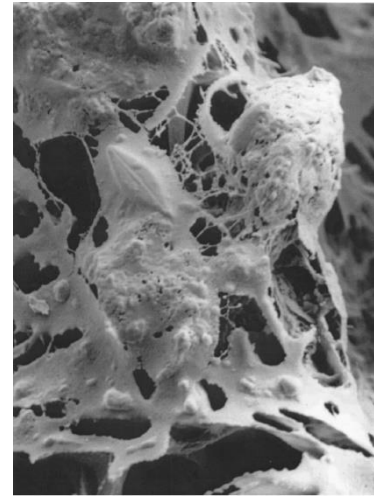


Figure 41 - Benthic diatom (\diamond) embedded in EPS (about 20 μm) (Black et al., 2002)

Their presence depends on a variety of factors including season (light, temperature, nutrient availability), nature of the subsoil and the intensity of herbivore grazing (Friend, 2001). Friend conducted an analysis on various influential parameters in an estuary in the UK to investigate if intertidal flat morphology is controlled by the influence of benthic organisms. A non-cohesive intertidal flat was selected, to minimize particle cohesion effects by clay minerals, and to focus upon the adhesive effects of EPS. He looked at hydrodynamics and chemical- and biological components, varying in space and time.

The only positive correlation he found (with a p-value smaller than 0.05), between critical shear stress and any of the biochemical parameters, was chlorophyll-a. This is a pigment and is essential in photosynthesis, allowing the algae to absorb energy from light.

Table 3 - Correlation chlorophyll-a and critical shear stress (Friend, 2001)

$\text{Chlorophyll-a} \left[\frac{\mu\text{g}}{\text{gDW}} \right] \quad r = 0.662$ $p = 0.027$
--

This parameter is thus strongly dependent on light intensity. The highest values occur at times when photosynthesis is the highest and that is at the end of spring and start of summer. By regression on the values that were found, the relation depicted in Figure 42 was found.

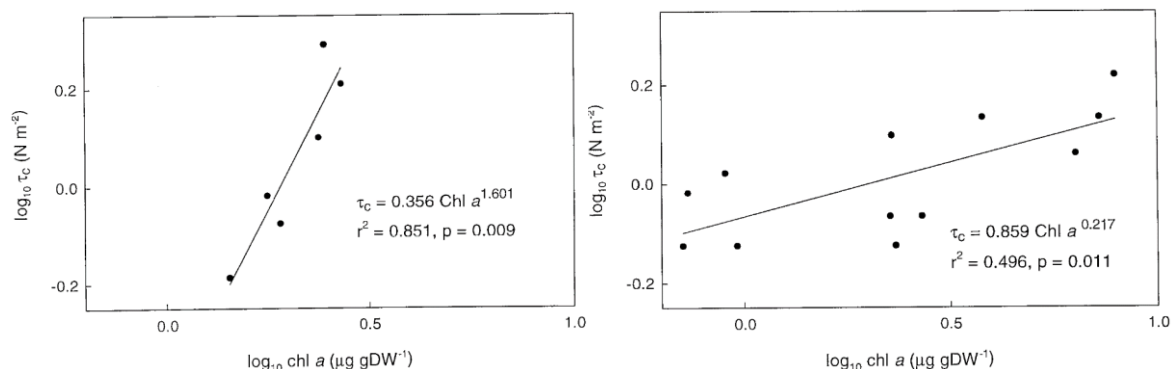


Figure 42 - Critical shear stress and chlorophyll-a on a more landward station in March and April (L) and on a more seaward measuring station in March, April and May (R) (Friend, 2001)

Besides the relation with critical shear stress, Wooldridge also found a positive correlation between clay coat coverage and chlorophyll-a (as mentioned before, Figure 34). If the conditions are good, diatom biofilms can completely cover the sediment surface. In this situation, traditional sediment transport approaches are redundant, as the boundary character may be changed from rough to smooth. When the

tide comes in and covers these layers with sand, a layered pattern of permeable and less permeable layers, due to EPS, emerges (Black et al., 2002).

Bio (de)stabilization by bioturbation

The burrowing, particle sorting and tube-building activities (i.e., bioturbation activities) of benthic fauna, such as snails, crustaceans, polychaetes and bivalves (in Dutch respectively: *slakken*, *schaaldieren*, *borstelwormen en tweekleppigen zoals oesters*) also affect natural sediments. These animals influence engineering properties of interest, when assessing piping or other sediment transport means, such as porosity and permeability. They destabilize the bed by burrowing but also stabilize by particle sorting and distribution of EPS. The depth to which bioturbation reaches is larger than just the EPS layers mentioned before. For example, the lugworm burrows to about 15 cm and clams can even reach to 30 cm. Macrofaunal (de)stabilization has potentially far-reaching engineering consequences (Black et al., 2002).

The lugworm (*Arenicola marina*, in Dutch: *Zeepier*, Figure 2.2) is a widespread and dominant large burrower at European Atlantic shores, and a major source of bioturbation on the intertidal flats in the Wadden Sea (Volkenborn et al., 2007). The lugworm is a sub-surface, deposit-feeding brush worm, and a dominant member of the macrobenthos on many of the intertidal flats throughout its range in North West Europe. In the Dutch *Wadden Sea*, *Arenicola marina* comprised 20-30% of the benthic biomass in 2001, and the average density in measurements by Friend in 2001 was 17 m⁻² (maximum 50 m⁻²) (Friend, 2001).

The lugworm has a cylindrical body, up to 20 cm in length, and lives in a U-shaped shaft at 15 to 20 cm depths. The shaft consists of a head shaft and a tail shaft, through which respectively feeding and defecation occurs. Feeding occurs in short bursts of a few minutes, with defecation occurring every 15-40 minutes, depending on the size of the worm. Lugworms feed on benthic microalgae, bacteria, micro and meiofauna (meio: living in marine and freshwater areas). The digging in, feeding from and defecation on (i.e. 'gardening' of) the sediment has caused the lugworm to be called an 'ecosystem engineer'. The interplay between physical and biological processes which affect sediment stability is illustrated in the case of the lugworm, which both consumes EPS and disrupts the sediment fabric by bioturbation (Friend, 2001).

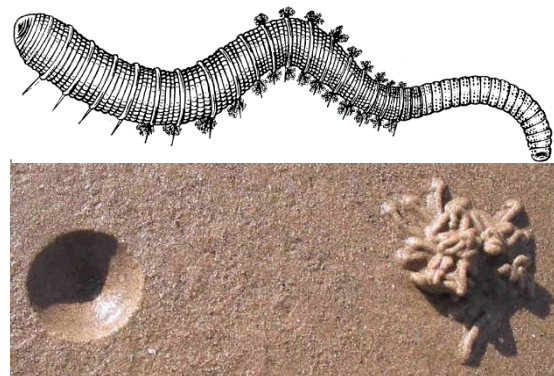


Figure 43 - Lugworm, feeding shaft and fecal mound (Clipground, 2019)

In 2007, Volkenborn et al. did research on the effects of the presence of the lugworm on grain size, organic content and chlorophyll-a concentration. They found that the impact of the presence of the lugworm was larger in fine grained soils. Lugworm presence, significantly enhanced the accumulation of fine particles in the first 5 cm from the surface (Volkenborn et al., 2007). This leads to a layered pattern of fine and coarse layers, enhancing heterogeneity. Defecation on the surface (Figure 43) leads to an increase in surface roughness, thereby increasing resuspension. The organic content and chlorophyll-a concentration were higher in this zone without the worms. Due to mixing and feeding, the organic content went down (Volkenborn et al., 2007).

Conclusion

EPS binds particles, creating aggregates which influence the permeability and cohesion. EPS concentration is measured the best by chlorophyll-a concentration and is influenced by diatoms, benthic fauna, bacteria, oxygen and sunlight.

3.2.5.d. Predicting

The ways to measure piping resistance and the direction to focus on in future research are described in this paragraph. To create a method to evaluate the strength of tidal sand, the parameters which best represent the strength must be measured. Taking this into account when assessing flood defenses requires more data on the involved parameters but an onset is made. The strength parameters are evaluated when the soil has been buried for a long time. For the mentioned parameters, the way to measure and the uncertainties when doing so, are described.

Sludge content

The sludge content must be defined from the grain size distribution in weight percentage smaller than 16 μm . Also, the gap ratio must be known which can be read from the grains size distribution as well.

Organic content

Measuring the weight percentage of organic and fine material is done as in a regular soil sampling analysis. The organic content is burned from the sample, leaving the opportunity to weigh and calculate the percentage of organic content of the soil sample. To show the difference in organic content between fluvial and marine sediments; the mean organic content in marine deposits in the Netherlands is 5.2% and of fluvial sand 1.2% (Veer, 2006).

Chlorophyll-a

Pigments are present in all photosynthetic organisms and function primarily as light harvesting units for photosynthesis. The type that has a positive correlation with EPS is chlorophyll-a (as mentioned before). If the concentration of chlorophyll-a (and its breakdown products) in the soil can be preserved and measured, it can give an indication on the amount of EPS (biofilm) that is present in the soil.

Changes in chemical and biological indicators such as chlorophyll-a, preserved in the sediment, can provide information on the physical environment. In addition, pigments are useful as biomarkers due to their ability to represent a precise class of biological organisms. Chlorophyll-a is found in all photosynthetic algae and higher plants. When chlorophyll-a degrades, the main remnant is pheophytin-a. Reuss (2005) made a classification of the stability of the pigments (classes 1-4, 1 stable and 4 unstable) and classified chlorophyll-a as 3 and pheophytin-a as 1. This study also shows that carbohydrates, which are also present in EPS, are the least stable group (Reuss, 2005).

Most of these breakdown products are detectable by regular pigment analysis. The most extensive degradation takes place during deposition and when they are positioned in the surface sediment, exposed to oxygen and light. The chlorophyll-a is affected by photo-oxidation within hours to weeks. The oxidation, depending on the accretion rate, continues for weeks to months. In this period, the rearranging and digestion by benthic fauna also affects the degradation (Reuss, 2005). When the sediment is covered deeper, the degradation is mostly due to the water flows through permeable sediments. The water flow enhances the decay of trapped organic particles by providing oxygen and other reactants that are necessary for decomposition (Boudreau et al., 2001).

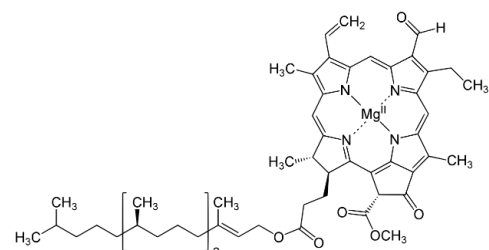


Figure 44 - Chemical structure of chlorophyll-a (Reuss, 2005)

Table 4 - Influence and consequences of and on chlorophyll-a preservation and concentration

Influence	Consequence
Settling velocity	Higher settling velocity means better preservation
Accretion rate	Higher accretion rate means better preservation
Water depth	Greater depth means better preservation
Hydrodynamic conditions	Certain loading may cause a local increase of chlorophyll concentrations. Quiet conditions mean better preservation.

Sampling site	The most reliable sampling sites are found at places where no significant changes in morphology and preservation conditions have occurred around the time of burial.
Grainsize/permeability	Larger grains / higher permeability means faster decomposition

Wooldridge et al. (2017) also investigated biofilm degradation. They found that in the presence of chemical compounds Mg^{2+} and Ca^{2+} , that are present in estuarine waters, EPS biofilm fractions become water insoluble and resistant to degradation (Wooldridge et al., 2017).

Despite the degradation, pigments are often the only remains of algae. For almost 30 years, pigment analysis is used to investigate climate change and consistency and changes of both lake bottoms and estuaries. The sampling must be done by collecting cores. Preferably the core must be protected from light, heat and oxygen. Keeping the samples cold and dark reduces degradation of the pigments. Pigment concentration is measured by high-performance liquid chromatography (HPLC). This is a separation method where the molecules are dissolved and are under high pressure pushed through a tube where the small and good dissolvable molecules pass first. A sensor detects different molecules and registers concentration.

The conclusion is that the chlorophyll concentration is a good marker for the presence of EPS. Chlorophyll-a and its breakdown components seem to be the best measurable and preserved parameters in the sediment over time. Thereby, knowledge of the sedimentation environment is of great importance to create a reliable vision of the chlorophyll-a level. Determining the best sampling locations and depth for a project may reduce the uncertainties introduced by the influences mentioned in Table 4.

Underwood et al. conducted research on the measuring of EPS and found values of chlorophyll-a in sediments from the *Blackwater estuary* in *Essex* (England) at different locations in the tidal basin (Table 5). It is not known in which season these measurements were taken, which is of great importance because EPS production varies a lot with the seasons. The difference between location, often resulting in a different assemblage of the algal biomass, results in a large difference in chlorophyll-a content. This means that to compare chlorophyll-a levels, the composition of the algal biomass is important. Besides the difference between location and composition, also the variation on a similar location is very high.

Table 5 - Chlorophyll-a levels *Blackwater Estuary, Essex* (Underwood et al., 1995)

Location	Assemblage	Chl-a concent. [$\mu\text{g/g}$]
Upper saltmarsh	25% diatoms and 75% bacteria	145.3 \pm 62.3
Cyanobacterial mat	25% diatoms and 75% bacteria	71.3 \pm 41.7
Lower saltmarsh	70% diatoms and 30% bacteria	144.1 \pm 39.6
Mudflat biofilm	100% diatoms	41.4 \pm 20.3

Closer to the *Hedwigepolder*, in the *Westerschelde*, Widdows et al. conducted research on the role of physical and biological processes in sediment dynamic on the *Molenplaat* (Figure 45). They measured the chlorophyll-a level on different locations on the tidal flat in June and September 1996 and 1997 (Table 6). The concentration depends strongly on season and location on the flat. The values in the *Westerschelde* are considerably lower than in *Essex*. Since the season of measuring in *Essex* and the algal biomass composition of the *Molenplaat* are both not known, it is impossible to say what causes this difference. It is also possible that the difference in hydraulic conditions at both locations play a big role since the difference between the locations on the *Molenplaat* already show larger differences.

Table 6 - Chlorophyll-a levels Molenplaat (Widdows et al., 2004)

Location		Chl a con- cent. June [µg/g]	Chl a con- cent. Sept. [µg/g]
Top tidal flat	1996	35.6	5.4
	1997	64.0	6.8
Top tidal flat	1996	26.1	2.6
	1997	10.6	5.7
Above mid-tide level	1996	2.4	1.9
	1997	7.1	1.8
Above mid-tide level	1996	1.2	0.8
	1997	1.3	0.75
Between low- and mid- tide level	1996	35.5	2.0
	1997	12.6	4.9

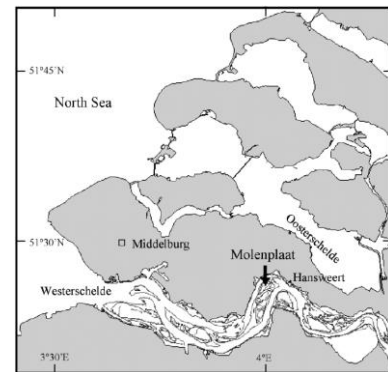


Figure 45 - Molenplaat in the Westerschelde (Widdows et al., 2004)

Conclusion

The large number of influential parameters explains why no simple relationship (comparable to the Shield's curve) is possible for the incipient motion of cohesive sediments (Friend, 2001).

From literature research it can be concluded that EPS content (as chlorophyll-a), grain size distribution and organic content have the highest potential of being an appropriate marker for increased erosion resistance in tidal sediments. The quantification of the chlorophyll-a concentration is a difficult task and has a high uncertainty in both time and space. Research must be conducted on the preservation of EPS and chlorophyll-a when it has been buried.

Accounting for additional strength

Although models for cohesive sediment transport in estuaries are available, they are largely based upon simplified empirical expressions for the bottom boundary condition. Almost all engineering transport models use the critical bed shear stress as a boundary condition (Black et al., 2002).

Paterson (2000), discussed the desire within cohesive sediment transport for a quantitative predictive relationship relating sediment properties to erosion potential. The critical shear stress for non-cohesive, relatively organic-free sediments can be determined sufficiently accurately by using one of the versions of the Shields function from knowledge of grain density, -size and the fluid properties. Analytical expressions for cohesive sediments have yet to be developed (Black et al., 2002; Paterson et al., 2000). Including sediment biochemical properties (such as chlorophyll-a, organic content and EPS content) makes the derivation of such an analytical expression even more hard to find.

It is usually possible to find erosion criteria, expressed in critical shear stress from flume experiments, and consequently it should also be possible to express the erosion coefficient in terms of sediment properties. This must involve laboratory experimentation, where there is control over the independent variable, rather than direct field experimentation where direct cause-effect relationships are difficult to discern. Field experiments show that a lot of correlations need to be defined to find the influence of a certain parameter.

To give an onset of how the influence of cohesion can be expressed, the following advice from literature is given. The difference in erosion resistance due to cohesion can be expressed in the following parameter/index: 1) Shields parameter ψ_c and 2) bio stabilization index S_B .

Shields parameter

The Sellmeijer equation is calibrated on a critical Shields parameter (ψ_c , Eq.12) of 0.1 in laminar flow (Figure 46). Increasing the bedding angle (θ) in this equation results in a higher critical shear stress, representing an increase in cohesion between particles. Since Sellmeijer's model is calibrated on a value of 37° , a new calibration must be performed for the new value(s) that would belong to tidal sediments.

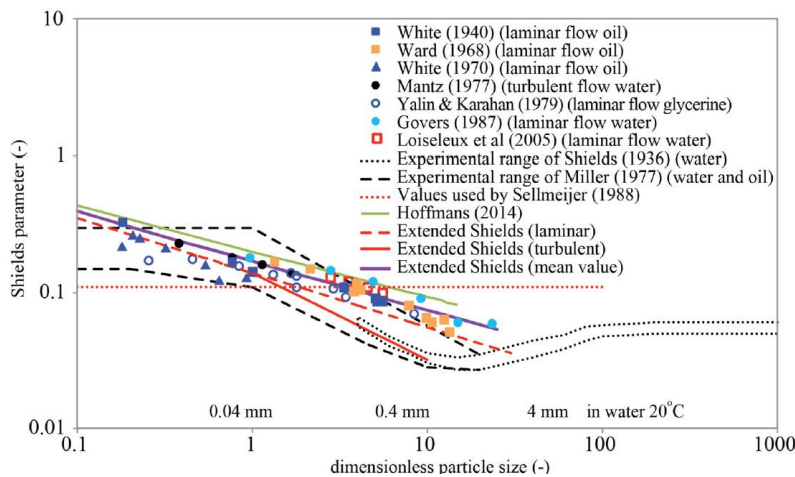


Figure 46 - Shields diagram (Hoffmans & Van Rijn, 2018)

$$\Psi_c = \eta \frac{\pi}{6} \tan \theta \quad Eq.12$$

Bio stabilization index

Friend (2001) suggested that critical shear stresses in the natural environment are always likely to be above the Shields curve because of the more biotic environment. Therefore, it is important that sediment transport formulae based upon the abiotic threshold for the initial motion or resuspension of sands, should incorporate a bio stabilization factor (Eq.13) to account for 'natural' shear stress values (Friend, 2001). Bio stabilization index S_B (Friend, 2001; Manzenrieder, 1983):

$$S_B = \left[\frac{\tau_{0,crit}(measured)}{\tau_{0,crit}(Shields)} \right] \quad Eq.13$$

For heavily colonized sediment, S_B can reach up to six or seven (Black et al., 2002).

As an indication of the extra strength of the soils tested in the field, he plotted the results of the CSM (Cohesive Strength Meter) measurements in the Shields diagram (Figure 47). The CSM uses the eroding stress of a perpendicular jet, directed at the sediment surface (about 0.0007 m²), to bring the sediment underneath the device in suspension (Friend, 2001). It shows that initiation of motion occurs at higher Shields values.

Sample remolding

An important notion upon retrieving soil samples and the effects of remolding the samples was given by Bennet et al. (1990). They conducted experimental research on the effects of particle orientation, arrangement and spatial distribution on determining porosity and permeability. They concluded that the microstructure, mineralogy and particle size distribution play a critical role in determining the physical and mechanical properties of tidal sediments. The study shows a difference of an order of magnitude between laboratory permeability and in situ measurements. Remolding of the sample profoundly reduces the permeability because of the rearrangement of fine particles (Bennett et al., 1990). This should be considered when conducting experiments on the influence of the discussed microstructures in tidal sediments.

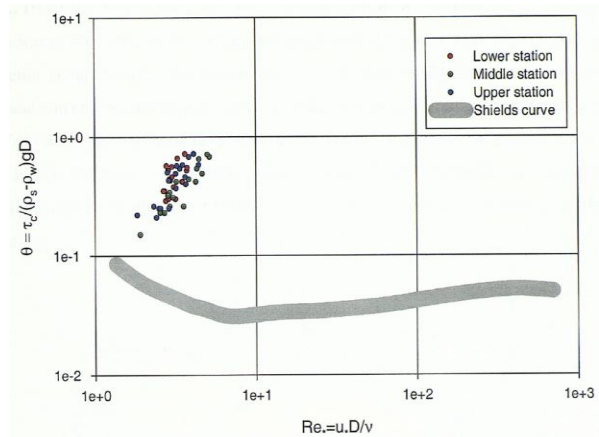


Figure 47 - Results of the CSM field measurements by Friend plotted on a Shields diagram with an indication of the Shields curve (Friend, 2001)

3.2.6. Lab experiments on tidal sand

Experiments on piping through tidal deposits are recently conducted at Deltares. This data is used in this thesis. Besides these experiments, no experiments on this specific topic has been conducted. Scale experiments have been conducted on suffusion, washing out of fine grains from the soil skeleton. In these experiments the fine fraction is not sieved out, as in other experiments is done. The most important findings from these experiments are listed below.

Loire sand 2011 (Hijma & Oost, 2019)

In 2011, tests were carried out on Loire sand. This sand had a relatively high uniformity coefficient of 3.3 and relatively much fine material (3% lutum, 4% silt). During the test it was noticeable that the fine material (probably smaller than 60 μm) leached from a 30 cm head drop. This resulted in many small pipes, but only at a head drop of 120 cm did a "real" pipe arise and at 180 cm a large and wide pipe formed. When comparing the critical head difference with the results from Sellmeijer, the measured critical head difference was found to be 3.1-4.6 times higher.

Richards and Reddy 2012 (Richards & Reddy, 2012)

The research by Richards and Reddy focused specifically on the differences in the piping process between non-cohesive and cohesive material. In the experiments, the sand is in a triaxial cell. Three modes of piping behavior were recognized: concentrated leak erosion, backward erosion, and suffusion. The amount and type of the fines present in the soils significantly influenced the initiation and mode of piping. The presence of non-plastic fines significantly reduced the required seepage velocity to initiate piping (critical seepage velocity), whereas the presence of plastic fines greatly increased the hydraulic gradient required to initiate piping. Concentrated leak erosion occurred along the soil/apparatus interface in soils with plastic fines at very low seepage velocity but required very high hydraulic gradients. Backward erosion was the primary mode of failure in non-cohesive soils. Suffusion was the primary mode of piping in soils that contain very fine non-plastic fines. Initiation of suffusion required seepage velocity an order of magnitude less than that required to induce backward erosion. Once suffusion initiated, it progressed to backward erosion of the soil skeleton at much lower seepage velocity than required for similar soils without non-plastic fines.

Negrinelli et al. 2016 (Negrinelli et al., 2016)

Their research focused on piping in heterogeneous sand and they used the same test set-up used in the current research. The tests performed with "micro-scale heterogeneity" are the most relevant here. The micro-scale heterogeneity is applied by filling the test set-up with water and always introducing a limited amount of soil into the water. Due to differential fall speeds, a layer forms that becomes finer towards the top. Repeating this procedure results in a structure with "fining-upward" sequences. A comparison of the critical head drops between the micro-scale heterogeneity tests and the sand-mixed tests showed that with micro-scale heterogeneity the critical head drop is 28% to 46% higher. The tests without stratification are described by Van Beek (2015) (Van Beek, 2015). The explanation for this is sought on the one hand in the physical barriers that arise during layered application, but also in a decrease in bulk permeability (Hijma & Oost, 2019).

4. Modelling and analysis SSE

In this chapter, the small-scale piping experiments on tidal sand (SSE), conducted by Deltares, are modelled. The obtained results are analysed to find an answer to sub-question two. In short this means quantifying the resistance against piping in tidal sand. This is done by comparing the results of the experiments with the outcomes of the modelling and analysis of the experiments.

In the first paragraph the experimental set-up and results of the experiments are discussed. The second paragraph describes the modelling in 2D with Sellmeijer's formula and modelling software D-Geo Flow. The third paragraph contains the analysis of the results.

4.1. Experiments on tidal sand

4.1.1. Experiment set-up

The piping erosion process in tidal sands is investigated by Deltares with small-scale experiments with a circular outlet configuration. The experiments were performed using a setup consisting of a rigid box filled with sand covered by a transparent plate, a water supply system and several riser tubes to measure pore pressure at various locations in the sand sample (Negrinelli et al., 2016) (Figure 48). The riser tubes are placed in the box as depicted on the left side of Figure 48. The set-up is used in other scale experiments where the pressure differences in the cross direction were important. In this case, the data from these tubes is not relevant but the set-up is appropriate to perform the experiments.

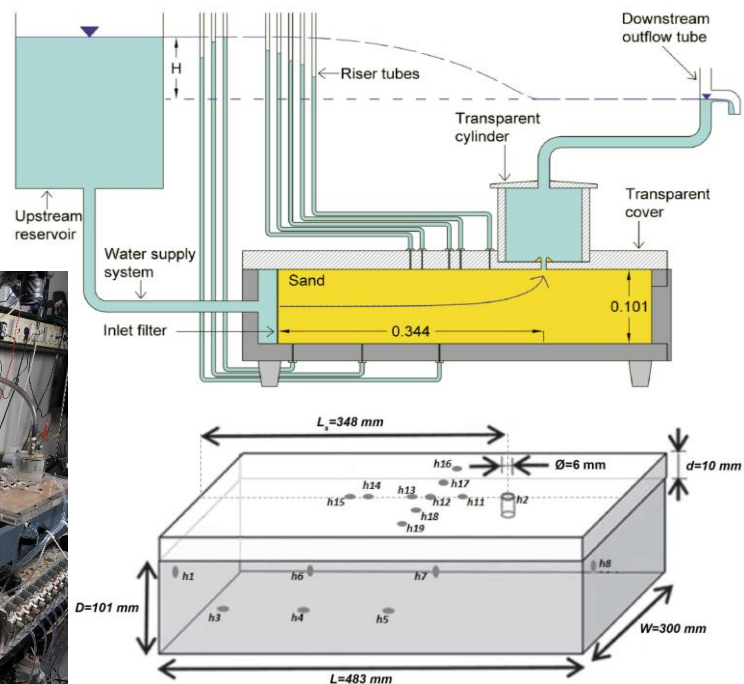


Figure 48 - Pictures of the experiment, measuring discharge and writing down the rise heights (L), schematic of the flow and riser tube measurements (T) and placement of the riser tubes (R) (Hijma & Oost, 2019; Negrinelli et al., 2016)

4.1.2. Material from the field

Tidal sand is collected from the *Grevelingenmeer*, *Vijffluizen* in *Friesland*. Besides retrieved soils, also soil mixes were prepared. The sand from the *Grevelingen* was collected at a location which was near to the tidal channel *Springersdiep* (Figure 49) before construction of the *Brouwersdam*. This material can be identified as weakly silty sand. The material from *Friesland* comes from a tidal channel deposit and can be identified as strongly silty and strongly sandy clay. The material is dried and remolded before applying.



Figure 49 - Location of the Springersdiep on a map from 1960, the sand sample was retrieved at the red circle on the map (Hijma & Oost, 2019)

The first three of the ten experiments were conducted on weakly silty mixed tidal sand from the *Grevelingen* (G). In the fourth experiment, two vertical clay layers perpendicular to the flow were applied and in the fifth test one clay layer. For applying the clay layers, a subset of fine material from the tidal sand was first obtained. This is done by pouring the tidal sand into a water column and then suctioning off the suspended material. In this way, fine material is obtained that corresponds to material that settles under natural conditions and forms a clay layer during the turning of the tide (see also 3.2.3). At the desired location in the container, this fine material is used in the thin layer of water to form a clay layer. During the fourth test this was done in two places, with the upstream layer having a thickness of about 10 mm and the downstream layer having a thickness of about 5 mm. In the fifth test, one layer of 5 mm was applied. Two grain size samples were taken from the clay layer which showed that the d_{50} is between 2-3 μm . The clay consists of 45% lutum, 52% silt and 3% extremely fine to very fine sand and can therefore be labelled as moderately silty clay. The strongly silty sand and strongly sandy clay (F215) from *Friesland* was used in three experiments (sixth, seventh and eighth experiment). This material had a much lower permeability than the sand from the *Grevelingen*. Finally, two experiments with Baskarp (B) sand with added Kaolinite clay (K, deemed to have no cohesion caused by biochemical influences), one and three weight percentage respectively. This Kaolinite clay represents the fine fraction in between the larger Baskarp grains. Both mixes are classified as weakly silty sand. The soil characteristics are given in Annex I.

Ideally, at least two identical experiments must be carried out for each test set-up in order to be able to compare the results. Due to time constraints, it was not possible to do two identical experiments with clay layers and Kaolinite. Instead, two experiments with different clay layers and different Kaolinite content were performed. The clay layers are present over the entire width/height and thus form a vertical screen of clay. In the first three experiments, the tidal sand is mixed. This means that the sand from the *Grevelingen* is first dried and then stirred. When applying the sand, the container is tilted and the downstream side is removed. Subsequently, a thin layer of water is applied via a hose at the bottom of the tray and sand is sprinkled in from above through this thin layer of water (in accordance with Van der Poel and Schenkeveld, 1998). The sand is tamped in between to obtain the desired relative density. This density is determined separately after the test. Subsequently, small amounts of water and sand are added to the container until the container is full, with tamping in between. Because thin layers of water are used, the sand does not separate into a fine and coarser fraction and is therefore applied well mixed.

4.1.3. Results

The results of the experiments are presented in Table 7. It is directly observed that the results differ a lot from each other (min. 19 cm and max. 180 cm). There are three noteworthy odd results. The first one is that large differences between experiments conducted on the same material are observed. This probably has to do with very small differences in the preparation of the sand sample, influencing the permeability, which has a large impact on the piping process. Also, remolding, drying and re-wetting of the material has an influence on the outcome. Another odd result is obtained in experiment G211. This experiment contains a vertical clay layer but the critical head difference is almost equal to the experiments without a clay layer. There is no reasonable explanation for this result at this stage. The third odd result is that the critical head difference in experiment F213 is 180 cm. This is very (almost unrealistically) high and this is because the fines content is such that the soil is identified as sandy clay.

Table 7 - Results critical head difference SSE

Nr.		$H_{c,m}$ [cm]
1	G207	36
2	G208	26
3	G209	25
4	G210	116
5	G211	26
6	F213	180
7	F214	60
8	F215	50
9	B & 1%K	19
10	B & 3%K	81

4.2. 2D modelling

To model the scale experiments on tidal deposits, D-Geo Flow is used (Deltares, version 1.3.0.38595). In D-Geo Flow, cross-sections can be modelled and 2D piping calculation can be performed. In D-Geo Flow a piping module is present to predict whether progressive piping can occur or not, given a certain water level. This module is based on Sellmeijer's model, in which the force balance of the grains in the erosion channel is assessed. In D-Geo Flow the subsoil can be modelled and 2D transient groundwater flow calculations can be performed. In these calculations, time-dependency and changes in the phreatic level are incorporated.

4.2.1. D-Geo Flow

The program has six main input categories: program settings, materials, boreholes, boundary conditions, a pipe and the mesh.

Program settings

The program settings first ask in how many timesteps the desired water level must be increased. The second setting is the output interval, the time between two calculations. It is useful to have multiple output steps per water level increase so the output interval should not be lower than the timestep chosen before. The third setting is the MPicard number. MPicard controls the step size by which the pipe height is adjusted to achieve equilibrium. The step size is $100 \cdot d_{70} / \text{MPicard}$. A larger step size (smaller MPicard) results in a lower accuracy but faster calculation and vice versa (Deltares, 2017).

Materials

Two types of material are distinguished; soil and water. For the water the compressibility, density and viscosity must be given and for the soil, the following:

Porosity (n) [-]

Only used in transient flow calculations in which the permeability changes over time. This option is not yet incorporated.

Compressibility (β) [m^2/N]

Belongs to transient flow calculations.

Grain particle density (ρ_s) [kN/m^3]

Submerged particle weight, being $1650 \text{ kN}/\text{m}^3$.

Particle diameter (d_{70}) [m]

White's constant (η) [-]

Calibration parameter, being 0.25.

Bedding angle (θ) [$^\circ$]

Calibrated at 37° .

Hydraulic conductivity ($K_{x,y}$) [m/day]

Boreholes

The cross section (Figure 50) is built from boreholes, in between which the layers are interpolated. The input consists of; x-location, top level, soil type and layering.

Boundary conditions

Because the cross section is cut from the rest of the world, boundary conditions at these cuts are needed. D-Geo Flow knows 5 types of boundaries (Deltares, 2017; Knops, 2018):

1. Head boundary: A constant head, must be assigned to the boundaries which are in contact with a uniform head in time and space;
2. Flux boundary: A boundary at which water is crossing the boundary in or out of the model;
3. Seepage boundary: A boundary through which water can seep into the outer atmosphere;
4. Submerging boundary: A variable head must be assigned to the boundaries which are in contact with a water level that is variable in time;
5. No-flow boundary: Assigned to locations where no flow crosses the boundary.

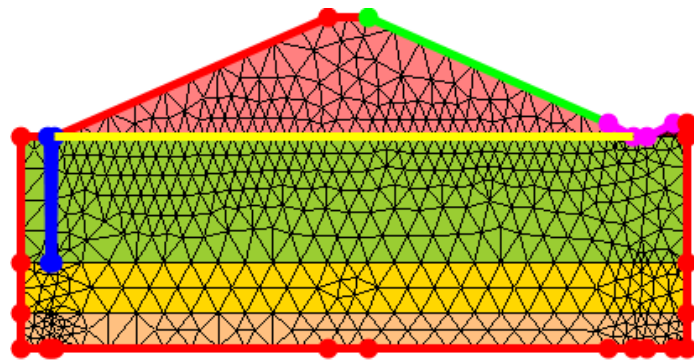


Figure 50 - Example of a cross section with an infiltration pipe in D-Geo Flow; pipe (yellow), mesh (black) and boundaries (blue = river water level, red = no flow boundary, pink = polder water level and green = seepage boundary)

Pipe

In D-Geo Flow, a pipe must be added manually and must be in contact with the outer atmosphere on both sides. This means that entry and exit points must already be added in the model, by use of the boreholes. The pipe can only grow between two horizontal layers of soil (Figure 50).

Mesh

The last step in setting up the model is generating the mesh. In the grid menu, two values must be chosen: The default mesh coarseness and the pipe coarseness. The mesh coarseness is the size of one side of an element in the grid. The pipe coarseness is the factor by which the elements around the pipe are smaller than the normal elements. Large elements lead to more inaccurate results and vice versa.

4.2.1.a. Limitations

The limitations of D-Geo Flow are listed below:

- **Validation**
The model is not validated with field- and experimental data.
- **Changing cross section**
All boreholes need to be changed when a layer is added and materials can only be used in one layer, otherwise a new soil type must be made and assigned.
- **Horizontal pipe**
D-Geo Flow can only calculate horizontal erosion and this erosion is placed underneath the dike body.
- **Complex cross-sections**
Complex geometries with small elements besides larger elements will give errors. This is mainly because D-Geo Flow will create elements with more than 3 sides. These errors are solved by choosing different grid properties, resulting in smaller grid cells which results in longer calculation times.

4.2.2. Input parameters D-Geo Flow

Modelling in D-Geo Flow starts with defining the timesteps in which the measurements in the program need to be done. In the experiments on tidal sands, the water level is raised 1 cm every 5 minutes. This situation is recreated in the model and the output is set to be produced every minute. This leads to an accuracy of 2 mm in the critical head results.

Also, an MPicard number is provided, which determines the depth of the pipe difference (accuracy). A value of 1000 is recommended in the manual and is also used in the model. A value of 2000 (more accurate) results in a very long calculation time and not a lot of difference in the outcome. A value of 500 (less accurate) results in a very conservative critical head difference in a short calculation time.

The grainsize is determined per experiment. The values range from 110–171 μm , see Annex I. The permeability required a more extensive investigation.

4.2.2.a. Permeability

The permeability of the sand used in the experiments is determined by use of Darcy's law in Eq.14. The discharge is measured during the experiment and the head difference between two head sensors is known per timestep at which the discharge is measured as well.

$$k = \frac{Q \cdot L}{A \cdot \Delta h} \quad \text{Eq.14}$$

Sensors 3 and 4 on the bottom (Figure 48) give the most constant values of the permeability during the experiment. For the experiments with clay layers, the total head difference is used to find the permeability of the clay layers.

The permeability of the sand is an important parameter in piping calculations. In the experiments, it is observed that the permeability changes over time (Figure 53). These changes over time are not practical. Only a single value for the permeability per layer and for all timesteps is supplied D-Geo Flow calculations and only a single value for the permeability in Sellmeijer's formula for the whole aquifer is supplied. One value must be supplied and thus chosen from graphs like Figure 51 for every experiment.

The way to come to this single value for the permeability per experiment is described in the paragraphs below. The differences in permeability during the experiments are caused by measuring uncertainties, outflow of fines, converging flow lines and growth of the pipe.

Measuring uncertainties

The measuring of discharge and head is of great importance to the permeability. The discharge is measured by weighing the amount of water flowing out of the box over one minute. This is done every five minutes. This approach leads, especially in the beginning of the experiment when discharges are very low (a few drops per minute), to large uncertainties. The head is measured every 5 minutes at 19 sensors, this leads to a lot of measuring and writing, which could lead to mistakes. The head in the box needs to adapt to the applied head, usually (in case of fluvial sand) this is going very fast (30 sec.) but in case of the tidal sand, this is not known. This could lead to a situation in which the head is applied too fast resulting in pipe-growth without equilibrium (pipe growth and progression at similar head).

To be able to give an indication of the measuring uncertainties, the measuring error is determined. Due to the above-mentioned reasons, eQ (error in discharge) is chosen to be 1 ml/min, eL (error in seepage length) and eA (error in flow surface) are 0 because of the standard size of the box and the error in head measurements (eh) is 2 mm. The error in permeability due to measuring uncertainties (eK) is calculated as follows:

$$eK(Q, eQ, L, eL, A, eA, h, eh) := \sqrt{\left(\frac{d}{dQ} k(Q, L, A, h) \cdot eQ\right)^2 + \left(\frac{d}{dL} k(Q, L, A, h) \cdot eL\right)^2 + \left(\frac{d}{dA} k(Q, L, A, h) \cdot eA\right)^2 + \left(\frac{d}{dh} k(Q, L, A, h) \cdot eh\right)^2}$$

An example of the determination of the permeability and the visualization of the error are given in Figure 51. It can be observed that the error in permeability is very high at the beginning of the experiment, when discharges are low. The chosen value is in line with the trend in the middle part of the experiment, as close as possible to the permeability just before the start of pipe growth. The permeability over head in the other experiments are added in Annex III and the chosen permeabilities in Annex I.

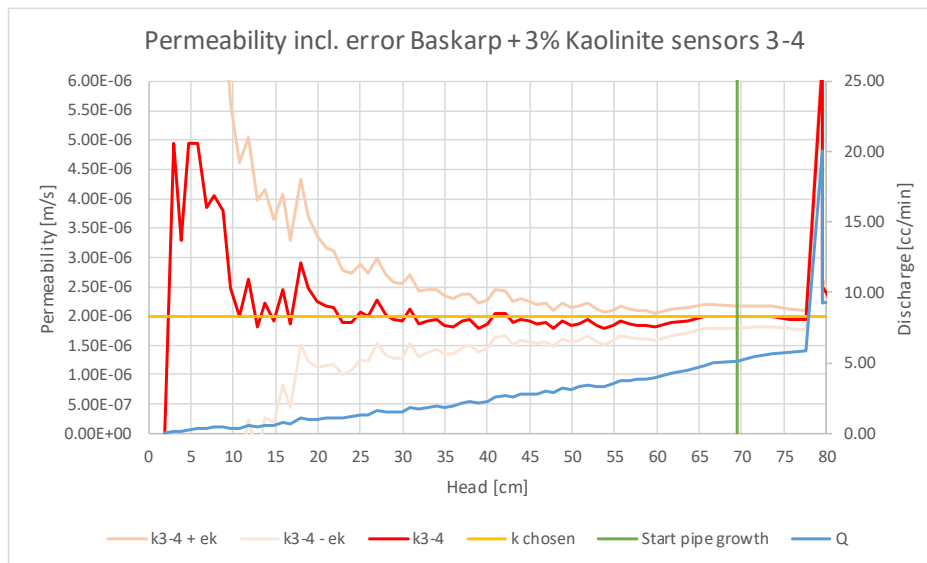


Figure 51 - Permeability of the experiment on Baskarp with 3 w% Kaolinite. The error bands are shown in light red and the discharge in blue. The green line indicates the applied head at which the pipe started growing visibly

Outflow of fines

Figure 53 shows two groups of permeabilities in the SSE. The first group starts high and then drops fast to become stable. This is assumed to be due to the uncertainties in permeability but also due to the outflow of fines to the exit. The first group of soils looks more like Figure 52a, when the head difference is applied, the fines can flow out of the larger grain matrix towards the outflow. The number of fines near the outflow becomes very high, thereby clogging the outflow, leading to a lower overall permeability after a while. The second group has a more stable and low permeability. It is assumed that this groups grain structure looks more like Figure 52b. When the head difference is applied, the fines cannot flow out because of the higher number of fines being present. Therefore, the permeability is low at the start and increases slowly during the experiment. The groups are clearly divided in terms of average: uniformity (8 times higher in group 2), permeability (4 times lower in group 2) and fines content (4 times higher in group 2).

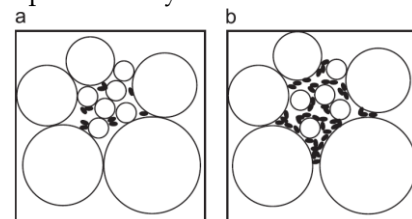


Figure 52 - Gap-graded soils with a low fines content and medium fines content (Chang & Zhang, 2013)

Flow lines

The uncertainty in permeability is also linked to the flow lines during the experiment. The flow will concentrate at the top of the box because the outflow is situated at the top as well. Since sensors 3 and 4 are situated at the bottom, somewhat higher heads will be measured than at the top where flow velocities are higher. A second influence is that the inflow of the box is not over the whole width. At both sides, a 5 cm reduction is present. This causes the flow to be concentrated in the center of the box. The used flow area (A) is the whole width multiplied by the height. The reduction at the inflow may lead to an underestimation of the permeability.

Growth of the pipe

The permeability during the experiments changes when the pipe starts to grow. The loss of material creates more space for the water to flow. The flow velocity in the pipe goes up, leading to lower pressures. The lower pressures cause an increase of attraction of water around the pipe. One of the experiments displayed in Figure 51, shows that at the end of the test, the permeability shoots up. Other experiments show also differences in permeability right after pipe growth is observed. The choice of permeability to use in the calculations is before pipe growth has been observed.

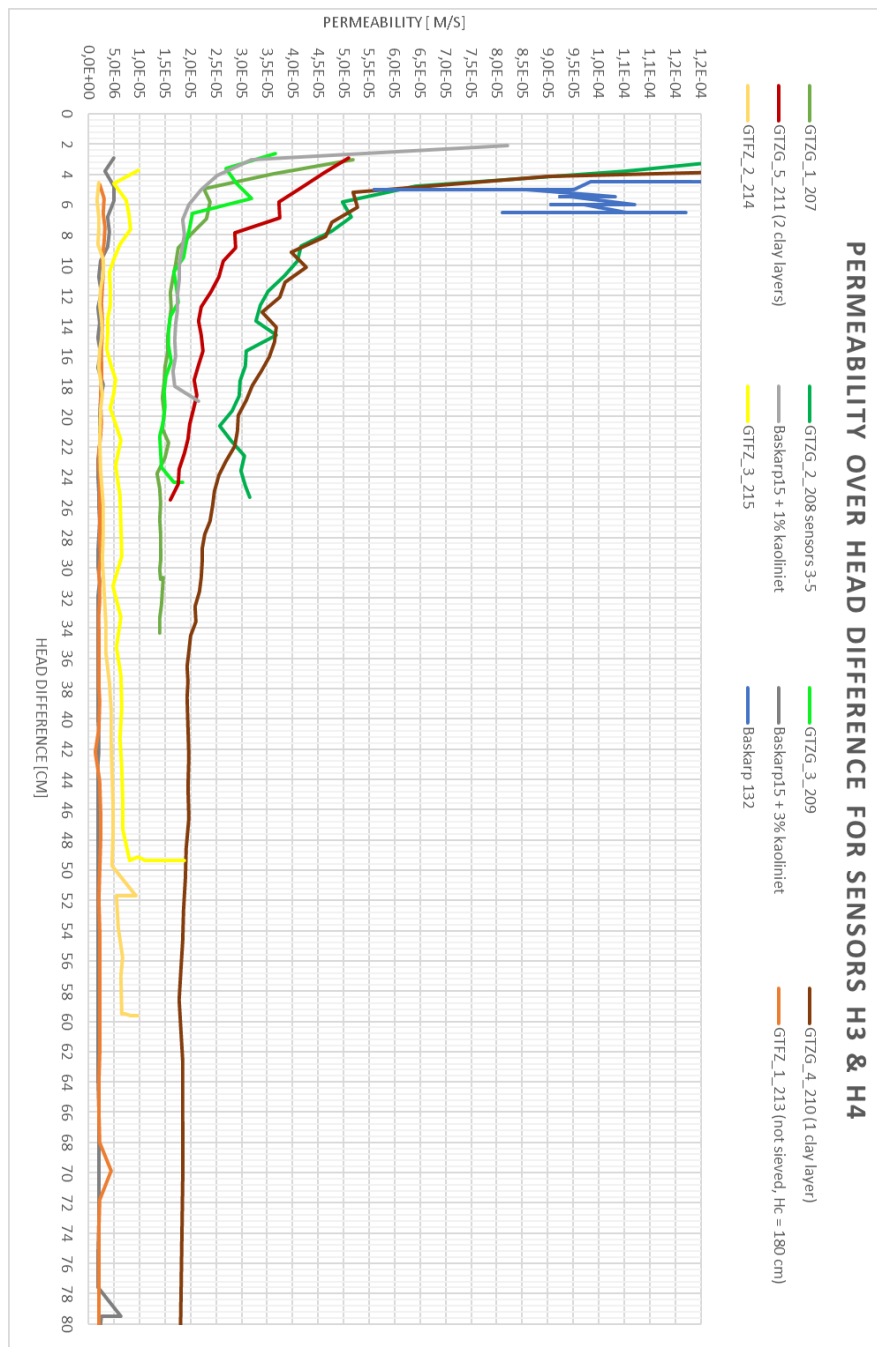


Figure 53 - Permeability over head difference for the small-scale experiments on tidal sands. Green=Grevelingen sand, Brown=Grevelingen sand with clay layers, Orange=Friesland sand and Grey=Baskarp sand with Kaolinite clay

4.2.3. Model configuration

The next step is to model the experiment set-up in D-Geo Flow (Figure 54). The yellow part is the tidal sand, the top red layer is an impermeable layer which represents the plexiglass cover. The inflow is given in blue, representing the high-water level over the entire filter. The outflow is situated at the small purple line with a width of 6 mm. The mesh is set to create grid cells of 1 cm wide and close to the pipe 5 times as small. Constant head boundaries are assigned to the inflow (blue) and the outflow (purple). The remaining boundaries (red) are no flow boundaries.

4.2.4. Sensitivity

The critical head difference is expected to be very sensitive to the permeability. The sensitivity of the permeability on the critical head difference is determined by calculating the critical head values with the lowest and the highest permeability measured in the experiments.

Anisotropy is not considered because it is expected that the effect of anisotropy is very limited due to the remolding of the sample and the small scale.

The 3D-effect is expected to be fully present since the hole type of outflow requires the flow

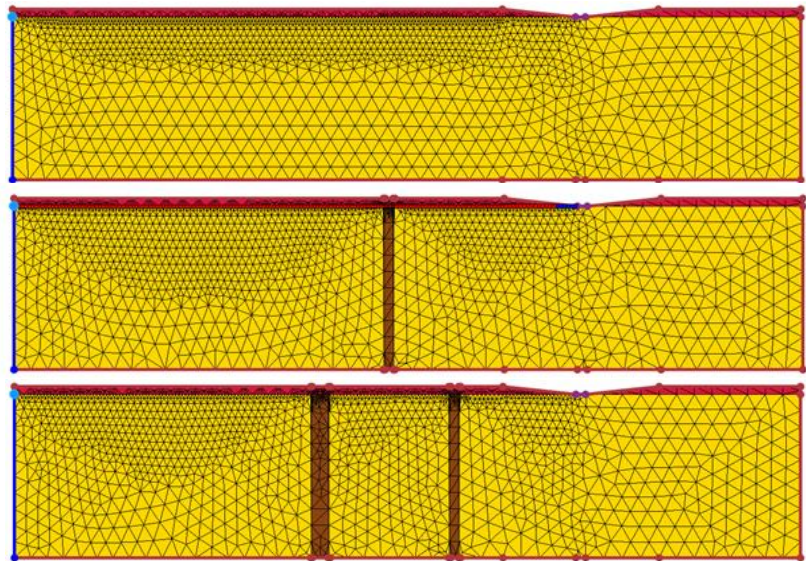


Figure 54 - Model set-up D-Geo Flow for the experiments with and without vertical clay layers

lines to concentrate towards the outflow. To give insight into the 3D-effect at this scale and with the same type of outflow, experiments on fluvial sand by Van Beek (2015) are used (Van Beek, 2015). Ten experiments with the exact same set-up but with a higher permeability and larger grains than the tidal sand experiments are performed, all of which the measured data from the experiments is known.

4.2.5. Results

The critical head differences calculated with Sellmeijer's formula and calculated with D-Geo Flow in the tidal- and fluvial sand experiments are presented in Table 8 and visualized in Figure 55. The results in Table 8 compare 3D experiment results with 2D calculations. This is further evaluated in 4.3.1..

Table 8 - Results SSE on tidal sand and fluvial sand (3D) compared to 2D calculations with Sellmeijer's formula and D-Geo Flow

Tidal sand experiments				Fluvial sand experiments			
Exp.#	$H_{c,measured}$ [cm]	$H_{c,Sell}$ [cm]	$H_{c,DgeoFlow}$ [cm]	Exp.#	$H_{c,measured}$ [cm]	$H_{c,Sell}$ [cm]	$H_{c,DgeoFlow}$ [cm]
G207	36	31.3	25.8	B132	6.5	15.9	15.0
G208	26	24.0	20.6	B142	8	20.4	16.8
G209	25	31.0	25.8	S170	35	24.7	19.6
G210 - 2 clay layers	116	45.5	30.6	E169	8.5	18	14.2
G211 - 1 clay layer	26	36.9	24.0	O163	18.5	16.1	17.0
F213	180	45.3	38.2	O140	9.5	16.2	15.0
F214	60	42.9	36.6	W130	10.6	13.2	12.0
F215	50	38.7	32.8	W131	8.6	12.9	11.8
Baskarp + 1%K	19	32.2	26.0	I166	21	27	20.8
Baskarp + 3%K	81	65.5	48.2	I168	20.5	29.8	23.8

A clear difference between the calculations with Sellmeijer's formula and D-Geo Flow is observed. The critical head differences of the experiments on fluvial sand by Van Beek (2015), calculated in D-Geo Flow are on average 13% lower than the ones calculated with Sellmeijer's formula. For the experiments on tidal sands, this is found to be 21% on average. It is not known where this difference comes from.

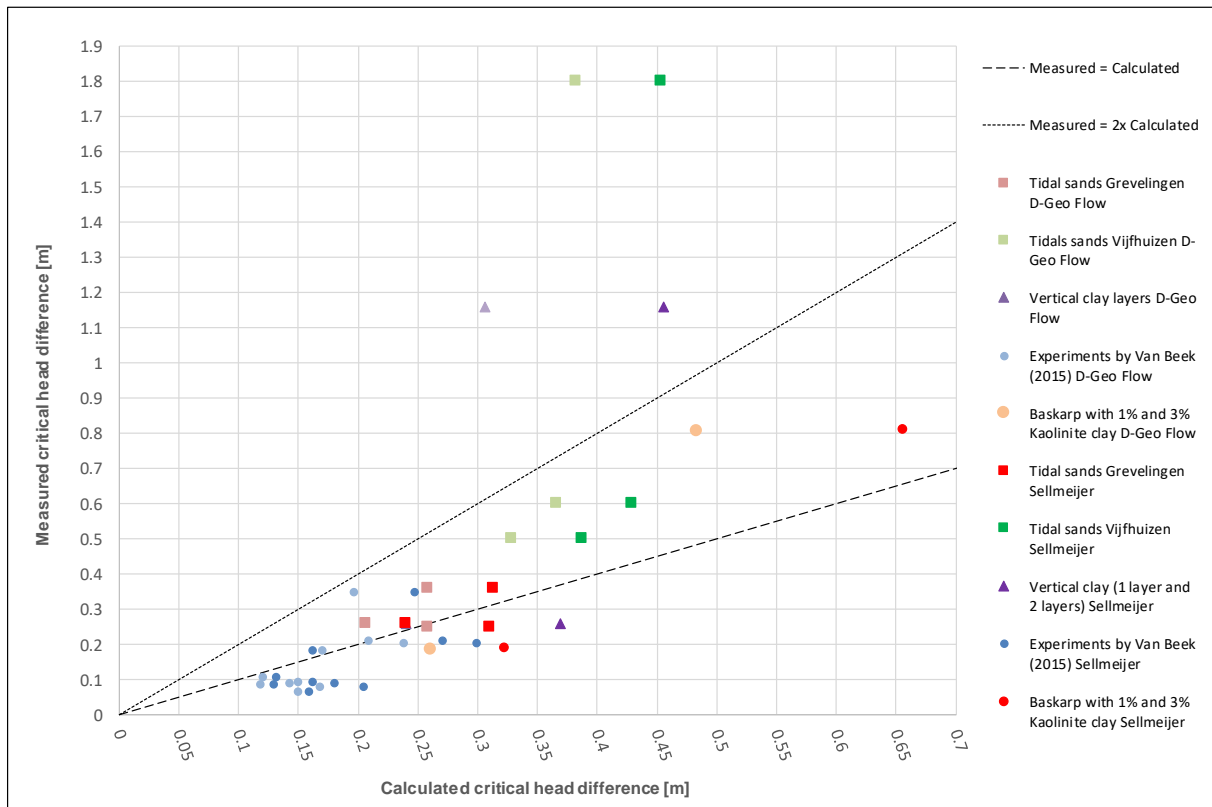


Figure 55 - Results SSE, measured and calculated with Sellmeijer's formula and D-Geo Flow

4.3. Analysis

On the retrieved results from Sellmeijer's formula and D-Geo Flow calculations, the data from the experiments and the known characteristics of the material, an analysis is conducted to see if there are differences in strength between fluvial sand and tidal sand. As a first step, the 3D-effect is quantified. Next, the strength which remains (when the 2D results are divided by the 3D-factor, see 4.3.1) is calculated. That remaining additional strength can be assigned to 1) fine material (all experiments except with clay layers, especially the experiments with Kaolinite clay), 2) vertical barriers and 3) cohesion.

4.3.1. 3D-effect

To obtain a factor over the critical head difference to account for the 3D-effect, the experiments (By Van Beek, as mentioned earlier) on fluvial sand are used. These experiments are used because they have the same set-up (small scale and hole type of outflow) as the experiments on tidal sand and the calculated results are not influenced by the processes that are expected to influence the results in tidal sand. When the results from Sellmeijer and D-Geo Flow calculations are compared to the experiments, the average 3D-effect factor ($H_{c,2D}/H_{c,experiment(3D)}$) is 1.5. This factor is also affected by the modelling error of D-Geo Flow. It is expected that the difference between this 1.5 and the value of 2 found by Van Beek (2015) is explained by: 1) Van Beek used small- and medium scale experiments. The 3D factors found there vary between one and two, as presented in Figure 56. As described in 3.1.3.g, the critical head depends on the width of the model. The width determines the bending and concentration of the flow lines. The found 3D factor of 1.5 could be linked to the small-scale. 2) It is expected that the 3D-effect is also linked to permeability (lower permeability means lower 3D-effect). This is not considered due to time constraints but due to the lower permeabilities it is expected that the 3D-effect is lower in tidal sand than in fluvial sand because when the permeability is low, less water from the surrounded soil is attracted by the exit. The calculated critical head differences with Sellmeijer's formula and D-Geo Flow are divided by the 3D-factor of 1.5 (small-scale!).

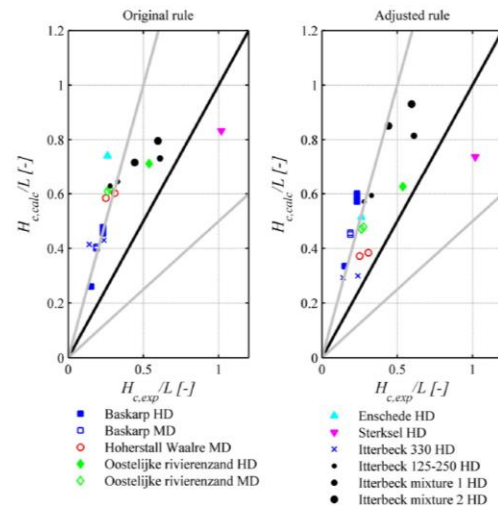


Figure 56 – Results of small- and medium scale experiments with a hole type of out-flow (3D) calculated with Sellmeijer's model (2D, original and adjusted form) (Van Beek, 2015)

Another option to determine the 3D-effect was by use of the 3D piping module DgFlow. This has been done but due to large uncertainties in model input parameters and of course the unknown influence of strength, the results were not useful to quantify the 3D-effect. The performed work on this 3D modelling is included in Annex VIII.

4.3.2. Tidal sand strength

The influence of tidal sand on the difference between critical gradients measured in experiments and calculated with piping models is measured by the Strength Factor ($SF = H_{c,measured} / H_{c,calculated}$). This factor indicates by what factor the model outcomes (calibrated on fluvial sands) differ from the values measured in the experiments, thereby indicating the effects which are not yet considered in the piping assessment. The mean SF in the experiments on tidal sand is 2.5 (when the 3D-effect is considered). That is the average of 2.2 calculated with the Sellmeijer formula and 2.8 calculated with D-Geo Flow. This means that the water level difference over the flood defense, situated upon tidal sand layers, at which piping will occur can be 2.5 times higher than calculated with Sellmeijer's model.

Sensitivity to permeability

The SF, when the highest permeabilities found in the experiments (see 4.2.2.a) are used, on average goes up with 18% and down by 10% when the lowest permeabilities are used. This leads to an upper bound of the SF of 3.0 and a lower bound of 2.3.

Subdivision of effects

The additional strength can be assigned to: 1) fine material (all experiments except with clay layers, especially the experiments with Kaolinite clay), 2) obstacles to the flow and 3) cohesion. The analysis on these influences is performed in the next paragraphs.

4.3.2.a. Weight percentage of fines

As suggested by Hijma & Oost (2019), the fines content indeed shows a positive correlation with the increase in strength (Figure 57). The experiments that are not used in this analysis, because they are influenced by other processes, are the ones with vertical clay layers. The results show that when fines are added to the sand, the head difference at which piping occurs goes up. The presence of these fines, as discussed in 3.2.5.b, affects the internal stability (which influences the permeability), uniformity and grainsize d_{70} of the soil. Since uniformity (representing the grainsize distribution) is not considered in Sellmeijer's model, the absence could be the reason of the large differences between the calculated and measured values. The processes which are thought to causes the additional strength are 1) that the fines surround the larger grains, causing the grains to be less easily removed and 2) physical cohesion.

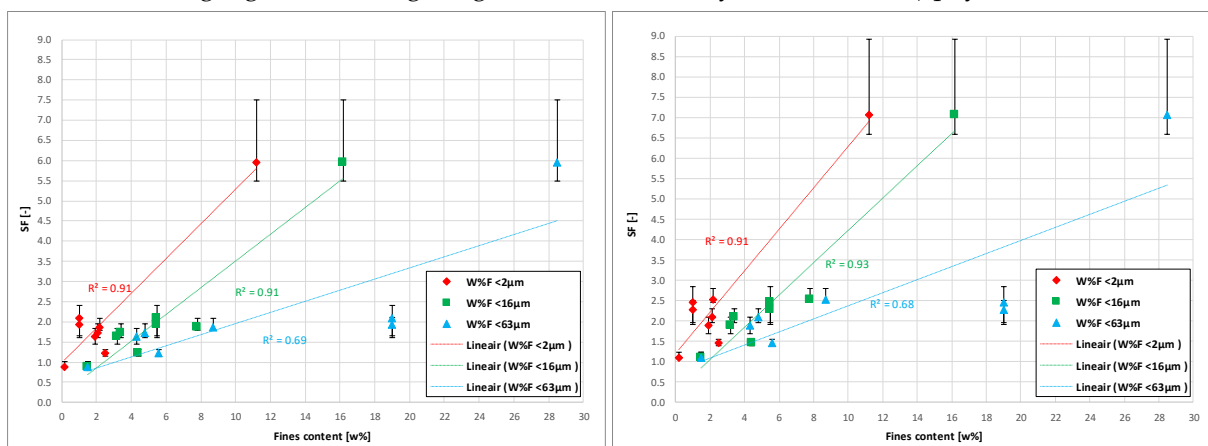


Figure 57 – SF (strength) over $w^0\%$ of fines (left Sellmeijer and right D-Geo Flow). The black bars represent the bound when the minimum and maximum permeability, measured in the experiments, is used to calculate the strength

When linear regression is performed, the highest coefficient of determination (R^2) is found for the weight percentage of fines in the grainsize $<16 \mu\text{m}$. When only the experiments with Baskarp sand and Kaolinite clay are considered, where cohesion and vertical clay layers are excluded, the additional strength follows the path drawn in Figure 58.

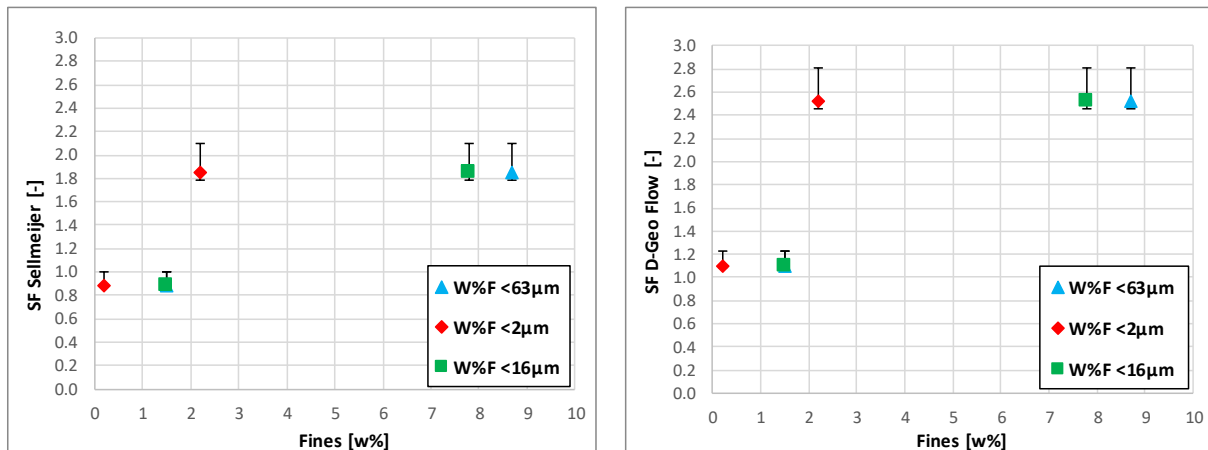


Figure 58 – SF (strength) over w% of fines of the experiments with Baskarp sand and Kaolinite clay (left Sellmeijer and right D-Geo Flow). The black bars represent the experiments the bound when the minimum and maximum permeability, measured in the experiments, is used to calculate the strength

Permeability

An important notion is that the fines content influences the permeability, which is an important influence in the piping process. In the experiments the permeability went down with increasing percentage of fines. Kong et al. (2011) also found that the increase of fines has a large impact on the permeability. The permeability went down significantly when the percentage of fines was in between 10-25%. Below 5% the effect was minor (Kong et al., 2011). Figure 59 shows the correlation between the percentage of fines and the permeability in the SSE, when looking at the different grain size fractions.

Permeability is accounted for in Sellmeijer’s model. This means that another effect, caused by the presence of fine grains, must lead to such a significant increase in piping resistance.

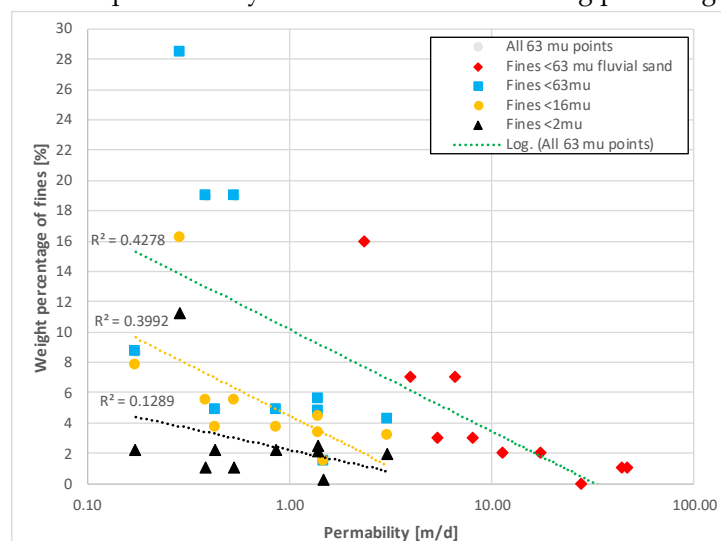


Figure 59 - Permeability over percentage of fines

Grainsize distribution

Besides permeability, also the grainsize distribution is affected by the addition of fine grains. The grainsize is incorporated in Sellmeijer’s model by use of the d_{70} . The d_{70} of tidal sand is expected to be somewhat lower than of fluvial sand. This would lead to lower critical head differences because smaller grains are more easily eroded from the pipe. Since d_{70} is directly supplied in Sellmeijer’s formula, it means that this does not explain the increase in piping resistance. A means to represent the grainsize distribution in tidal sands is the uniformity coefficient. The uniformity coefficient of tidal sand is expected to be higher than the uniformity of fluvial sand. This is expected because the combination of large grains and fine material causes tidal sand to be less well-sorted than fluvial sand. This means that d_{60} and d_{10} are further from each other, resulting in a higher uniformity coefficient. In Figure 60 the

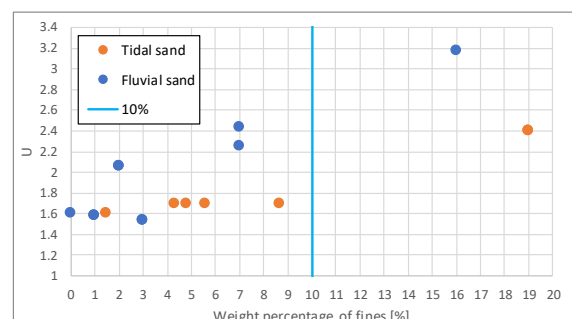


Figure 60 - Uniformity over fines percentage (<63 µm)

uniformity coefficients of the material in the SSE is presented. This graph shows that an increase in uniformity coefficient will be more significant if the fines percentage is higher (i.e. the d_{10} is a lot lower when the fines percentage is above 10%).

Van Beek (2019) showed that with an increasing uniformity coefficient, the critical gradients increase (Figure 61). For the experiments on tidal sand the influence of uniformity coefficient on the Strength Factor is evaluated (Figure 61) with the lowest bound in purple), except for the experiments with clay layers. A positive correlation is found between the Strength Factor and the uniformity coefficient. Since the values of the uniformity coefficient are relatively close together, more data should be gathered to confirm this relation. An advice is to use a uniformity with d_{60} and d_5 instead of d_{10} . In that case, the fines are better represented and the relation is expected to be clearer. This would require a new calibration of Sellmeijer's model.

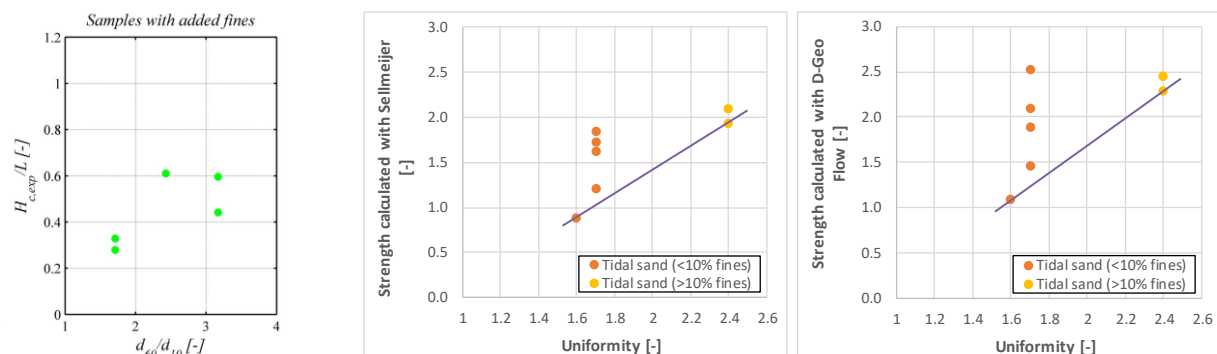


Figure 61 - SF (strength) over uniformity coefficient (Van Beek, 2015) (L) and strength factor varying over uniformity (middle Sellmeijer and right D-Geo Flow) (R)

4.3.2.b. Obstacles to flow

To assess the influence of obstacles to the flow, the experiments with vertical clay layers are evaluated. It is observed that the pipe develops to the clay layers, then stops until the local gradient is high enough to grow through the clay layer. When the clay layer breaks, the pipe immediately progresses towards the next obstacle or the end. It is therefore assumed that other influences like fines and cohesion are influenced a lot by the presence of obstacles to the flow. In the experiments it is observed that every layer needs a pressure built up, therefore it is assumed that the number of layers is important to the piping process in aquifers with vertical layers. More experiments on different scales must be performed to underline this theory because only two experiments are available with a maximum of two layers. The results of the experiments are given in Figure 62. The x-axis is scaled by use of Eq.15 because it is expected that the number of layers, total width of these less permeable layers and the distance over which these layers are spread are important to the observed process.

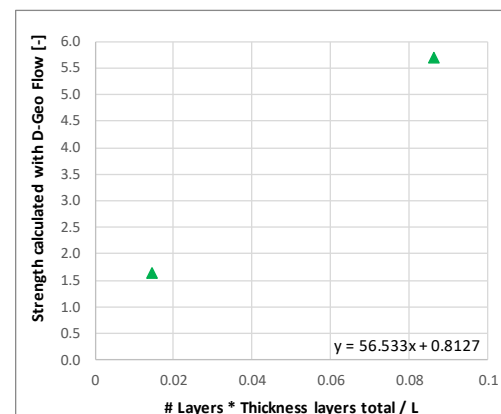


Figure 62 - SF (strength) in relation to number of layers, width of the layers and seepage length (G210 and G211)

$$\frac{\#_{layers} \cdot W_{layers,total}}{L} \quad Eq.15$$

4.3.2.c. Cohesion

Physical and/or biological cohesion is assumed to be present in the soils from the *Grevelingen* and *Friesland* although they are remolded and applied homogenous. In these experiments (as shown above) also the influence of fines is present, an attempt is made to remove this influence by the known relation between the SF and w% of fines <16 μm (4.3.2.a) in the Baskarp with Kaolinite experiments. This is done by linear regression between datapoints in Figure 58, resulting in:

$$SF_{F, Sellmeijer} = 0.154 \cdot W\% F < 16\mu m + 0.653 \quad Eq.16$$

$$SF_{F, DGeoFlow} = 0.226 \cdot W\% F < 16\mu m + 0.757 \quad Eq.17$$

Since the w% of fines <16 μm is also known for the experiments where cohesion is expected, the SF can be reduced by Eq.16 and Eq.17, depending on the w% of fines <16 μm. This results in an average Strength Factor due to cohesion (SF_c) of 1.8 calculated with Sellmeijer and 1.7 calculated with D-Geo Flow.

Incorporating cohesion in Sellmeijer's model

A means of taking cohesion into account in Sellmeijer's model is to change the calibrated bedding angle. When cohesion is present between soil particles, they are less easily removed when drag forces are applied, i.e. the critical shear stress is higher. As described in (3.1.3.d), the critical shear stress depends on the bedding angle (Eq.18) in White's formulation. When the bedding angle increases, the critical shear stress increases.

$$\tau_c = \eta \frac{\pi}{6} \gamma_p' d \tan(\theta) \quad Eq.18$$

The experiments on tidal sand are recalculated with Sellmeijer's formula with an increasing bedding angle to come to the strength in tidal sand of 1.8. The bedding angle at which the calculated strength is 1.8 is 46° instead of the calibrated value in Sellmeijer's model of 37°. The bedding angle influences the critical head difference linearly. An important notion is that it is not sure which erosion process (primary or secondary) is affected by the cohesion. This should be investigated to know if the approach via adaptation of the bedding angle in Sellmeijer's model (which only contains secondary erosion) is the right approach.

Sellmeijer's model is calibrated on a critical Shields parameter (ψ_c) of 0.1 (as mentioned in 3.1.3.d). The critical Shields value in laminar flow Eq.19 for a bedding angle of 46° is 0.136. No clear match with Shields values from literature are found. A further analysis is recommended.

$$\Psi_c = \eta \frac{\pi}{6} \tan \theta \quad Eq.19$$

4.3.2.d. Scale effect

An important difference between the small-scale experiments and the tidal sand underneath dikes is the scale at which piping occurs. Since modelling and experiments are performed at the same scale, this is not an issue for the comparison between the resulting heads (SF). The applicability of the SF on a larger scale depends on the scale dependency of the processes which cause the additional strength. Below, it is argued per process whether it is expected that a scale increase will lead to an increase or decrease of the Strength Factor.

Fine material

A scale increase is expected to lead to more severe clogging of the pores, reducing the permeability strongly at the start of water flow through the exit. A scale increase is therefore expected to lead to a higher Strength Factor. This depends largely on the amount of fine material and the seepage length and should be investigated further by performing experiments on small-, medium and large-scale, using the same material.

Obstacles to the flow

In the SSE, a large dependency of the additional strength (SF) is found with an increasing number of vertical layers. With increasing scale, it is expected that more obstacles to the flow are present (may it be horizontal or vertical layers). Since the variation in permeability in the aquifer can also cause regions to have a higher permeability, the effect could be dampened because the flow will search for the route with the least resistance. In the large-scale experiment it is important to know the layering pattern beforehand and monitor the flow pattern during the experiment. It is not expected that a scale increase will lead to a lower Strength Factor.

Cohesion

The soil in the SSE is dried, remolded and applied homogenous. It is expected that in-situ soil contains undisturbed laminae of cohesive material and chemical concentrations which result in much more bonding between grains than when the sample is dried and remolded. This leads to a higher critical shear stress and more anisotropy because these laminae are horizontal. A negative influence of an increasing scale is the variability of the biofilms. The biofilms are most likely not present over the full seepage length and will differ in composition. Also, the pipe is deeper on a large scale, requiring the biofilm to be present over a larger depth, otherwise the pipe will grow underneath the biofilm. When the bedding angle will be adapted to account for cohesion, the influence works linear on all scales in the Sellmeijer formula.

It is expected that an increase in scale (essentially in-situ so dike-scale) will lead to an increase of the Strength Factor. This needs to be validated with experiments consisting of the same material on different scales.

5. Piping experiment *Hedwigepolder*

In this chapter, the large-scale piping experiment on tidal sand in the *Hedwigepolder*, which is planned for 2021 by Fugro, Deltares and Waterschap Hollandse Delta, is designed. This design is based upon the gained knowledge about tidal sediments in the previous chapters. In the first paragraph main goals and requirements are set. The second paragraph describes the location and in the third paragraph, the sub-soil is analysed. In the fourth, fifth, sixth and seventh paragraph's, the design choices, optimal design, compartments and measurements are discussed respectively.

5.1. Goals and requirements

In this paragraph, the goals that are set by Fugro, Deltares and Waterschap Hollandse Delta, commissioned by the HWBP (HoogWaterBescherminingsProgramma; Dutch alliance of waterboards and the government to secure water safety in 2050) are specified towards a design.

The main objective is to use the practical experiment in the *Hedwigepolder* to determine the actual strength of tidal sand against piping, characterize the strength properties, translate this knowledge and make it applicable for assessment and reinforcement projects of flood defenses in the Netherlands.

The practical experiment serves to validate the opportunities for inclusion of additional strength within the tidal sand by the following influences as discussed in the previous chapter, based on the small-scale experiments:

Fine fraction	}	Strength
Cohesion		
Small scale layering	}	Load (D-Geo Flow)
Vertical layering		
Anisotropy		

The objective is assessed and specified by use of the commonly used SMART-Principle:

Specific

The goal is divided in three parts. The first sub-goal is the validation of the suggested additional strength in tidal sand compared to fluvial sand. This is the critical head difference that will be measured in the experiment compared to the calculated critical head difference with piping models. This will also lead to more understanding of the scale effects. The second sub-goal is the characterization of the strength parameters. The mentioned strength causes in the previous chapter need to be measured and quantified. The final sub-goal is to make the method to quantify the strength increase in tidal sand applicable in piping reinforcement projects. This requires a relation between the SF and the suspected influential parameters which can be measured in the field. A calibration of the Sellmeijer formula or a safety factor to apply over the critical head difference will follow.

Measurable

The measuring of the pipe development needs to be conducted in such a way that the results are accurate enough to perform the validation. The experimental data will be analysed to find a relation between the SF and the influential parameters which can be measured in the field.

Acceptable

The goals are acceptable to all stakeholders: 1) reduction in reinforcement costs for the HWBP in future projects in tidal sand areas and 2) for Deltares, Fugro and Waterschap Hollandse Delta to gain knowledge on different sand types, how they erode and what the influence of the earlier mentioned factors is on the piping assessment.

Realistic

The goals are realistic. By use of small-scale experiments on the earlier mentioned influence factors, the potential of this experiment and the usability in flood safety practice is shown.

Time dependent

The experiment will be executed in 2021 and will take approximately a month time. The analysis of the results will take more time.

In this stage, that leads to the following requirements for the design:

- I. pipe development must occur through the tidal sand layer;
- II. lifting of the cover layer at unwanted locations must be prevented;
- III. measurements must be precise enough to conduct the analysis and to follow the head levels in the aquifer real-time during the experiment.

The experiment must be as realistic as possible; therefore, the following assumptions are made:

- the seepage length is preferred to be large (dike base scale);
- the head gradients at the outflow must be high enough to force piping to occur;
- flow along the sheet pile walls must be limited to prevent pipe growth along the walls;
- the inflow of water must be equal over the width between the sheet pile walls to recreate a realistic piping situation.

5.2. Project location

The experiment will be conducted in the *Hertogin Hedwigepolder* in Zeeland. A 400 m long dike stretch is reserved for piping experiments on the dike that will be removed in the future (Figure 63). The project area reaches towards the tree line further up the road. In this photo, the polder side of the dike is presented at which the outflow will be forced. More about the location can be found in the introduction (1.1).



Figure 63 - Location overview at the Lingestraat in the Hedwigepolder, retrieved from Google maps Street View

5.3. (Sub)surface analysis

5.3.1. Soil drillings and CPT's

Dinoloket (TNO, 2009) provides soil drillings in the polder. From these drillings, the soil profile is constructed in GeoTopv1.3 (Figure 64). The soil profile consists of a clayey surface layer and a fine sandy layer underneath, both part of the *Naaldwijk* formation (tidal clay and tidal sand, light green in Figure 64), a peat layer from the *Nieuwkoop* formation (brown), the coarser sandy *Boxtel* formation and the bottom layer is the Pleistocene coarse sand layer from the *Oosterhout* formation. By use of CPT's retrieved from the Belgian DOV (Dutch: Databank Ondergrond Vlaanderen), a more specific soil profile is constructed Figure 65. The soil in the yellow rectangle (in the photo in Figure 64) is tidal sand from the *Naaldwijk* formation in which the experiment will be performed. This gives an idea about the layering of the soil, cm thick layering with locally some shells and remolded peat.

The *Hedwigepolder* is situated in an area where the Pleistocene sand lies relatively high in the subsurface compared to the rest of the Netherlands. This Pleistocene sand layer is covered by a peat layer and on top of that, tidal sand is situated.

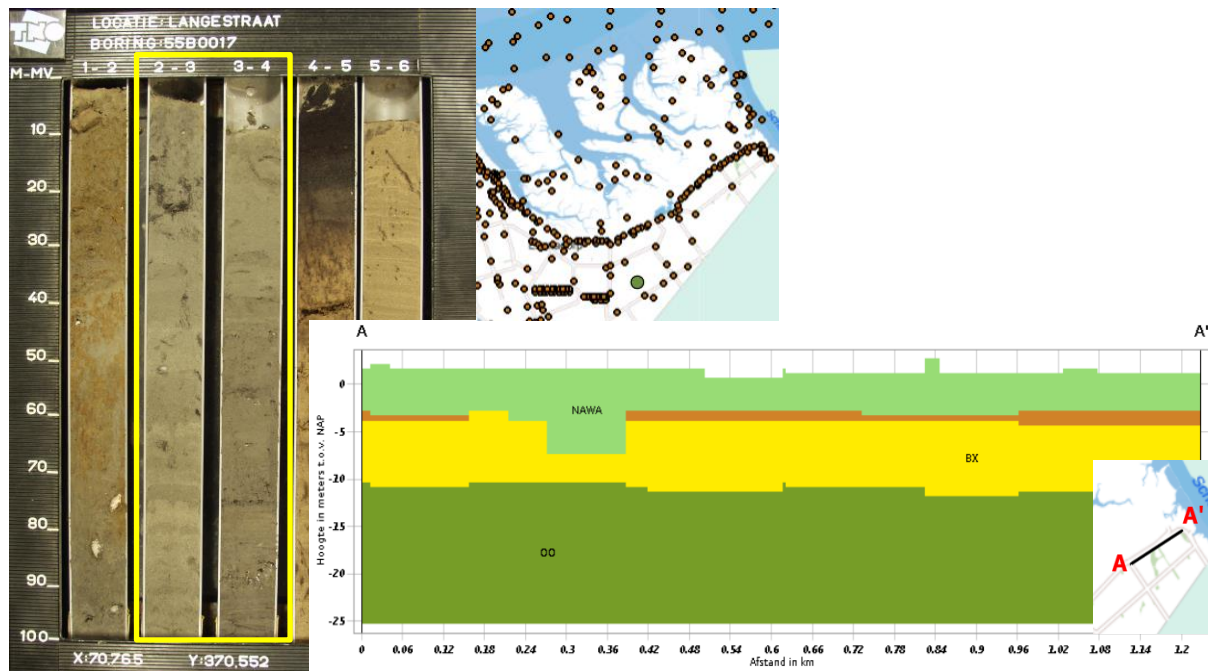


Figure 64 – Soil profile along the dike constructed from soil drillings on the orange dots in the overview figure. NAWA being the *Naaldwijk* formation, BX the *Boxtel* formation and OO the *Oosterhout* formation (see 3.2.3). The green dot is the location of the soil drilling of which the photo is made and the yellow rectangle in the picture is the soil on which the experiment will be performed

5.3.2. Soil parameters

The layers and soil parameters, found in the geotechnical profile, are described.

Surface layer

The surface layer is a clay tidal flat deposit, of the *Naaldwijk* formation. This layer will be removed at the exit to overcome the cover layer resistance and specifically look at BEP. Van Asselen et al. gives an anisotropy factor (A) for silty clay of 10.

Tidal sand layer

The tidal sand layer is a part of the *Naaldwijk* formation, more precisely the *Walcheren* member. It consists of grey fine tidal-channel sand with little thin clay and silt layers and shell fragments. The clay layers are mm to cm thick. The lower part of the layer contains remolded peat. The SOS-code is H_mg_zk with a d_{70} of 130 μm and a permeability of 4 m/d. The permeability is a very important parameter in the piping calculations. The project related CPT's, drillings and soils analysis are not available yet. That is why a comparable study on tidal sand is used to get a better view on the plausible permeability values. The project *Spui-West* is a dike reinforcement project, situated in the same lithological member as the *Hedwigepolder*, in which tidal sand plays an important role. HPT-AMPT measurements (technology in which horizontal and vertical permeability of the soil are determined) are performed to quantify the permeability of the sand. This resulted in an average horizontal permeability of 4.5 m/d with a standard deviation of 2.3 m/d. This is close to the SOS-permeability found in the *Hedwigepolder*. The average anisotropy factor (A) is 8, larger than predicted by Van Asselen et al., see 3.1.3.f. The coefficient of variation is not known for the anisotropy factor. Van Asselen et al. mentions that is largely depend on the fluctuation scales of different parameters of the soil. A safe value of 0.5 is used.

Peat

The third layer from the top, a peat layer in the *Nieuwkoop* formation, has a very low permeability. The *Nieuwkoop* formation is often situated on top of *Boxtel* sand and the member which is considered here is *Basisveen*. The low permeability creates an optimal chance to create a situation in which purely the tidal sand will contribute to the groundwater flow.

Pleistocene sand: *Boxtel* formation

The sand layer situated underneath the peat is part of the *Boxtel* formation. This formation most likely consists of aeolian deposits at the top with sandy brook deposits below. This layer consists of fine to coarse sand and has a d_{70} of 210 μm and the permeability is 15 m/d. At locations where the peat layer is not present, it is expected that a large amount of water (depending on the vertical permeability and the layer thickness of the tidal sand) will flow out in this sand layer because of the relatively high permeability compared to the tidal sand. Van Asselen et al. gives an anisotropy factor (A) of 4.

Pleistocene sand: *Oosterhout* formation

Underneath the *Boxtel* sand, a Pleistocene marine sand layer is situated. This sand is part of the *Oosterhout* formation. The soil properties are equal to the those of the riverbed sand. This is not expected to be the case in reality but not enough data is available to determine the actual permeability. It is expected that the *Oosterhout* formation contains more fines and it's mean grain size is lower because it is a marine deposit. Since this is the third aquifer from the top it is not expected that it has a large influence on the results from the piping calculations.

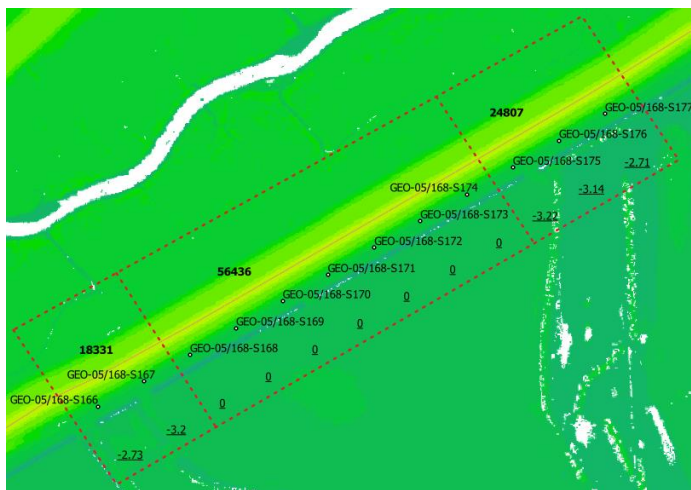
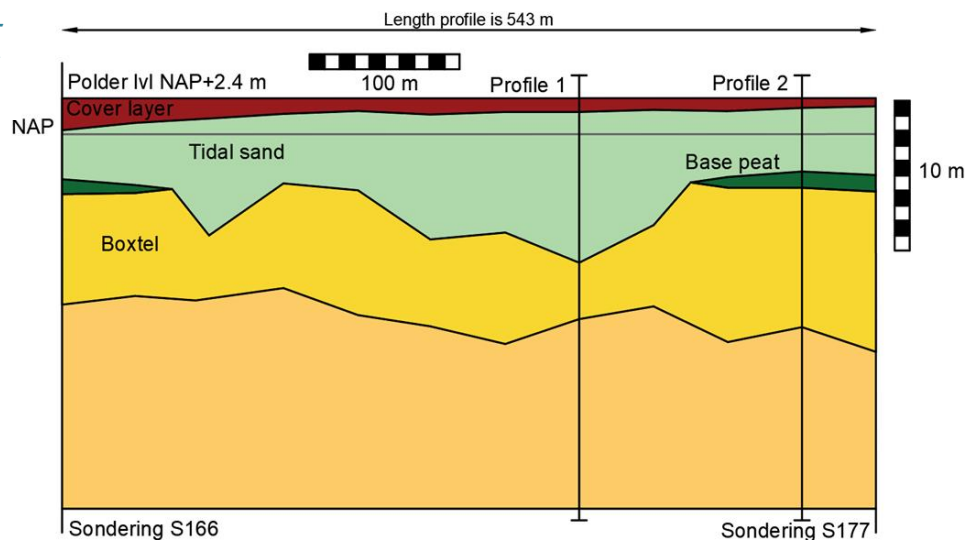


Figure 66 - Project area with CPT's, 50 m from each other. The underlined numbers are the depth of the underside of the peat layer (0 if not present) in the rectangle in the middle there is no peat layer present

Figure 65 - Geotechnical length profile, from left to right in Figure 66.



In common design practice, the design value of the strength is determined by dividing the strength by an overall safety factor. This overall safety factor consists of two partial safety factors: the uncertainty in 1) geometry and 2) modelling (Jonkman, 2018). In the geometry factor, soil layering and hydraulic gradients are considered. This factor lies between 1 and 1.3 and depends largely on layering scenarios (MIM, 2017). In the modelling factor, parameter-, model- and required safety level uncertainty are considered. The factor for modelling lies between 1.2 and 1.8 and is completely depending on the target failure probability of a stretch of dike. These two factors are multiplied by each other after which, in this case, the resistance would be multiplied by that factor of safety.

The partial safety factor for modelling (largely depending on the required safety level) is not considered because the safety level is not of importance because no human lives or economic damage is involved when the construction fails. The partial safety factor for soil layering and hydraulic gradients is applied because, especially in tidal sand, variations in layer forms, permeability and grain size are expected. Since these effects are also considered in the Strength Factor (SF), as determined in 4.3.2, this factor of 1.3 is decided to be a part of the factor 2.5 for strength in tidal sand.

The characteristic values of the soil parameters are determined by use of the recommended coefficients of variation (V) from the Dutch schematization manual for piping (MIM, 2017) and the mean values described in 5.3.2. The coefficients of variation are 0.12 for d_{70} , 0.5 for the horizontal permeability and 0.5 for the anisotropy factor (estimated by analysis of the mentioned values by Van Asselen et al.) (Van Asselen et al., 2018). The accompanying standard deviations ($\sigma = \mu \cdot V$) are given in Table 9.

Table 9 - Soil characteristics Hedwigepolder

	Clay	σ	Tidal sand	σ	Peat	Boxtel sand	σ	Oosterhout sand	σ
d_{70} [μm]	130	16	130	16	-	210	25	210	25
k_h [m/d]	0.050*	0.025	4	2	-	15	8	15	8
A [-]	10	5	8	4	-	4	2	4	2
k_v [m/d]	0.025	-	1.4	-	0	3.8	-	3.8	-

*A wrong indication of the permeability of clay, retrieved from SOS, lead to a change from 4 m/d to 0.05 m/d, see Figure 74

For every soil parameter in the Sellmeijer formula, to calculate the critical head difference, it is determined whether a value of the mean plus or minus 1.64 standard deviations must be used, such that the critical head difference is not underestimated. This is done for every layer separately. As explained in 3.1.3.b, a large grain size, a low horizontal permeability and a low vertical permeability cause a higher critical head difference. The characteristic soil parameter values are presented Table 10.

Table 10 - Characteristic soil properties values

	d_{70} [μm]	k_h [m/d]	A [-]	k_v [m/d]
Clay cover	156	0.10*	1.8	0.05*
Tidal sand	156	0.7	14.4	0.05
Boxtel sand	251	27.3	1.0	27.3
Oosterhout sand	251	27.3	1.0	27.3

*As mentioned under Table 9, the mean permeability is adapted

Table 11 - Sensitivity in permeability

	Charac.	50%	150%
k_h [m/d]	0.7	0.4	1.1
k_v [m/d]	0.05	0.03	0.08

The uncertainty and influence of the permeability of tidal sand are very large. Therefore, the sensitivity is evaluated. Calculations of the critical head difference are performed with permeabilities 50% lower and 50% higher than the characteristic values (Table 11).

5.4. Hydraulic boundary conditions

The prevailing hydraulic boundary conditions comprise of the polder water level and the water level in the *Schelde*. The polder water level roughly varies between NAP+0.5 m in summer and NAP+0.13 m in winter (Figure 68). The average polder water level is NAP+0.75 m. Since the exact time of the experiment is not known at this moment, the average polder water level is used in the design.

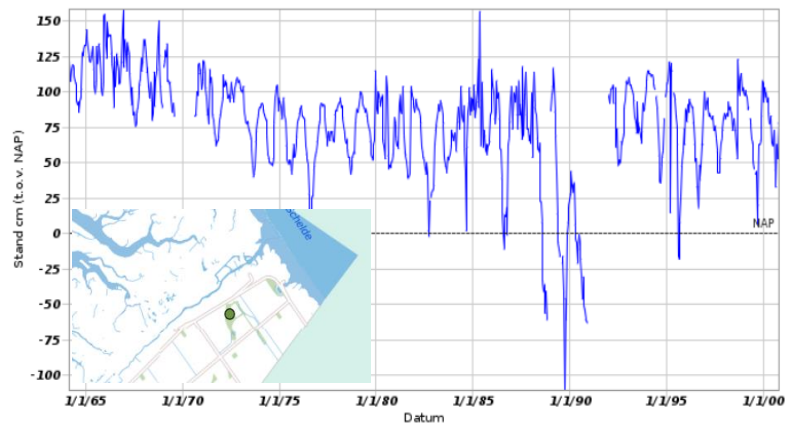


Figure 68 - Polder water level Hedwigepolder from 1964 until 2000 at the green dot on the map (TNO, 2009)

The water level in the *Schelde* is analysed at the closest measuring location: *Schaar van de Noord* (Figure 69). The mean water level lies around NAP+0.5 m. The ground level at the *Schelde* side of the dike is NAP+2.4 m. The maximum water level in the winter of 2018 was NAP+3.5 m. This means that the water depth at the toe of the dike was 1.1 m. The waves measured at the same location have a significant height (H_s) of 14.8 cm and a maximum of 94 cm.

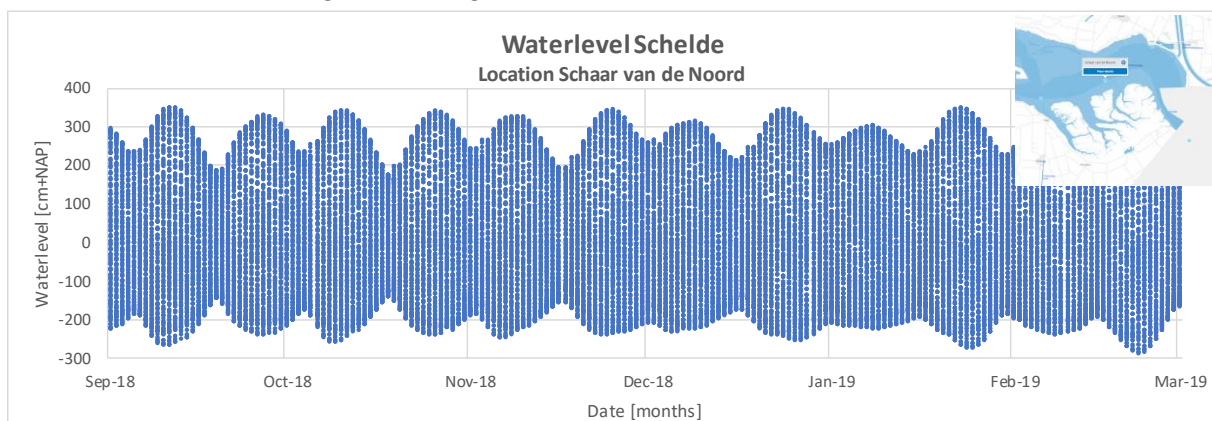


Figure 69 - Tidal record at *Schaar van de Noord* September 2018 - March 2019 (RWS, 2020)

5.5. Design choices

The base requirement for the experiment is that a water level difference must be created over the dike to force piping. Constructing a cofferdam in which the water will be raised and infiltrates into the aquifer is the first option evaluated. After the first calculations it was clear that the water level must be far above the crest level of the dike and this leads to high costs and an enormous construction. The second

option is to construct infiltration pipes into the aquifer with sheet pile walls that direct the flow towards the outflow point (Figure 70). With this option, the seepage length can be determined because the pipes can be installed at any position in the dike. This is very important because of the high expected water level which is needed to force pipe-growth. When the seepage length is shorter, the needed head difference to force piping will be less. The cover layer will be removed over a certain width to overcome the cover layer resistance, thereby removing the process of lifting and cracking of the cover layer. In this way it is the most certain where the pipe

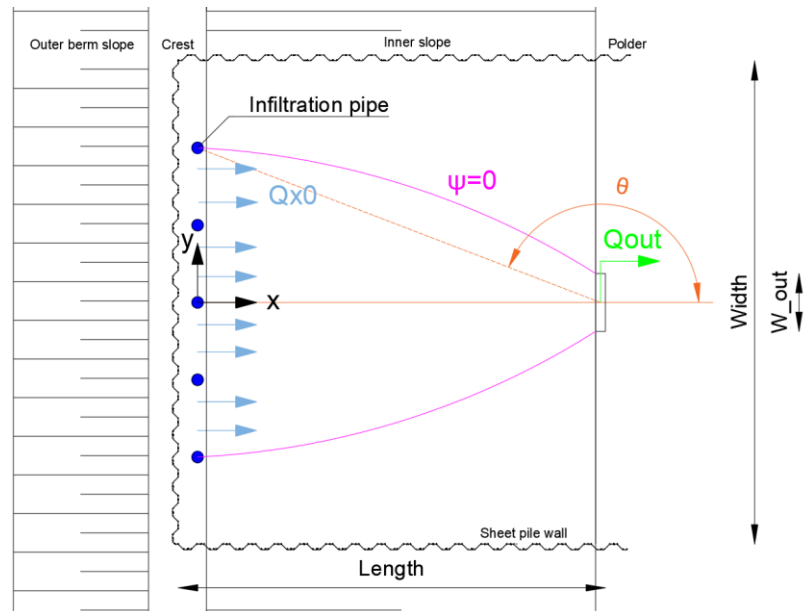


Figure 70 - Top view of the piping experiment

will start to grow. The possible design choices which have an influence on the other requirements are: 1) length (x-direction, Figure 70), 2) width (y-direction), 3) outflow width and 4) number of infiltration pipes.

A finite difference model (Figure 71) is constructed in Excel to determine the head distribution during the experiment. Assumed that no additional water is stored, the flow is confined and by use of Darcy's law, the head in a cell is calculated with Eq.21. In this equation, the discharge (Q) is positive when extracted from a cell, $h_{\#}$ is the head in a neighbour cell and T is the transmissivity (kD) of the aquifer.

$$h = \frac{h_1 + h_2 + h_3 + h_4}{4} - \frac{Q}{4T} \quad \text{Eq.21}$$

And along an impermeable wall:

$$h_{wall} = \frac{h_5 + h_6 + h_7}{3} - \frac{Q}{3T} \quad \text{Eq.22}$$

The discharge in x-direction between two cells (Q_x) is calculated with:

$$Q_x = T \cdot (h - h_2) \Rightarrow kD \cdot (h - h_2) \quad \text{Eq.23}$$

Disadvantages of this method are: 1) only one layer can be modelled. This means that only the cross section with a peat layer underneath the aquifer can be modelled. The peat layer prevents outflow to lower layers. 2) The mesh is coarse (0.5 m cells). 3) The permeability near the walls is hard to predict. 4) Water will be attracted towards the pipe when it starts to grow. This causes changes in the flow pattern, which are not considered in this model. 5) Anisotropy cannot be modelled, a single value for the permeability is used in the entire model. Benefits of this method are: 1) the insight in the calculations and 2) the ability to change the model relatively easy.

The boundary conditions are a steady head at a far distance, a steady inflow head at the critical head difference, no flow through the bottom of the aquifer and a steady polder head in the outflow.

The top view of the project area in the model (Figure 72) is divided in five types of square cells (0.5 m · 0.5 m):

- I. Orange: head depending on the four cells aside;
- II. Blue: polder head at a relatively far distance from the cofferdam and outflow (NAP+0.75 m);
- III. Green and yellow: head near the sheet pile wall, depending on the three head levels aside. The green and yellow cells are not connected to each other, meaning that no water can flow through the sheet pile walls;
- IV. Black: inflow cell where the head can be set to a steady level;
- V. Red: outflow cell where the head is set equal to the polder head.

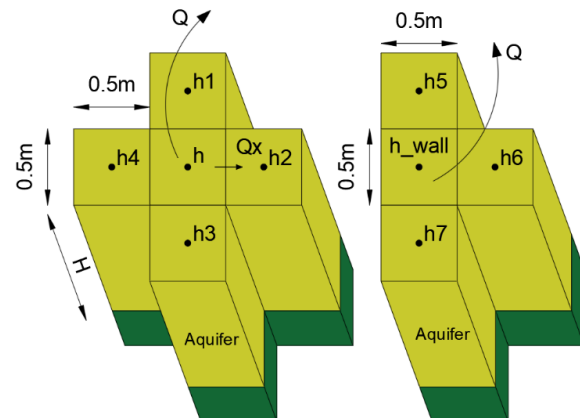


Figure 71 - Finite difference model

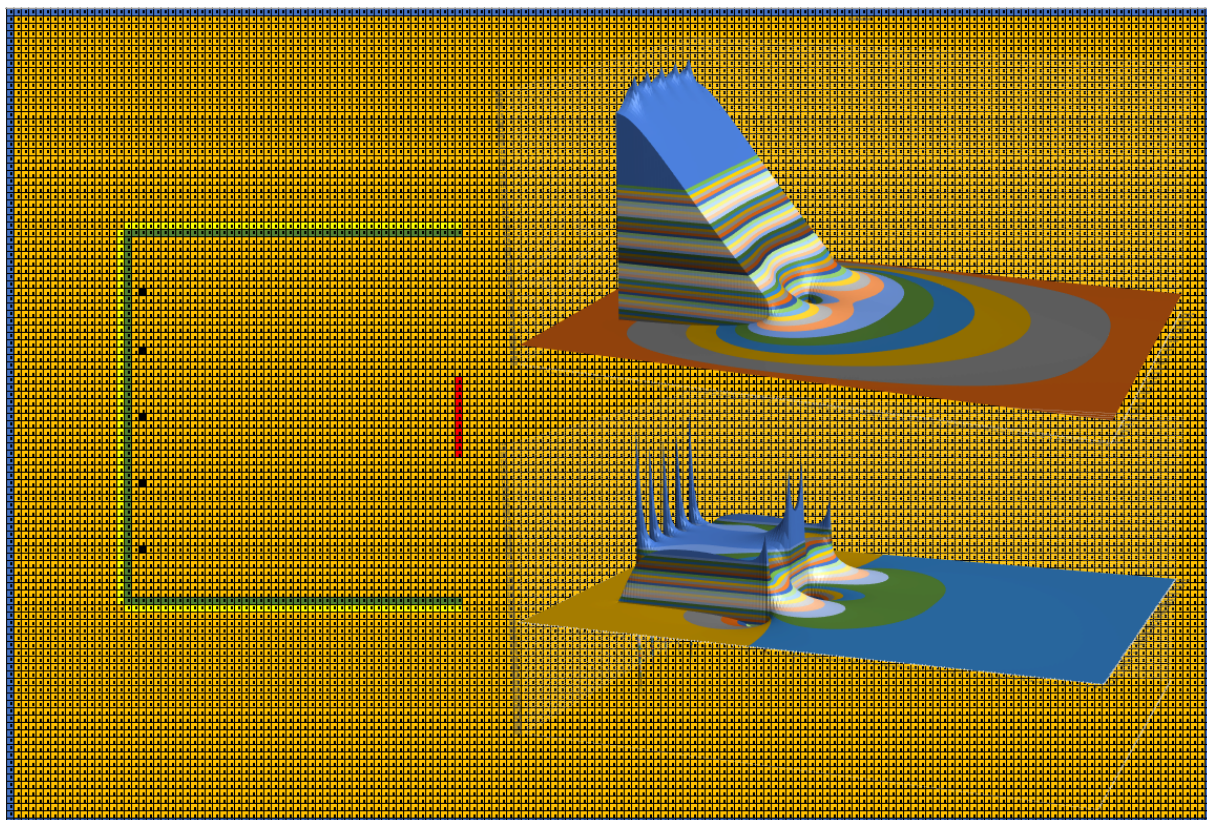


Figure 72 - Top view of the project area (with 5 inflow points, a length of 22.5 m, a width of 25 m and an outflow width of 3 m) in the finite difference model in Excel. The 3D graphs on the right are indications of the head (top) and the discharge in x-direction (bottom)

To analyse the effect of changes in length, outflow width, number of infiltration pipes, the permeability along the walls and different head levels, cross calculations are made with the variations in Table 12.

Table 12 - Variations in input parameters FD-model

	Low	Middle	High
L [m] – Distance between inflow and outflow (5.5.1)	10.5	14	22.5
W_{out} [m] – Width of the outflow hole	1	3 (base)	5
#Pipes [#] – Number of infiltration pipes divided over the width	1	3 (base)	5
k_{wall} [m/d] – Permeability in the cells next to the wall	$1 \cdot k$	$1.2 \cdot k$ (base)	$1.5 \cdot k$
h_{in} [NAP+m] – Critical head differences (characteristic permeability, 50% of the characteristic permeability and the head expected when head development over time is considered to lag	10.0 (base)	11.8	15.3

From every calculation, the following information is collected:

- 1) Head gradient near the wall (i_w). When gradients along the wall are higher, the flow is higher and this will lead to influence of the boundary on the result, which must be kept low.
- 2) Head drop from the inflow to the wall ($\Delta h_{inflow-wall}$). When this is large, the inflow is less realistic.
- 3) Inflow discharge (Q_{in}), which is estimated by multiplying the average specific discharge with the width between the sheet pile walls.
- 4) Outflow discharge (Q_{out}), which is estimated by subtracting the discharge to the polder in x-direction from the discharge in x-direction before the outflow. When the width to depth ratio of the pipe is known, an estimation can be made of the secondary erosion in the pipe.
- 5) With the discharges, a width (W) can be determined at a length (L) from the outflow at which the discharge is 0. The streamline at the border where the discharge is zero is defined as the line where the stream function (Ψ , Eq.24) is 0 (Figure 70). A simplification is made to the model by estimating the discharge over the width at the inflow (Q_{x0}), this is the discharge per meter of width.

$$\Psi = \frac{Q_{out}}{2\pi} \theta - Q_{x0} \cdot y \quad Eq.24$$

In which θ is the angle between the flow direction through the center of the outflow and the maximum y-coordinate at the inflow and y is the distance from the center of the cofferdam construction to the wall.

- 6) Head gradient at the outflow (i_{out}). This is an indication for initiation of piping. A rule of thumb is that fluidisation of the sand occurs when the local gradient is around 1. This is slightly higher than the horizontal gradient required to move sand grains in horizontal direction (Van Beek, 2015).

In the following paragraphs, the four design choices are discussed.

5.5.1. Length

The seepage length is linked to the water level which is needed to force pipe development. To determine which water level belongs to which seepage length, D-Geo Flow is used. The modelling of the subsoil starts with the cross section as defined (Figure 73, the dimensions of the dike do not matter, only the seepage length is of importance). The experiment will be conducted without the cover layer at the

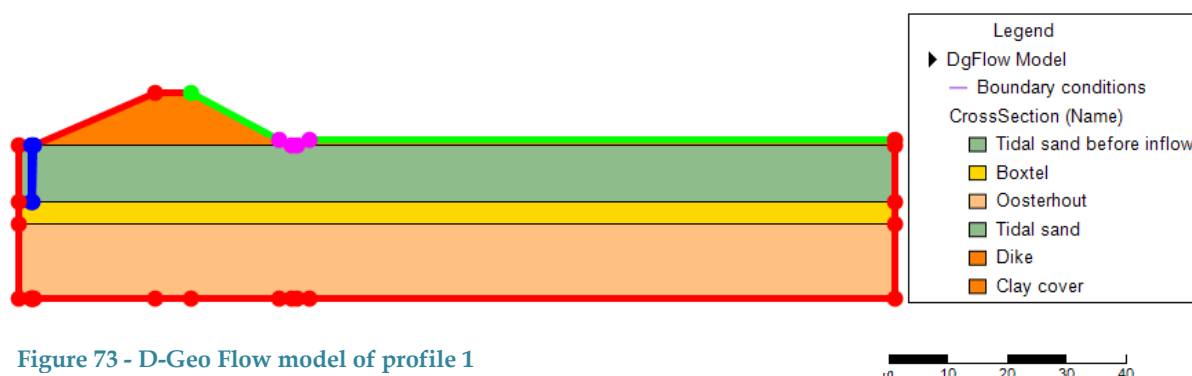
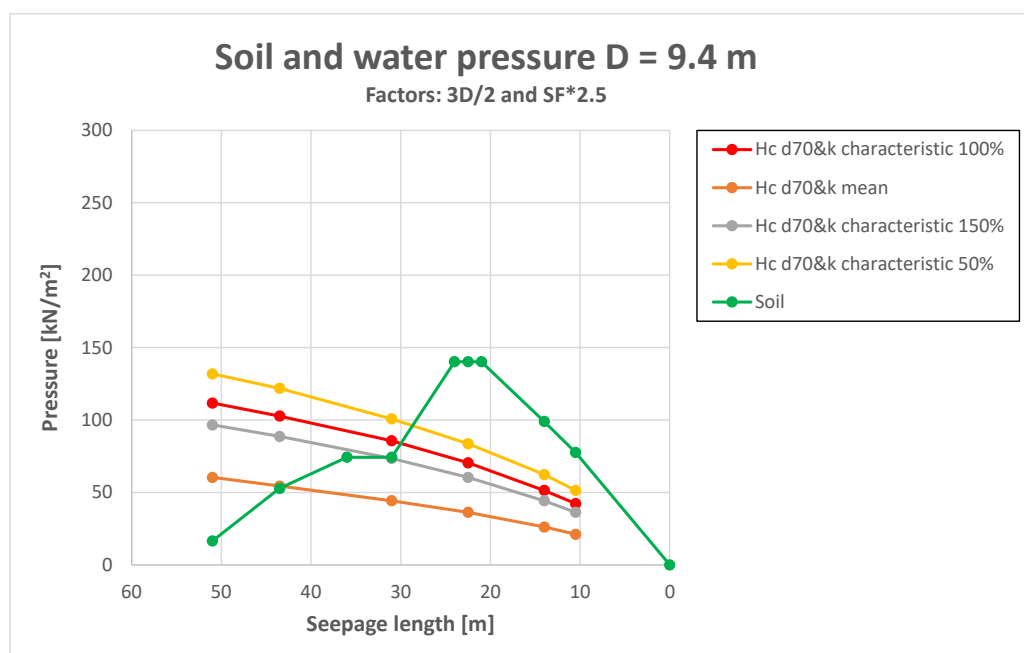


Figure 73 - D-Geo Flow model of profile 1

inflow. The blue boundary represents the inflow boundary through an infiltration tube. The red boundaries are no-flow boundaries. The green lines are seepage boundaries and the pink lines are the outflow. The water level is raised with 50 cm/h, the mesh is set to create grid cells of 1 m and near the pipe 2 times as small and output is generated every 10 minutes. This is done for the two cross sections and the variations in permeability as mentioned in Table 12.

The results from D-geo Flow must be corrected towards the expected higher value because of the presence of tidal sand and the 3D-effect. Because of the lack in knowledge of the soil content, no distinction between the processes causing the additional strength can be made. Therefore, the general result, found in the small-scale experiments, of $SF = 2.5$ is applied. The scale effect on the Strength Factor is described in 4.3.2.d. The outflow hole is not stretched over the total width of the cofferdam; therefore, 3D-effects are expected. As explained in 3.1.3.g, this leads to higher outflow gradients, reducing the critical head difference. Therefore, the critical head difference is reduced by a factor two. This 3D factor of two (found by Van Beek) is used because of the unknown scale effects and the fact that the findings by Van Beek are more substantiated (small- and medium-scale).

The results of the calculations multiplied by the SF, divided by the 3D factor and multiplied by the unit weight of water (10 kN/m^3), becoming the pore water pressures, are given in Figure 74. The water level difference which needs to be applied (in meters) automatically follows from a division by 10 kN/m^3 . The top of the aquifer lies at NAP+0.8 m, the head differences are calculated with respect to this level. This means that when the values in Figure 74 are divided by 10 and then added to 0.8, the water level relative to NAP is found.



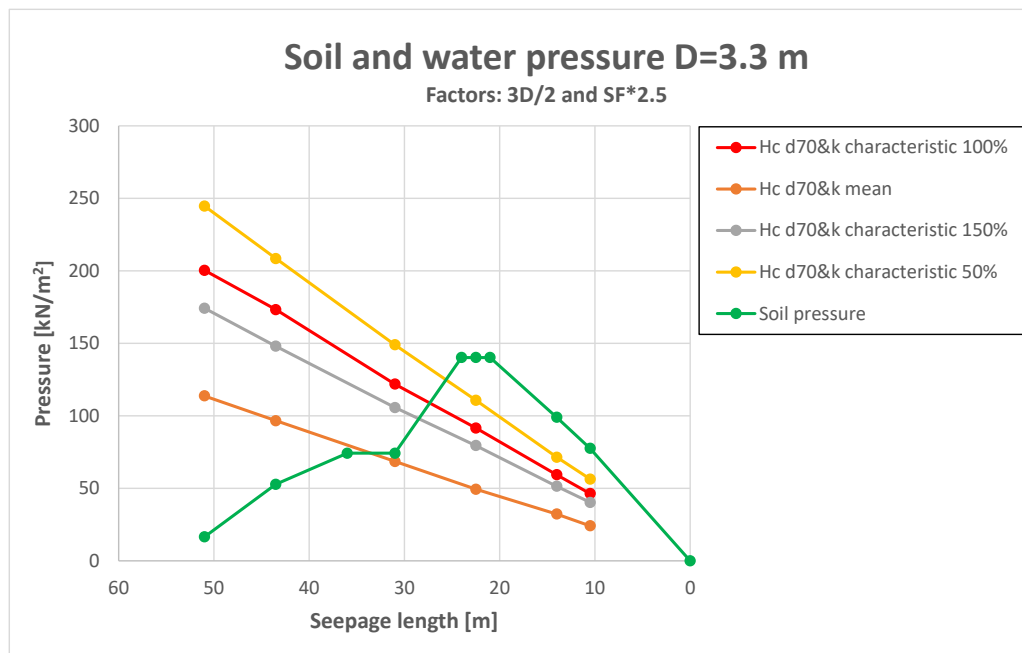


Figure 74 - Pressure on the surface between the cover layer and the aquifer for cross section 1 (top) and 2 (bottom). The pressures are water pressure caused by the critical head differences and soil pressure. As mentioned in Table 9, the permeability of the cover layer is assumed to be lower. When this is considered, the critical head difference is approximately 5% lower

Sheet-pile wall length (x-direction)

The length of the sheet pile walls between the in- and outflow (x-direction) is determined by the seepage length. They are placed over the whole length because when they are not, the head gradients at the outflow decrease fast because the water flows away to the sides and less towards the outflow. These gradients are the most important for initiation of piping and thus are desired to be controlled as good as possible. Therefore, the length of the sheet pile walls is equal to the seepage length.

Lifting of the cover layer close to the infiltration pipes

The pore water pressure which is exerted on the soil at the top of the aquifer results in an upward pressure which could lift the cover layer. The weight of the cover layer must be high enough to prevent lifting of the cover layer. The total stress in kN/m² is calculated by use of Eq.25.

$$\sigma = \gamma'_{submerged} \cdot d \quad Eq.25$$

In which σ is the vertical soil stress in kN/m², $\gamma'_{submerged}$ is the submerged unit weight of the soil (16.5 kN/m³) and d is the thickness of the soil on top of the aquifer in meters. The locations where the effective stress σ' ($= \sigma - \text{pore water pressure}$) is negative, the cover layer will lift up (Figure 74). The locations at which the soil pressure exceeds the water pressure needed to force pipe development are useful to perform the experiment. These locations are halfway the slope from the outflow ($L=10.5$ m), two thirds of the slope from the outflow ($L=14$ m) and in the middle of the crest of the dike ($L=22.5$ m).

Time dependency

A water level difference must be created, as mentioned, this will be done with infiltration pipes and sheet pile walls directing the flow. In a natural high water situation, the water level raises slowly, meaning that the head in the aquifer changes slowly with it. In the experiment, when increasing the water level, it is important to wait with the following head increase until the pressures in the aquifer are distributed over the seepage length. To achieve this, the adaptation of the head must be estimated.

The adaptation of the head in time in confined flow is estimated at a distance x from the inflow of water by use of the Edelman equation (Eq.26). This gives an estimation because at the outflow, the confining

aquitard is removed, creating an outflow of water from the aquifer, resulting in faster adaptation. The results from this analysis are thus conservative and only give an indication.

$$h(x,t) = \Delta h \cdot \operatorname{erfc}(u) \tag{Eq.26}$$

$$u = \sqrt{\frac{S \cdot x^2}{4T \cdot (t - t_0)}} \tag{Eq.27}$$

With the complimentary error function:

$$\operatorname{erfc}(u) = \frac{2}{\sqrt{\pi}} \int_u^\infty e^{-\tau^2} d\tau \tag{Eq.28}$$

The waterlevel difference between the inflow and just before the outflow (assumed to be approximately L) is calculated with this equation. The storage coefficient S is the aquifer thickness (D) multiplied by the specific storage (S_s) which ranges, if assumed that the value of dense sand is applicable, between 1E-4 m⁻¹ and 2E-4 m⁻¹ (Batu, 1998). The average is used, 1.5E-4 m⁻¹. From a practical point of view, the head will not be increased more often than once per hour. The minimal of an hour is needed to observe and analyse the heads in between steps. A choice can be made for the head increase per hour. A first estimation is 0.5 m per hour. When the characteristic head difference is applied, the adaptation at the outflow is presented in Table 13.

Table 13 - Adaptation of the head near the outflow with the head increasing by 0.5 m per hour

	h_{applied} [NAP+m]	h_{adaptation} [NAP+m]		
		L=22.5	L=14	L=10.5
D=3.3 m	9.91 (19 h)	7.12	8.24	8.73
D=9.4 m	7.80 (14 h)	5.16	6.08	6.48

Figure 75 shows the adaptation of the water level at a distance x (L) from the inflow. The head at that distance adapts towards the applied head at the inflow. The head adapts faster when the distance is short. Another way to improve the adaptation is to lower the head increase per hour. To stay within a reasonable timeframe for the experiment, about 48 hours, the head increase is not lowered to 0.1 m but a reasonable 0.3 m (Table 14). If the HPT-AMPT measurements (which will be done) show that the permeability is even lower, calculations with a head increase of 0.1 m should be made. This was also the case in the *IJkdijk* experiment. A larger head increase of 1 m is also considered but the lag for L = 10.5 m, k = 0.72 m/d is already 23%. A larger head increase per hour than 0.5 m is not recommended.

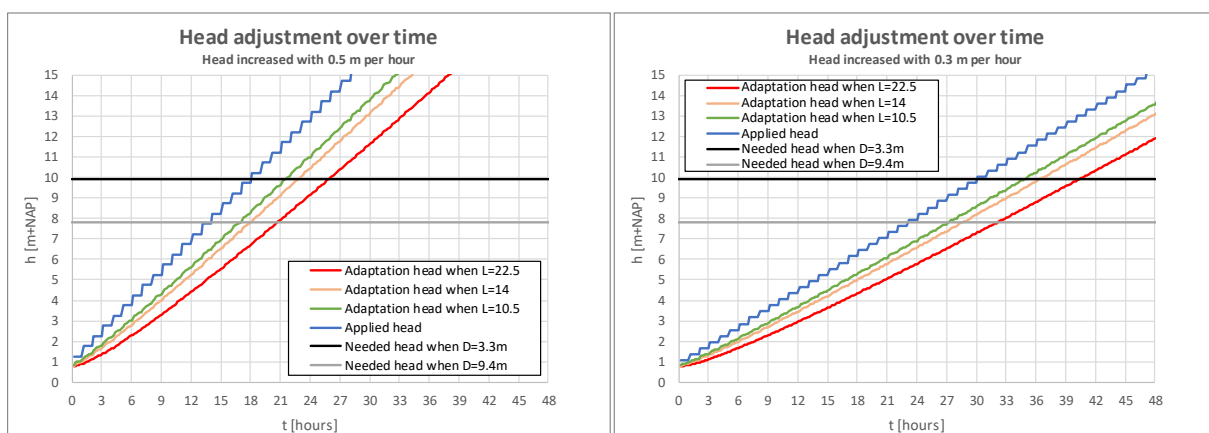


Figure 75 - Head adjustment over time for different lengths when the head is increased with 0.5 or 0.3 m per hour

When the needed head for failure is applied, the head near the outflow lags a certain percentage of the needed water level (Table 14). This lag is defined for different values of the permeability and accompanying critical head difference.

Table 14 – Head lag near the outflow with sensitivity of the head development to permeability and head increase steps

k [m/d]	h [NAP+m]	Head lag [% w.r.t. applied head]		
		L=22.5	L=14	L=10.5
$\Delta h = 0.3 \text{ m} ; D = 3.3 \text{ m}$				
4	5.7	-12%	-7%	-5%
1.1	8.7	-20%	-12%	-9%
0.72	9.9	-23%	-14%	-10%
0.4	11.8	-29%	-19%	-14%
$\Delta h = 0.3 \text{ m} ; D = 9.4 \text{ m}$				
4	4.38	-11%	-6%	-4%
1.1	6.79	-22%	-14%	-11%
0.72	7.8	-26%	-17%	-13%
0.4	9.11	-30%	-19%	-14%
$\Delta h = 0.5 \text{ m} ; D = 3.3 \text{ m}$				
4	5.69	-15%	-9%	-7%
1.1	8.7	-25%	-16%	-12%
0.72	9.91	-28%	-17%	-12%
0.4	11.83	-38%	-25%	-19%
$\Delta h = 0.5 \text{ m} ; D = 9.4 \text{ m}$				
4	4.38	-20%	-14%	-3%
1.1	6.79	-28%	-19%	-14%
0.72	7.8	-34%	-22%	-17%
0.4	9.11	-39%	-26%	-18%

The largest lag is found in the situation where the permeability is low and the head increase large. The lowest lag in the opposite situation. To create the desired head (i.e. overcome the lag), the following two options remain:

- I. Increase the water level with 0.5 m per hour until the desired head is reached. A negative consequence of this method is that the water level will keep increasing slowly after the desired water level is reached.
- II. Wait until the head at the outflow is adapted as can be followed with the installed pressure transducers. A negative consequence of this method is that it might take a long time.

Based on the available time for a single experiment and the desired adaptation, the head increase per hour and the seepage length can be chosen.

5.5.2. Number of inflow pipes

The inflow of water into the aquifer goes by infiltration pipes with a diameter of 0.6 m (flow surface almost equal to the surface of a grid cell 0.5^2). To generate a realistic situation, the water must flow into the aquifer equally over the width. This means that the pipes have to be spaced over the width in such a way that the head is equally distributed over the width.

A number of 1, 3 and 5 pipe(s) is considered. The results from the calculations show that with an increasing number of pipes:

- The gradient at the outflow goes up because more water is infiltrated, raising the gradients;

- The inflow discharge goes up because the infiltration area is larger;
- The outflow discharge increases because the inflow discharge increases;
- The maximum wall gradient increases because water is infiltrated closer to the wall;
- The head difference between inflow and wall goes down because the water is infiltrated closer to the wall.

This is presented in the table below, where the values in the cells represent the cases of 1 pipe and 5 pipes.

Distance [m]	i_{out} [-]	Q_{in} [m ³ /d]	Q_{out} [m ³ /d]	i_w [-]	Δh [m]
L=22.5	0.65-1.00	6.2-10.0	4.2-6.6	0.3-0.4	4.7-1.3
L=14	0.82-1.48	7.8-14.7	5.4-9.6	0.3-0.6	5.9-1.8
L=10.5	0.97-1.82	8.8-18.2	6.3-12.0	0.3-0.7	6.5-2.2

5.5.3. Outflow width

Removing the cover layer on the polder side results in an outflow hole. The width of the hole has an influence on the flow pattern. The values of the outflow width for which these influences are considered are 1, 3 and 5 m. The results from the calculations show that with an increasing outflow width:

- The gradient at the outflow goes down because the outflow area is larger;
- The flow width goes up because the discharges are higher;
- The inflow discharge goes up because the discharge out increases because the outflow area is larger;
- The outflow discharge increases because more flow is attracted by the wider outflow;
- The maximum wall gradient goes down by a maximum of 0.05. The flow is more attracted to the centre;
- The head difference between inflow and wall goes up by a maximum of 0.34. The flow is more attracted to the centre.

This is presented in the table below, where the values in the cells represent the cases of 1 and 5 m outflow width.

Distance [m]	i_{out} [-]	W [m]	Q_{in} [m ³ /d]	Q_{out} [m ³ /d]
L=22.5	1.18-0.84	12.3-16.2	9.0-9.5	4.8-7.0
L=14	1.67-1.21	11.9-15.3	12.5-13.7	6.8-10.0
L=10.5	2.02-1.48	11.8-14.9	14.9-16.7	8.4-12.4

A negative influence of a large outflow width is that the higher gradients will be situated at the position most close to the wall. This will lead to more chance of the pipe growing towards the wall or that the pipe will not grow through the center, where the most pressure sensors are installed.

5.5.4. Width

The width of the experiment is important because of the boundary effects near the sheet pile walls. The flow will be attracted towards the sheet pile walls because it is expected that the permeability is slightly higher near the wall-grain interface. The scenario that the pipe will grow along the wall has to be eliminated because that is not a natural pipe growth and interferes with the research on tidal sand strength. If the pipe grows along the wall, it is likely that it will start to grow towards the wall from the outflow and follow the wall until the inflow.

The following three options to prevent or indicate pipe growth along the wall are:

- I. In the small-scale experiments it is observed that in some cases the erosion pipe diverts to the side (y-direction) and grows along the wall. The length to width ratio of the small-scale experiments is 1.16. To prevent the pipe from growing to the wall, the length to width ratio is chosen to be 0.9, reasonably lower than 1.16.
- II. Calculate the distance needed between the walls for the flow. This can be done based on the discharges in and out of the sheet piled area and results in a width for which no flow will go along the walls (Eq.24). Q_{xo} and Q_{out} are estimated by use of the finite difference model. The

maximum width found in the cross calculations is 16.4 m, this is lower than the chosen 25 m (ratio length to width of $0.9 = 22.5/25$). Based on the calculated discharges in the finite difference model, the conclusion is that no flow goes along the wall when the width is larger than 16.4 m.

III. Analyse the head gradients along the wall. Transport of material through pores is mostly determined by the applied head gradient. Since the gradients are influenced by the growth of the pipe, which is not incorporated in the finite difference model, the wall gradients are not reliable. Besides that, the permeability along the wall, which is not known, also influences the gradients. However, they give insight in which parameters influence the gradients positively or negatively. The head gradient along the wall goes up when:

- The length is low;
- The outflow hole is small, very small difference of 0.05;
- More pipes are installed;
- The input head is high.

This is presented in the table below.

Distance [m]	Change in wall gradient when #pipes 1 or 5	Changes in wall gradient when h_{in} is 10 or 15.3 NAP+m
L=22.5	0.3-0.4	0.4-0.6
L=14	0.3-0.6	0.5-0.8
L=10.5	0.3-0.7	0.6-0.9

5.5.5. Sensitivity head and wall permeability

The variation in input head, has an influence on the design choices. When a choice is made for a worse scenario (low permeability), the head needs to be higher. With increasing head input:

- The outflow gradient goes up because the overall gradient becomes higher as well;
- The flow width goes down;
- The inflow discharge goes up because of the higher inflow gradient. The outflow discharge goes up because of the higher gradients;
- The outflow discharge goes up because of the higher gradients;
- The maximum wall gradient increases because all head gradients are higher;
- The head difference between inflow and wall increases because all head gradients are higher.

This is presented in the table below, where the values in the cells represent the cases of a low and a high head.

Distance [m]	i_{out} [-]	W [m]	Q_{in} [m ³ /d]	Q_{out} [m ³ /d]	i_w [-]	Δh [m]
L=22.5	0.92-1.46	16.4-14.4	8.8-14.8	6.5-9.5	0.4-0.6	2.0-3.4
L=14	1.34-2.09	14.1-13.8	13.1-20.8	8.7-13.5	0.5-0.8	8.7-13.5
L=10.5	1.63-2.56	13.8-13.6	15.9-25.2	10.7-16.7	0.6-0.9	3.4-5.5

The variation in wall permeability, has an influence on the design choices. With increasing near-wall permeability: 1) the width is going up by a maximum of 0.75 m and 2) the maximum head gradient does not change but the maximum discharge along the wall does ($Q_{wall} = i_w \cdot H \cdot k_{wall}$ [m³/d]).

Distance [m]	Q_{wall} [m ³ /d]
L=22.5	2.0-3.4
L=14	8.7-13.5
L=10.5	3.4-5.5

5.6. Optimal design

In this paragraph, the best choices in design options are substantiated. It is advised to choose the largest seepage length (22.5 m) to make optimal use of the opportunity to do a large-scale experiment. The needed water level in this case is expected to be above NAP+10 m. To limit the adaptation lag, the water level must be raised with maximal 0.3 m per hour. The height of NAP+10 m is reached after approximately 30 hours and lags 23% at that time. The head is expected to be fully adapted after +/-40 hours when the water level is further increased. In case soil permeability is not the characteristic value but the mean, the pipe could progress at a water level of about NAP+5.8 m. The width must be minimal 25 m to avoid much flow along the walls and growth of the pipe towards and along the walls. The number of pipes must be minimal 5. This is due to the outflow gradients, which must be above 1 and the head being equal over the width. The difference in head between the inflow and the wall in this case is 1.3 m. A negative influence of this choice is that the wall gradient can be up to 0.4 instead of 0.3 in case of one pipe. The outflow width must be 1 m to ensure large outflow gradients and to make the chance of the pipe growing towards the walls smaller. The discharge into the aquifer is about 9 m³/d and about 4.8 m³/d flows from the outflow hole at maximum gradients. An impression of this design is presented in Figure 76.

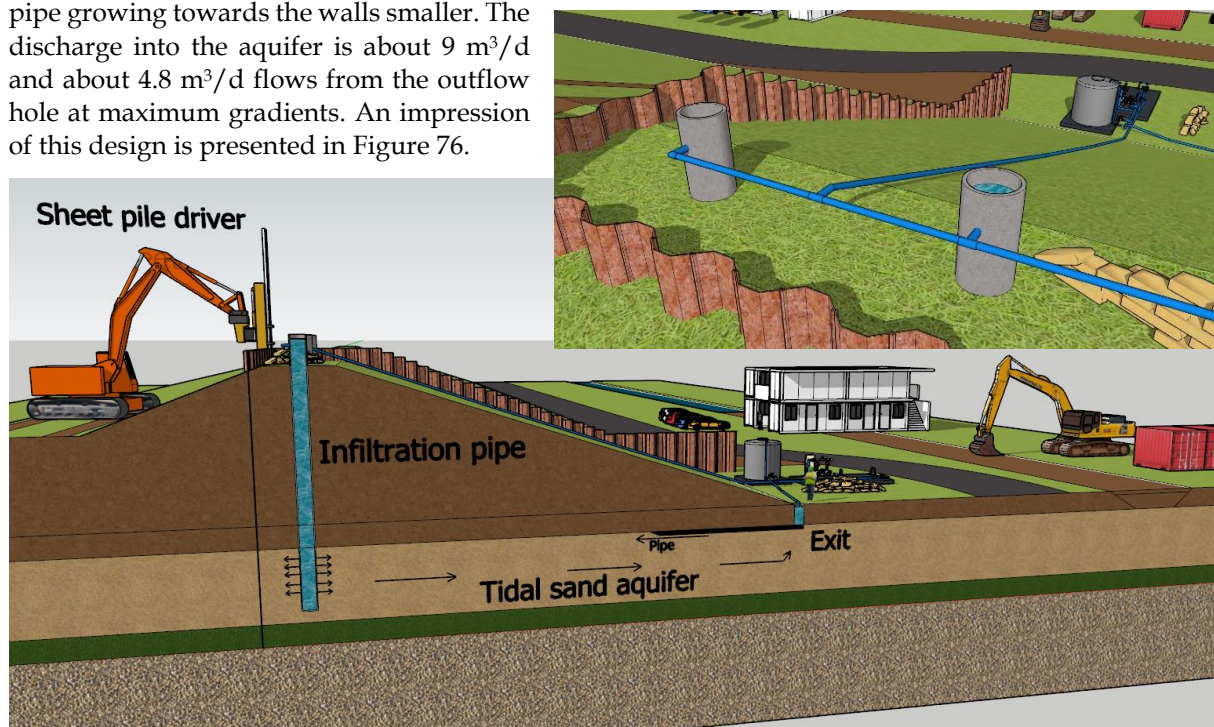


Figure 76 - Final design impression of the experiment in a cross section (bottom) and from the crest of the dike (top)

The water is pumped from a reservoir into the infiltration pipes. This reservoir is placed at the toe of the dike as stabilizing weight but when the dike is stable, it can be placed on the crest to reduce the pump capacity. The water flows towards the outflow hole through the tidal sand aquifer and is pumped back to the reservoir. In this way the water level in the infiltration pipes can be managed.

5.7. Experiment compartments

The project area is approximately 400 m wide. Not the whole area is suitable for the experiments. In the area where no peat layer is present (Profile 1 in 5.3.3), too much water will flow towards underlying layers and monitoring of the experiment will be much harder. Also, the costs are very high because the sheet pile walls must be installed very deep to prevent that too much water will flow away to the sides. These reasons contribute to the advised to use only the parts of the project area where a peat layer is present, this is approximately 150 m. Depending on the available budget, more experiments can be performed with a width of 25 m per experiment.

Prior to performing the destructive experiment, tests must be performed to gain knowledge on the in-flow capacity of the aquifer and the head adaptation over distance and time. Also, the measuring equipment can be tested in these small tests.

5.8. Measurements

Several rows of pore pressure meters will be placed at the interface of sand and clay to be able to monitor the pipe formation and head adaptation. They will be placed at the top of the tidal sand layer to be able to measure pressure differences when the pipe starts to grow. The accuracy needs to be at least 1 cm (measured in head) to be able to measure pipe developments and gradients. The placing pattern of the 71 pressure transducers is drafted in Figure 77. The sensors are placed in a funnel shape becoming smaller towards the outflow. The sensors are placed more closely to each other on the center line and towards the outflow to be able to track pipe development at locations where it is expected.

Besides pressure, also the temperature will be measured to detect failure by piping. Especially progressive erosion is measured well with this technique (De Vries et al., 2010). The water coming from the outflow will be pumped out to maintain the head difference and measure the discharge.

The flow pattern (due to differences in permeability) can be visualized by adding tracer dye to the water. Different colours will be added to the different infiltration pipes to be able to see which part of the aquifer accommodates the most flow. This can be an indication of the direction of pipe growth and obstacles to the flow.

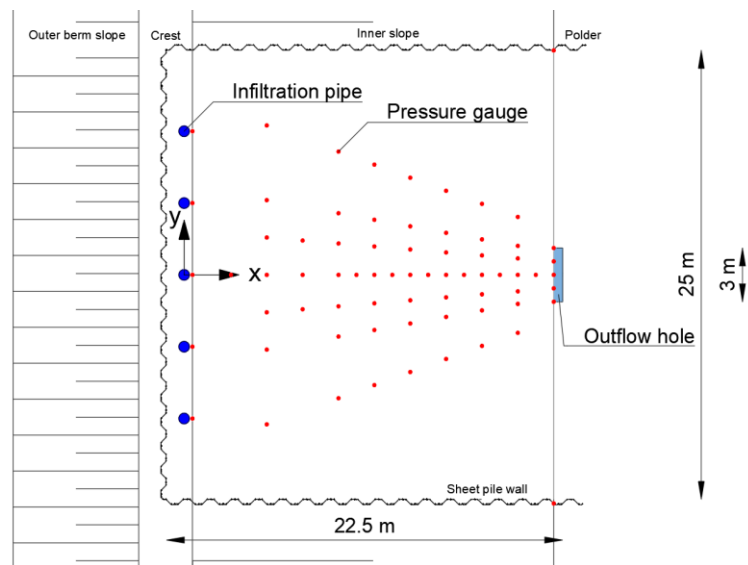


Figure 77 - Placing pattern pressure transducers

The parameters which need to be measured to be able to quantify the strength parameters are: 1) fine material in weight percentage ($d < 63 \mu\text{m}$, $d < 16 \mu\text{m}$ and $d < 2 \mu\text{m}$) (grain size distribution), 2) organic content in weight percentage, 3) chlorophyll a level, 4) vertical and horizontal permeability (anisotropy) and 5) the presence of vertical and horizontal layering which could form an obstacle to the flow (measured by CPT's and drillings).

6. Discussion

The main goals of this thesis are to improve the piping assessment of flood-defense systems in tidal areas and to design the large-scale piping experiment in the *Hedwigepolder*, hereby using gained knowledge from small-scale experiments on tidal sand. This chapter discusses the results of the executed research and the situations for which the results are valuable and valid. Parts of the discussion were already carried out in the chapters before as this was necessary for making the most suitable design.

The first part of the discussion reflects on whether the main objectives have been reached. The second parts discusses the most important findings of this thesis. This means discussing the quality of the results, the importance to the work field and future research. At the end of the chapter, future recommendations for research are listed.

6.1. Overall discussion

The main goal of this study is to improve the piping assessment in tidal sediments. To achieve this, several aspects must be studied of which three have been addressed in this research: 1) literature study on piping in tidal sand; 2) modelling and analysis of SSE and 3) design of a field test.

For the literature study first an analysis is made of how the piping process changes when going from fluvial sand to tidal sand. Looking back, this was the right approach to gain knowledge on the involved processes and to find a good measure for cohesion by EPS (extracellular polymeric substance, a viscous substance, secreted by diatoms, benthic fauna and bacteria) and fines in tidal sand and where the strength by cohesion depends on. EPS is a complex substance and its behavior under many circumstances is investigated in previous research by many researchers. Studying EPS and using this previous research can deliver new useful findings for the influence on piping. More knowledge needs to be gained from theory and from experts in this field. Previous research already hinted at a strong relation between the percentage of fines and the SF, but the SF is also depending on the amount of EPS. A good measure for this amount seems chlorophyll-a concentration, but at present this parameter has not been measured in piping-related research. When data becomes available in future research on both this concentration and the percentage of fines, it is expected that a combined relation can be obtained that can be used in piping assessments.

The analysis of the small-scale experiments delivered knowledge on the influence of fines, cohesion and vertical layering on the Strength Factor. The enormous influence was not expected at the start of the research. Clear relations have been found between suspected strength parameters and the SF. When the relations have been validated by future research, including large-scale experiments, the number of needed dike reinforcements in the tidal area is expected to decrease substantially. It has been shown how the strength is applicable in piping assessment by use of the fines content, uniformity or bedding angle. The used approach of analysing and modelling small-scale experiments had limitations like the number of available experiments, the application of the 3D factor and the determination of the permeability in the experiments.

The goal to make a substantiated design of the large-scale experiment is met by performing a subsoil analysis, cross calculations for different design options and using the results of the small-scale analysis to substantiate the expected strength. Uncertainties in this design are caused by the self-built finite difference model and the unknown soil parameters. Sensitivity analysis resulted in knowledge about the effects caused by changes in design options and soil parameters.

6.2. Discussion findings

6.2.1. Tidal sand cohesion

The most important findings from literature are the aspects which can explain the increased strength in tidal sands. This strength is thought to be caused by the presence of cohesion (largely influenced by fines). Fines are thought to cause a strength increase by embedding the larger sand grains, making them more erosion resistant. Cohesion is divided in physical and biological cohesion. Physical cohesion is caused by electrostatic forces which bind clay particles, which increases with salinity and evaporation-driven aggregation, which increases with fines content. The presence of iron in these more oxygen rich environments causes permeability reduction. Biological cohesion also influences the process. Tidal sediments contain bacteria, algae and benthic fauna which influence the EPS content that causes biological cohesion. Aggregates are formed consisting of fines, plant roots, larger sand grains and binding substance EPS and this aggregation increases with salinity. The presence of these aggregates enhances erosion resistance and reduces permeability. Indicating parameters for the increased erosion resistance in tidal sediments are organic content and chlorophyll-a concentration (component of EPS) which degrades in measurable components and is the best-preserved marker of EPS over time.

The downsides in the approach of measuring salinity, iron- and EPS content are: 1) the (yet) unknown relation between the parameters and piping resistance and 2) the large variability in strength increase and degradation in time and space. The degradation of EPS is a very important aspect because the soil on the location where piping is expected has been buried for a long time. Some EPS components are only slowly biodegradable due to the strength of the biofilms in which they live. The biofilm is a sponge-like system that provides surfaces for a diverse range of molecules. This leads to several benefits to the biofilm, such as nutrient intake and stabilization. Surface-attached biofilms are not only able to take up nutrients from the water but can also digest biodegradable components from the soil, which – if enough ‘food’ is present – can keep the biofilm alive and stable when buried. Besides the intake, biofilms are also capable of surviving exposure to antimicrobial compounds like toxic metals and small-molecule antibiotics. Chlorophyll-a degrades as well. The most important degradation when buried is due to groundwater flow by supply of oxygen and flushing out. When a sample is taken, the chlorophyll-a is degraded by oxygen and photo oxidation (which is higher with higher temperatures). The samples need to be kept in a closed, dark and cold container to preserve the chlorophyll-a. The mentioned influences need to be measured over time and at the locations in the aquifer where pipe growth is expected.

The coupling between biochemical soil parameters and physical processes in piping is relatively undiscovered terrain compared to geotechnical parameters. The ability to take the increased cohesion, caused by these physical and biochemical influences, into account in piping assessments in tidal sediment areas is a step forward in flood safety. This thesis supplies handles on how to quantify the cohesion and measure it in the field. It also gives a notice on how the EPS is formed and what the influences are on the concentration.

6.2.2. Tidal sand strength from SSE

The influence of tidal sand on the difference between critical gradients measured in experiments and calculated with piping models is measured by the Strength Factor ($SF = H_{c,measured} / H_{c,calculated}$). This factor indicates by what factor the model outcome (calibrated on fluvial sands) differs from the values measured in the experiments, thereby indicating the effects which are not yet considered in the piping assessment. This approach is essentially using the model error as a measure for additional strength. Therefore, the model error which would remain when the additional strength is considered, is assumed to be zero in this approach. It should be realized that the intrinsic modelling error (working both ways) is now included in the Strength Factor.

The calculated SF in the experiments on tidal sand is 2.5. This means that the critical head can be 2.5 times higher in the experiment than calculated with piping models.

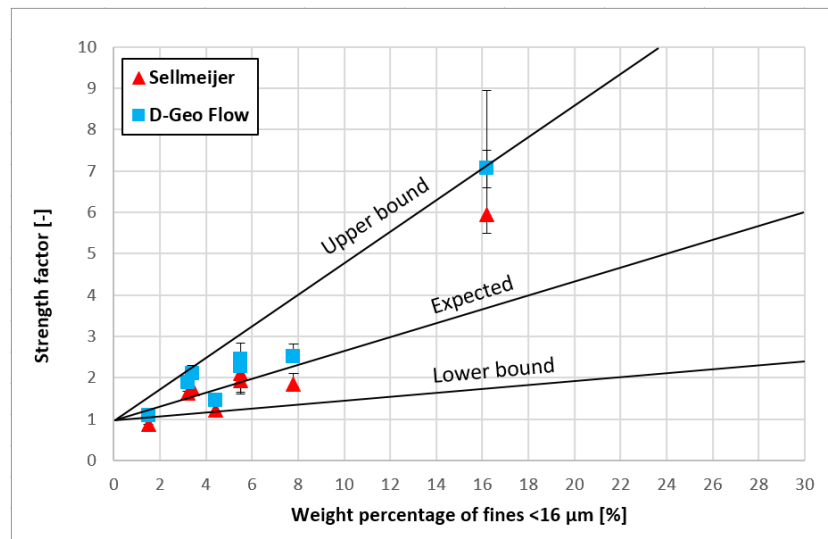


Figure 78 - Strength factor over weight percentage of fines <16 μm

This is caused by the presence of fine material, obstacles to the flow and cohesion. The best relation is found between the fines content <16 μm and the Strength Factor (SF). The fines content influences the permeability and d_{70} , but since they are incorporated in Sellmeijer's formula, these influences do not explain the increase in SF. The relation between fines and the SF is presented in Figure 78, in which also the bounds are given. It is directly clear that the highest point largely influences the result. That particular experiment contains large amounts of lutum and is classified as sandy clay. The amount of fines smaller than <16 μm in the *Naaldwijk* formation is known to be maximum 10 w% (Table 2). This means that the expected line is a better representation of the strength than the upper bound. The mean values are 7 w% in tidal flat sand and 3 w% in tidal channel sand, resulting in SF values of 1.5 and 2 respectively, which is quite high.

The data from the small-scale experiments shows that the Strength Factor due to cohesion (SF_c) is 1.8 (a part of the earlier mentioned 2.5). This is found by linear interpolation between data points of experiments without cohesion and using this knowledge to find the influence of cohesion in the other experiments. This approach contains a lot of uncertainty and requires confirmation by more experiments with cohesionless soil to separate influences. Cohesion causes the critical shear stress to be higher, which can be incorporated in Sellmeijer's formula by increasing the bedding angle (θ). For this data set, the angle goes from 37° to 46°. To use this in the field, different values for the bedding angle at different levels of cohesion need to be defined and the Sellmeijer's model needs to be recalibrated.

Heterogeneity, in the form of vertical clay layers, causes obstacles to the flow. Especially the pressure built up before such an obstacle breaches is important. That is why the thickness of the layers and the number of layers over the seepage length are important. A measure is given for the increased strength against piping for this data set. Since only two experiments with different size layers have been performed, the relation is very uncertain and should be supported by additional small-scale experiments with different sizes and numbers of clay layers. Since this measure also depends on scale the findings should also be validated in a large-scale experiment.

The uncertainties in the obtained results come from: 1) The number of experiments, which is only ten. 2) The model D-Geo Flow is not validated, 3) The 3D factor obtained from the analysis in this thesis comes to 1.5 (on small-scale). A negative point affecting the found 3D factor is that it is the mean between calculations with Sellmeijer's formula and with D-Geo Flow, which are known to deviate (a little). The 3D factor found by Van Beek was two but this is based on different scale experiments and the found values there were in between 1.5 and two. Because of the difference in scale, the more substantiated 3D factor by Van Beek of two is used. 4) The analysis is completely based on small-scale experiments. It is expected that the strength increases with scale. This is expected because much more fines are led towards the outflow, lowering the permeability more than on small-scale. Cohesion is expected to have more influence on large-scale because in-situ biofilms are not remolded and dried, as in the small-scale experiments. 5) It is not known if cohesion only has an influence on secondary erosion or also on primary erosion. Unfortunately, Sellmeijer's model only considers secondary erosion until now. The bedding angle can be used to incorporate cohesion in Sellmeijer's model but then it is assumed that it only influences secondary erosion. When primary erosion can be considered in Sellmeijer's model, the influence of cohesion on it must be investigated. 6) The remolding and drying of the sample causes disturbances in the iron and cohesion influence. In one of the experiments, large amounts of rust were observed. The soil has been dried completely and it is expected that when it is rewetted, the oxidized iron does not dissolve again, leading to a reduced effect on the permeability. In reality, the soil is not completely dried but it stays moisty. The drying and remolding causes the biofilms to be damaged or even completely removed. It is not known what the influence is but literature provides an indication of the reduction of the influence by remolding biofilms to be an order of magnitude. That is why experiments must be conducted on in-situ soil samples.

This research contributes to the improvement of piping assessment by delivering an approach how to incorporate cohesion into piping assessment. This can be done by increasing the bedding angle of the sand on the bottom of the pipe, introducing a uniformity coefficient defined as $U = d_{60}/d_5$ or by a factor over the critical head difference which is based on the weight percentage of fines $<16 \mu\text{m}$. In future research, a relation must be found between the SF and biofilms by measuring and analysing chlorophyll-a concentrations.

6.2.3. Piping experiment *Hedwigepolder*

The design of the experiment in the *Hedwigepolder* has led to dimensions of the experiment which are based on the characteristic soil parameters, the outcome of a finite difference model and the modelling of piping in D-Geo Flow. The largest uncertainty in these calculations is the permeability of the soil. that is why the calculations have been performed for the mean permeability found in WTI-SOS, the characteristic value and $\pm 50\%$ around the characteristic value. It is expected that piping will occur before the characteristic water level, calculated with D-Geo Flow, of NAP+10 m (NAP+ 8.7 m and NAP+11.8 m when $\pm 50\%$ around the characteristic permeability is used).

The quality of the design depends mainly on the uncertainties in the models and the soil parameters. The model which is used to define the water flow is a finite difference model in Excel with square cells of 0.25 m wide. This model is chosen due to time constrains and because such a model, which is built piece by piece, gives a lot of insight in the influential processes and can be adapted easily. The uncertainties which are introduced by using this approach are: 1) No pipe development is considered in the flow model. If this would have been the case, the flow pattern is changed because the water flow is concentrated towards the pipe. The results from the model are a good approximation when the pipe is not growing yet. It is expected that the pipe will start to grow before the critical head difference is reached (which indicates a progressive pipe growth). 2) The absence of time dependency in the flow model causes the results to be steady state. Therefore, the Edelman equation is used to know how the head at the outflow adapts to the head increase at the inflow over time. This is a good approximation, except the fact that the exit works like a pressure release. This means that because of the outflow of water, the head will adapt faster. Another large influence which causes uncertainty in the Edelman approximation is the specific storage of the tidal sand aquifer, which is unknown. The used value is of dense sand. If a more clayey sand type is chosen, the adaptation is less good. 3) As mentioned before,

the model D-Geo Flow is not validated yet. 4) The 3D factor is chosen to be 2, as found by Van Beek (2015), because the exit hole is very small. This is still a large influence on the results which is not yet validated on a large scale. 5) Instability of the slope is not considered due to time constraints. It is expected that due to the high pore pressure, the effective soil stress will drop, reducing the shear resistance which could lead to failure. This needs to be checked and if necessary, measures like counterweights at the toe must be installed to increase the resisting force against sliding. This has not been done in this thesis due to time constraints.

Design choices

The water level difference is created using five infiltration pipes at 22.5 m from the outflow. This length, in combination with the accompanying critical water level difference is chosen because the weight of the cover layer is not high enough when the seepage length is larger (i.e. a higher critical head). An option which is not considered is to put additional weight on top to prevent lifting of the cover layer. In that case, the seepage length can be larger but this will make the duration of the experiment longer.

Five infiltration pipes are recommended because in that case, the homogeneity of the inflow head over the width is the best. The values chosen at the start of the modelling (1, 3 and 5) could have been supplemented by seven, such that the homogeneity of the head is even better. This can be investigated in a later stage and will most likely depend on costs.

The width of the cofferdam construction is based on the discharges in and out. Since the discharges depend on pipe-growth, the discharge would change when pipe growth is considered in the flow model. That is why the rule of thumb to have a larger width than length is prevailing ($L/W = 0.9$).

The outflow hole is one meter wide. When the width is larger, the chance of the pipe growing towards the walls increases. Also, the 3D-effect will be less when the outflow width is larger, which is undesired because a 3D factor of 2 is used. The option, which was present at the start, to investigate the 3D-effect by creating an outflow width over the total width of the cofferdam is not considered feasible. The discharge needs to be a lot higher than the situation with a small outflow. Since it is expected that the strength in this experiment is very high, the uncertain 3D-effect will most likely be hard to discern from the effects that are studied. Since the 3D-effect can be estimated the best when the outflow is small, the analysis of the studied effects will be less hard when this small outflow is used.

This field test contributes to the improvement of the piping assessment by defining the expected strength on a large scale. The experiment on its turn will provide a lot of data on piping in tidal sediments to validate the findings in this thesis.

6.3. Future research recommendations

Several question about the additional strength of tidal deposits have been answered in this thesis. However, also new questions have raised. This is mainly because of the newly considered biochemical and fines content influence on piping. Below, the recommended research is listed, starting with the most important.

- I. The influence of scale on the SF must be substantiated. This influence is very important and will be hard to discern from other effects. That is why separate research must be conducted on the influence of scale on the different aspects (fines, cohesion and obstacles).
- II. More small-scale experiments must be conducted to further confirm the found relations. Only ten experiments are used so no statistics can be applied. Besides experiments with remolded material, also experiments with in-situ soil conditions must be performed to keep biofilms and iron conditions intact. When more experiments are conducted, the relations between the SF and influential parameters may change a lot.

- III. The chlorophyll-a level at the depth at which piping occurs must be determined over time. This needs to be coupled to the EPS content, what the state of the EPS is and how it varies with seasons.
- IV. The influence of EPS on soil erosion resistance has been examined a lot. In future research the influence of EPS and fines on piping resistance should be considered and the affected erosion process (primary or secondary). More data needs to be gathered to find a value of the Shields parameter for laminar flow in tidal sands.
- V. Research needs to be conducted on the influence of salinity on the binding between particles in sand-clay mixtures which are present in tidal sediments.
- VI. The influence of iron oxidation and accompanying oxygen levels on piping and permeability needs to be examined in a well-controlled experiment.

7. Conclusion

7.1. Introduction

In this thesis, a literature study and an analysis of small-scale experiments is performed to gain knowledge on how to design the large-scale experiment on piping in tidal sediment in the *Hedwigepolder* and how to measure and account for the expected resistance against piping in tidal sediments. These effects have been investigated in order to improve the current safety assessment (Sellmeijer's model) on piping, which is currently calibrated on fluvial sand. This chapter presents the final conclusions based on the previous chapters of this thesis.

7.2. Main research question

This paragraph contains the conclusion by means of an answer to the research question. The research question served to achieve the following objective: "Improve piping assessment in tidal areas and to design the large-scale piping experiment in the *Hedwigepolder* with gained knowledge from small-scale experiments on tidal sand.". The accompanying main research question is:

"What is the most suitable design of the field experiments on flow and piping through sandy tidal deposits in the Hertogin Hedwigepolder?"

This main research question is answered by the supply of an optimal design of the large-scale experiment on piping in tidal sediment in the *Hedwigepolder*, which is planned for 2021.

The main requirement of the design is to force piping underneath the dike, which can be well measured to analyse the impact of the sediment type on the process. This will be done by constructing a cofferdam construction with one open side, as presented in Figure 79. The water level needed to force piping is calculated with D-Geo Flow and lies just above the crest level of the dike at NAP+10 m. The water is infiltrated into the aquifer by infiltration pipes. This is done because when a cofferdam would be installed at the outer toe of the dike, it would have to be enormous. The water is pumped from a reservoir into the infiltration pipes. This reservoir is placed at the toe of the dike as stabilizing weight but when the dike is deemed stable, it can be placed on the crest to reduce pump capacity. The water flows towards the exit through the tidal sand aquifer and is pumped back to the reservoir. In this way the water level in the infiltration pipes is controlled. The seepage length of 22.5 m is chosen such that lifting of the cover layer besides the infiltration pipe is prevented. Five infiltration pipes are installed to secure the homogeneity of the inflow head over the width. The width of the cofferdam is 25 m because in small-scale experiments the pipe tended to grow towards the sides in some cases ($L/W = 1.16$). That is why a rule of thumb is used to have a larger width than length in the ratio of $L/W = 0.9$. The outflow hole is one meter wide. When the outflow width is larger, the chance of the pipe growing towards the walls increases, which must be prevented. Also, the 3D-effect will be less when the outflow width is larger, which is undesired because a 3D factor of 2 is used, indicating much bending of the flow lines.

The duration of the experiment is estimated by calculation of the adaptation of the head over the seepage length. To limit the adaptation lag, the water level must be raised with 0.3 m per hour. The height of NAP+10 m is reached after 30 hours and lags 23% at that time. When the water level is further increased, the head is fully adapted after 10 hours (40 in total). In case soil permeability is not the characteristic value but the mean, the pipe could progress at a water level of 5.8 m +NAP.

Before the experiment starts, tests will be done to measure the permeability of the soil. When more is known about the permeability, a better estimation of the required water level for piping and the adaptation time can be made. During the experiment, the pressure is measured to detect pipe growth. The flow pattern (due to differences in permeability) will be visualized by adding tracer dye to the water. Different colours will be added to the different pipes to be able to see which part of the aquifer

accommodates the most flow. This can be an indication of the direction of pipe growth and obstacles to the flow. The parameters which need to be measured to be able to quantify the strength parameters afterward are: 1) fine material in weight percentage ($d < 63 \mu\text{m}$, $d < 16 \mu\text{m}$ and $d < 2 \mu\text{m}$) (grain size distribution), 2) organic content in weight percentage, 3) chlorophyll-a level, 4) vertical and horizontal permeability (anisotropy) and 5) the presence of vertical and horizontal layering which could form an obstacle to the flow (measured by CPT's and drillings).

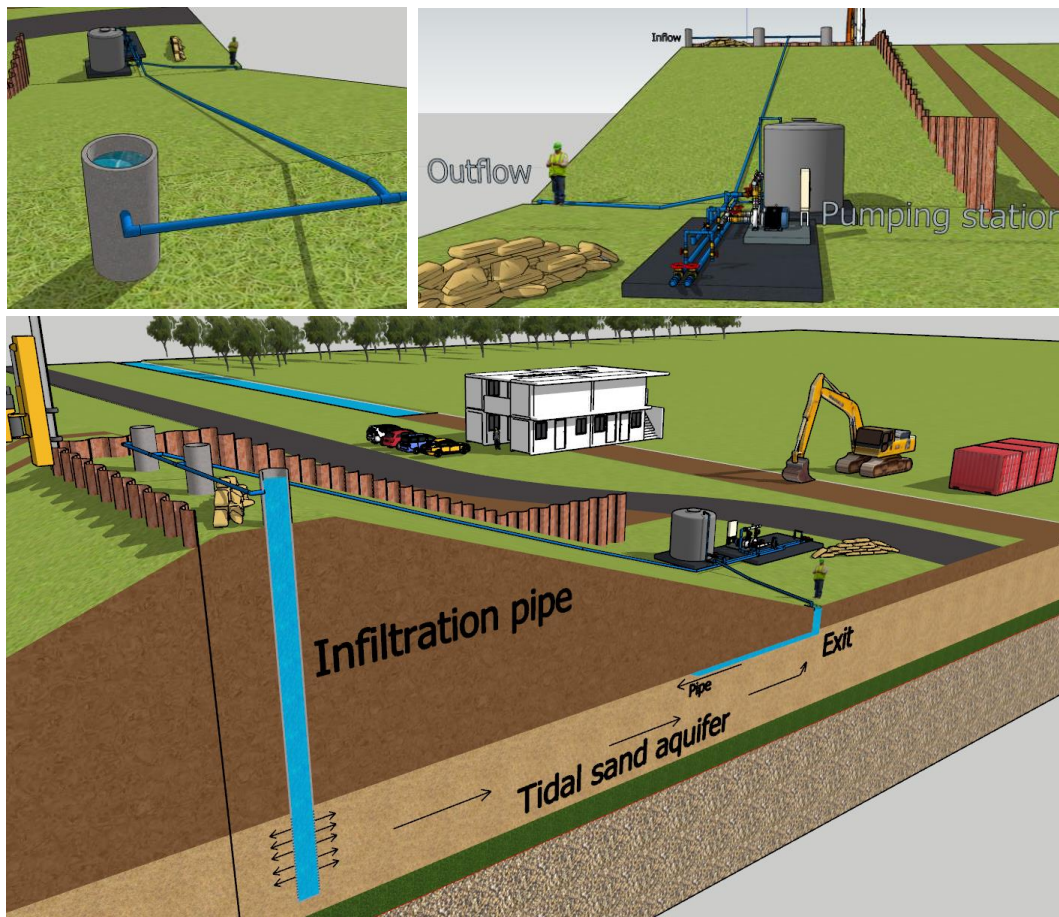


Figure 79 - Experiment set-up Hedwigepolder

7.2.1. Sub-question 1

“What are the differences between the piping erosion process in tidal sands and fluvial sands?”

The most important findings from literature are the aspects which can explain the increased strength (SF) in tidal sands. This strength is assumed to be caused by the presence of cohesion (largely influenced by fines). Fines are thought to cause a strength increase by embedding the larger sand grains, making them more erosion resistant. Cohesion is divided in physical and biological cohesion. Physical cohesion is mainly caused by electrostatic forces which bind clay particles due to a negative surface charge, which increases with salinity and evaporation-driven aggregate formation, which means that when fines $< 5 \mu\text{m}$ are present, dried sediment forms solid bridges which increase the strength of the soil 10-100 times when wetted. The presence of iron in these more oxygen rich environments causes oxidation and precipitation, reducing the permeability. Biological cohesion also influences the process. The biochemical composition of fluvial and tidal sediments differs a lot. Tidal sediments contain bacteria, algae and benthic fauna which influence the EPS content that causes biological cohesion. Aggregates are formed consisting of: fines, plant roots, larger sand grains and binding substance EPS (as a biofilm). The presence of these aggregates enhances erosion resistance and reduces permeability. Since EPS is also bonded to clay particles by electrostatic forces, increased salinity causes additional cohesion when the EPS content is higher. Indicating parameters for the increased erosion resistance in tidal sediments are thus fines

content, organic content and chlorophyll-a concentration (component of EPS) which degrades in measurable components and is the best-preserved marker of EPS over time.

The fines content influences both types of cohesion, making their presence the most important parameter by which strength in tidal sands can be measured. The reason why this is so different compared to fluvial sand is that EPS, salinity and more often drying of the soil cause the fines to be more cohesive. The degradation of EPS is a very important aspect because the soil on the location where piping is expected has been buried for a long time. Some EPS components are only slowly biodegradable due to the strength of the biofilms in which they live. The biofilm is a sponge-like system that provides surfaces for a diverse range of molecules. This leads to several benefits to the biofilm, such as nutrient intake and stabilization. Surface-attached biofilms are not only able to take up nutrients from the water but can also digest biodegradable components from the soil, which – if enough ‘food’ is present – can keep the biofilm alive and stable when buried. Besides the intake, biofilms are also capable of surviving exposure to antimicrobial compounds like toxic metals and small-molecule antibiotics. Chlorophyll-a degrades as well. The most important degradation when buried is due to groundwater flow by supply of oxygen and flushing out. When a sample is taken, the chlorophyll-a is degraded by oxygen and photo oxidation (which is higher with higher temperatures). The samples need to be kept in a wet, closed, dark and cold container to preserve the chlorophyll-a concentration.

7.2.2. Sub-question 2

“What is the influence of tidal sands on the differences between the data from the small-scale experiments on tidal sands and the outcomes of the modelled scale-experiments in D-Geo flow?”

The influence of tidal sand on the difference between critical gradients measured in experiments and calculated with piping models is measured by the Strength Factor ($SF = H_{c,measured} / H_{c,calculated}$). This factor indicates by what factor the model outcome (calibrated on fluvial sands) differs from the values measured in the experiments, thereby indicating the effects which are not yet considered in the piping assessment. The SF in the experiments on tidal sand is 2.5. This means that the critical head can be 2.5 times higher in the experiment than calculated with Sellmeijer’s piping model.

The used 3D factor is 1.5, based on the same type of experiments (same scale and same outflow configuration) on fluvial sand by Van Beek in 2015. A substantiation of the influential effects and parameters on the additional strength against piping is made by finding a relation between the SF and known parameters of the used material. This resulted in the following conclusions.

The best relation between a soil parameter and the SF in the small-scale experiments is the fines content. This confirms the findings in sub-question one. In that literature review it is found that the fines influence the cohesion between particles and that larger grains are more embedded between fines, which increases erosion resistance. The fines content can be represented in the uniformity coefficient, but the uniformity coefficient is only affected when the fines content is sufficiently high (approximately 10% or higher). In this way, the fines content can be incorporated in the refined Sellmeijer model (see Annex V .a). An advice is to recalibrate the Sellmeijer formula with uniformity values where d_5 is used instead of d_{10} to better represent the fines content.

The data from the small-scale experiments shows that the Strength Factor due to cohesion (SF_c) is 1.8. Cohesion causes the critical shear stress to be higher, which could be incorporated in Sellmeijer’s formula by increasing the bedding angle (θ). For this data set, the angle goes from 37° to 46° . To use this in the field, different values for the bedding angle at different levels of cohesion need to be defined and the Sellmeijer model needs to be recalibrated.

Heterogeneity in the form of vertical clay layers obstructs the flow. Especially the pressure built up before such an obstacle breaches is important. That is why the thickness of the layers and the number of layers over the seepage length is of importance. In this thesis, a measure is given for the increased strength against piping for this data set. This measure depends on scale and should be validated in a large-scale experiment. Horizontal layering (which was not present in the small-scale experiments) on

meso- to meta-scale can be modelled in D-Geo Flow and on small-scale, as found by Van Beek (2018) causes an increase in strength of 20-80%.

Anisotropy is negligible in the small-scale experiments due to the remolding of the soil. Since the anisotropy is investigated by Van Asselen et al. and will be measured in the polder with HPT-AMPT measurements, these values are used in the design of the experiment in the *Hedwigepolder*. It is expected that a scale increase will lead to more anisotropy.

It is expected that a scale increase will lead to a higher SF because in-situ soil contains intact biofilms, in contrary to the remolded material in the small-scale experiments. Also, presence of fine material, washing out towards the outflow and clog the outflow, leading to more severe clogging of the pores near the outflow, is expected to increase with scale but needs substantiation.

7.2.3. Sub-question 3

"How can the piping experiment in the Hertogin Hedwigepolder be designed?"

The answer to the question consists of the design choices. The assumptions made beforehand were that the experiment needs to be designed in such a way that:

1. **Sand boils will appear, and backward erosion piping occurs.** A subsoil analysis of the project area is made to be able to model the dike. The water level difference which is needed for backward erosion piping is calculated with D-Geo Flow for different seepage lengths. This water level is corrected by the 3D-effect and the expected strength in the tidal sand. In combination with the criterion that the cover layer may not lift close to the infiltration pipes, the seepage length is evaluated. Important in the calculations of the water level is the permeability, which is unknown. The calculations have been performed for the mean permeability found in WTI-SOS, the characteristic value and +/-50% around the characteristic value. The width, number of infiltration pipes and outflow width are calculated based on the expected heads, gradients and discharges, calculated with a self-built finite difference model. An analysis of the head over time, by use of the Edelman equation, is performed to determine the head increase which is needed. Cross calculations have been performed between all mentioned influences to find the optimal design, as given as an answer to the main research question.

The parameters which need to be measured to be able to divide this factor into factors which are linked to processes are: (1) fine material in weight percentage ($d < 63 \mu\text{m}$, $d < 16 \mu\text{m}$ and $d < 2 \mu\text{m}$) (grain size distribution), (2) organic content in weight percentage, (3) chlorophyll-a level, (4) vertical and horizontal permeability (anisotropy) and (5) the presence of vertical and horizontal layering which could form an obstacle to the flow by use of CPT's and drillings.

2. **The dike does not fail due to other failure mechanisms than piping** Other failure mechanisms (besides piping) which could occur are lifting of the cover layer and instability. Lifting of the cover layer is prevented by choosing a location at which the soil stress exceeds the pore water pressure induced by the locally applied head. Instability is not considered due to time constraints. It is expected that due to the high pore pressure, the effective soil stress will drop, reducing the shear resistance which could lead to failure. This needs to be checked and if necessary, a measure like a counterweight at the toe must be installed.
3. **Data obtained from the experiments is valuable to study the effects of tidal deposits on piping.** To be able to use the data to quantify the influences on the additional strength found in tidal sand, measurements are of great importance. That is why the tidal sand is precisely investigated before the experiments will take place. The above-mentioned soil parameters will be determined. While the experiments take place, the head is measured, pipe development is tracked, and flow patterns are monitored. Afterwards, a link between the soil parameters and the measured results during the experiments will be sought.

Literature List

- 't Hart, R., De Bruijn, H., & De Vries, G. (2016). *Fenomenologische beschrijving - Faalmechismen WTI Deltares*, Delft.
- Batu, V. (1998). *Aquifer hydraulics: a comprehensive guide to hydrogeologic data analysis*: John Wiley & Sons.
- Bennett, R. H., Fischer, K. M., Li, H., Baerwald, R., Hulbert, M. H., Yamamoto, T., Badiey, M., & Geotechnology. (1990). *In situ porosity and permeability of selected carbonate sediment: Great Bahama bank Part 2: Microfabric*, <https://doi.org/10.1080/10641199009388228>
- Black, K., Tolhurst, T., Paterson, D., & Hagerthey, S. (2002). *Working with Natural Cohesive Sediments*, vol. 128, [https://doi.org/10.1061/\(ASCE\)0733-9429\(2002\)128:1\(2\)](https://doi.org/10.1061/(ASCE)0733-9429(2002)128:1(2))
- Bosboom, J., & Stive, M. (2015). *Coastal Dynamics I*. Delft: University of Technology, section of hydraulic engineering
- Boudreau, B. P., Huettel, M., Forster, S., Jahnke, R. A., McLachlan, A., Middelburg, J. J., Nielsen, P., Sansone, F., Taghon, G., & Van Raaphorst, W. (2001). *Permeable marine sediments: overturning an old paradigm*, vol. 82, <https://doi.org/10.1029/EO082i011p00133-01>
- Cai, P., Sun, X., Wu, Y., Gao, C., Mortimer, M., Holden, P. A., Redmile-Gordon, M., & Huang, Q. (2019). *Soil biofilms: microbial interactions, challenges, and advanced techniques for ex-situ characterization*, <https://doi.org/10.1007/s42832-019-0017-7>
- Chang, D., & Zhang, L. (2013). *Extended internal stability criteria for soils under seepage*, vol. 53, <https://doi.org/10.1016/j.sandf.2013.06.008>
- Clipground. (2019). *Los Angeles*. Retrieved from <https://clipground.com/arenicola-marina-clipart.html>
- Costa, O., Raaijmakers, J., & Kuramae, E. (2018). *Microbial extracellular polymeric substances: ecological function and impact on soil aggregation*, <https://doi.org/10.3389/fmicb.2018.01636>
- De Groot, A., & van Straaten, L. (1964). *Mud transport studies in coastal waters from the western Scheldt to the Danish frontier*, <http://library.wur.nl/WebQuery/wurpubs/453780>
- De Vries, G., Koelwijjn, A., & Hopman, V. (2010). *Ijkdijk Full Scale Underseepage Erosion (Piping) Test: Evaluation of Innovative Sensor Technology*, [https://doi.org/10.1061/41147\(392\)63](https://doi.org/10.1061/41147(392)63)
- Decho. (1994). *Molecular-scale events influencing the macroscale cohesiveness of exopolymers*,
- Deen, M. (2015). *Dit is een rampgebied. vpro*. Retrieved from <https://www.vpro.nl/boeken/artikelen/vpro-gids/2015/september/37-Chris-de-Stoop.html>
- Deltares. (2017). *D-Geo Flow - User manual*,
- El Ganaoui, O., Schaaff, E., Boyer, P., Amielh, M., Anselmet, F., Grenz, C. J. E., Coastal, & Science, S. (2004). *The deposition and erosion of cohesive sediments determined by a multi-class model*, vol. 60, <https://doi.org/10.1016/j.ecss.2004.02.006>
- Flemming, H., & Wingender, J. (2010). *The biofilm matrix.*, <https://doi.org/10.1038/nrmicro2415>
- Flemming, H., Wingender, J., Szewzyk, U., Steinberg, P., Rice, S., & Kjelleberg, S. (2016). *Biofilms: An emergent form of bacterial life*, vol. 14, <https://doi.org/10.1038/nrmicro.2016.94>
- Förster, U., De Bruijn, H., Kruse, G., Hijma, M., & Vonhögen-Peters, L. (2012). *Onderzoeksrapport zandmeevoerende wellen Rijkswaterstaat*, publicaties.minienm.nl/download-bijlage/23912/onderzoeksrapport-zandmeevoerende-wellen.pdf
- Friend, P. (2001). *Biological influences on the stability of intertidal flat sediments*. University of Southampton, <http://eprints.soton.ac.uk/id/eprint/410548>
- Hijma, M., & Lam, K. (2015). *Globale stochastische ondergrondsschematisatie (WTI-SOS) voor de primaire waterkeringen Deltares*,
- Hijma, M., & Oost, A. (2019). *Getijdenafzettingen en piping: een quickscan* Deltares, Delft,
- Hoffmans, G. (2014). *An overview of piping models* Delft University of Technology, Delft, doi: 10.1201/b17703-3
- Hoffmans, G., & Van Rijn, L. (2018). *Hydraulic approach for predicting piping in dikes*, vol. 56, <https://doi.org/10.1080/00221686.2017.1315747>
- Huysmans, M., Peeters, L., Moermans, G., & Dassargues, A. (2008). *Relating small-scale sedimentary structures and permeability in a cross-bedded aquifer*, vol. 361, <https://doi.org/10.1016/j.jhydrol.2008.07.047>

- Ikelle, L. T., & Amundsen, L. (2018). *Introduction to petroleum seismology*: Society of Exploration Geophysicists.
- Jonkman, S. N. (2018). *Flood defences - lecture notes CIE5314* Delft University of Technology, Delft.
- Jonkman, S. N., & Cappendijk, P. (2006). *Veiligheid Nederland in kaart-inschatting van het aantal slachtoffers ten gevolge van overstroming*, vol. 7,
- Kanning, W. (2012). *The weakest link: spatial variability in the piping failure mechanism of dikes*, <https://doi.org/10.4233/uuid:5fb7b121-dc00-48aa-bda2-b163f10513bf>
- Knops, D. (2018). *Effects of the foreshore and heterogeneities of the subsoil on the safety analysis of piping HKV lijn in water*, Delft, Master thesis <http://resolver.tudelft.nl/uuid:e590425f-4177-4ab1-8ca8-93b1a85c2f2b>
- Kole, P. J. (2013). *DE HERTOGIN HEDWIGEPOLDER ONTPOLDEREN?* ,
- Kong, L., Li, X., & Tian, H. (2011). *Effect of fines content on permeability coefficient of sand and its correlation with state parameters*, vol. 32,
- Koopmans, G. F., Chardon, W. J., & Groenenberg, J. (2010). *Karakterisatie van ijzerslib en-zand: een verkenning van de mogelijkheden van het gebruik van deze reststoffen om fosfaatverliezen vanuit landbouwgronden naar het opperolaktewater te verminderen* Alterra,
- Kramer, R. (2014). *Piping under transient conditions* University of Twente, Enschede, Master thesis <https://doi.org/10.13140/2.1.1261.9044>
- Kwant, L. (2015). Retrieved from <https://www.wadgidsenweb.nl/helden/540-dollardeiland.html>
- Malarkey, J., Baas, J. H., Hope, J. A., Aspden, R. J., Parsons, D. R., Peakall, J., Paterson, D. M., Schindler, R. J., Ye, L., & Lichtman, I. (2015). *The pervasive role of biological cohesion in bedform development*, vol. 6, <https://doi.org/10.1038/ncomms7257>
- Manzenrieder, H. (1983). *Biological stabilisation effects on Wadden Areas from an engineering point of view*, Meetjesland. (2018). Retrieved from <https://www.npmeetjesland.be/event/7159/>
- Microsoft Corporation Earthstar Geographics, S. (Cartographer). (2019). Bing maps aerial view
- MIM. (2010). *Water Act*,
- MIM. (2017). *Schematiseringshandleiding piping - wbi*,
- Monien, P., Lettmann, K. A., Monien, D., Asendorf, S., Wöfl, A.-C., Lim, C. H., Thal, J., Schnetger, B., & Brumsack, H.-J. J. G. e. C. A. (2014). *Redox conditions and trace metal cycling in coastal sediments from the maritime Antarctic*, vol. 141, <https://doi.org/10.1016/j.gca.2014.06.003>
- Montalvo, C., Aguilar, C., Amador, L., Cerón, J., Cerón, R., Anguebes, F., & Cordova, A. (2014). *Metal contents in sediments (Cd, Cu, Mg, Fe, Mn) as indicators of pollution of Palizada River, Mexico*, vol. 3, <https://doi.org/10.5539/ep.v3n4p89>
- Negrinelli, G., Van Beek, V., & Ranzi, R. (2016). *Experimental and numerical investigation of backward erosion piping in heterogeneous sands*. Paper presented at the Scour and Erosion: Proceedings of the 8th International Conference on Scour and Erosion (Oxford, UK, 12-15 September 2016) <https://doi.org/10.1201/9781315375045-58>.
- Oldenbeuving, M., & De Jong, G. (2019). De strijd om de Hedwigepolder is gestreden, maar de pijn blijft. Retrieved from <https://eenvandaag.avrotros.nl/item/de-strijd-om-de-hedwigepolder-is-gestreden-maar-de-pijn-blijft/>
- OmroepZeeland. (2019). Hoe de Hedwigepolder er nu nog uitziet *omroep zeeland*. Retrieved from <https://www.omroepzeeland.nl/nieuws/110853/Hoe-de-Hedwigepolder-er-nu-nog-uitziet>
- Parsons, D. R., Schindler, R. J., Hope, J. A., Malarkey, J., Baas, J. H., Peakall, J., Manning, A. J., Ye, L., Simmons, S., & Paterson, D. M. (2016). *The role of biophysical cohesion on subaqueous bed form size*, vol. 43, <https://doi.org/10.1002/2016GL067667>
- Paterson, D., Tolhurst, T., Kelly, J., Honeywill, C., De Deckere, E., Huet, V., Shayler, S., Black, K., De Brouwer, J., & Davidson, I. (2000). *Variations in sediment properties, Skeffling mudflat, Humber Estuary, UK*, vol. 20, [https://doi.org/10.1016/S0278-4343\(00\)00028-5](https://doi.org/10.1016/S0278-4343(00)00028-5)
- Reuss, N. (2005). *Sediment pigments as biomarkers of environmental change* National Environmental Research Institute, Denmark, http://www2.dmu.dk/1_viden/2_Publikationer/3_ovrige/rappporter/phd_NIR.pdf
- Reynaud, J., & Dalrymple, R. (2012). Shallow-marine tidal deposits. In *Principles of Tidal Sedimentology* (pp. 335-369): Springer.

- Richards, K., & Reddy, K. (2012). *Experimental investigation of initiation of backward erosion piping in soils*, vol. 62, <https://doi.org/10.1680/geot.11.P.058>
- Rijkswaterstaat. (2019). Waterinfo. Retrieved from <https://waterinfo.rws.nl/#!/kaart/zouten/>
- Robbins, B., & Van Beek, V. (2015). *Backward erosion piping: a historical review and discussion of influential factors*. Paper presented at the ASDSO Dam Safety, New Orleans.
- RWS. (2020). Waterinfo - Astronomische-getij. Retrieved from <https://waterinfo.rws.nl/#!/kaart/astronomische-getij/>
- Seiphoori, A., Ma, X., Arratia, P., & Jerolmack, D. (2020). *Formation of stable aggregates by fluid-assembled solid bridges*, <https://doi.org/10.1073/pnas.1913855117>
- Sellmeijer, J. B. (1988). *On the mechanism of piping under impervious structures* Delft University of Technology, Delft, <http://lib.ugent.be/catalog/rug01:000198091>
- Sellmeijer, J. B. (2006). *Numerical computation of seepage erosion below dams (piping)* GeoDelft, Delft, <https://hdl.handle.net/20.500.11970/100072>
- Shehata, A. (2015). *Engineering Properties, Micro-and Nano-Structure of Bentonite-Sand Barrier Materials in Aggressive Environments of Deep Geological Repository for Nuclear Wastes*. University of Ottawa, <http://dx.doi.org/10.20381/ruor-5494>
- Sidik, W. S., Canakci, H., Kilic, I. H., & Celik, F. (2014). *Applicability of biocementation for organic soil and its effect on permeability*, vol. 7,
- Smitskamp, L., & Koks, L. (2013). *Activiteitenplan Project Herinrichting Hedwigepolder*,
- Spears, B., Saunders, J., Davidson, I., & Paterson, D. (2008). *Microalgal sediment biostabilisation along a salinity gradient in the Eden Estuary, Scotland: unravelling a paradox*, vol. 59, <https://doi.org/10.1071/MF07164>
- Stoop, N. (2018). *The effects of anisotropy and heterogeneity in the piping sensitive layer*. (Master thesis). Delft University of Technology, Delft. <http://resolver.tudelft.nl/uuid:dd40b31f-33f1-479e-a6e0-8cbf836763be>
- TAW. (1999). *Technisch rapport zandmeevoerende wellen* Rijkswaterstaat, <http://resolver.tudelft.nl/uuid:d5354144-9b49-48b2-a6cc-0e13d0e38691>
- TNO. (2009). DINOloket (Internet Portal for Geo-Information). Retrieved from <https://www.dinoloket.nl/ondergrondmodellen>
- Tolhurst, T., Gust, G., & Paterson, D. (2002). The influence of an extracellular polymeric substance (EPS) on cohesive sediment stability. In *Proceedings in marine science* (Vol. 5, pp. 409-425): Elsevier.
- Underwood, G., Paterson, D., & Parkes, R. (1995). *The measurement of microbial carbohydrate exopolymers from intertidal sediments*, vol. 40, <https://doi.org/10.4319/lo.1995.40.7.1243>
- Van Asselen, S., Hijma, M., & Kanning, W. (2018). *Anisotropie in doorlatendheid* Deltares, Delft,
- Van Baars, S., & Van Kempen, I. (2009). *The causes and mechanisms of historical dike failures in the Netherlands*, [www.dwa.de/portale/ewa/ewa.nsf/c125723b0047ec38/8428f628ab57becfc125766c003024b6/\\$file/historical%20dike%20failures.pdf](http://www.dwa.de/portale/ewa/ewa.nsf/c125723b0047ec38/8428f628ab57becfc125766c003024b6/$file/historical%20dike%20failures.pdf)
- Van Beek, V. (2015). *Backward erosion piping, initiation and progression* Delft University of Technology, Delft, <https://doi.org/10.4233/uuid:4b3ff166-b487-4f55-a710-2a2e00307311>
- Van Beek, V., Bezuijen, A., Sellmeijer, J., & Barends, F. (2014). *Initiation of backward erosion piping in uniform sands*, vol. 64, <https://doi.org/10.1680/geot.13.P.210>
- Van Beek, V., & Hoffmans, G. (2017). *Evaluation of Dutch backward erosion piping models and a future perspective* European Working Group on Internal Erosion, Delft, <http://resolver.tudelft.nl/uuid:bb0669f9-1c9e-4678-bec1-187165be6ed9>
- Van Beek, V., Knoeff, H., & Schweckendiek, T. (2011). *Piping: over 100 years of experience, from empiricism towards reliability-based design*, Delft, A tribute to Prof. Frans Barends <http://resolver.tudelft.nl/uuid:7bcf54c4-89bc-4349-88a2-9a62a934ab0d>
- Van Beek, V., Noordman, A., Robbins, B., & Griffiths, D. (2019). *EWG-11 3D Numerical Simulation of Backward Erosion Piping Tube Experiments*. Paper presented at the Book of Abstracts
- Van Beek, V., Wiersma, A., & Van Esch, J. (2018). *Invloed van micro-schaal laminae op het pipingproces*,
- Van Dam, J., & Beijersbergen, J. A. (1981). *Dijkdoorbraak Zalk 8 januari 1926* Centrum voor Onderzoek Waterkeringen,

- Van de Broek, M., Temmerman, S., Merckx, R., & Govers, G. (2016). *Controls on soil organic carbon stocks in tidal marshes along an estuarine salinity gradient*, vol. 13, <https://doi.org/10.5194/bg-13-6611-2016>
- Van der Meulen, M., De Lang, F., Maljers, D., Dubelaar, C., & Westerhoff, W. (2003). *Grondsoorten en delfstoffen bij naam* (D. W.-e. Waterbouwkunde Ed.). Delft.
- Van Esch, J. (2015). *WTI 2017: Toetsregel piping Validation piping module DgFlow (report including primary erosion)*, Delft.
- Van Goor, G., Hijma, M., Couperus, B., & Los, B. (2019). *Living Lab Hedwige-Prosperpolder*, Project exploration
- Vandenboer, K., Bezuijen, A., & Van Beek, V. M. (2014). *3D character of backward erosion piping: Small-scale experiments*. Paper presented at the Scour and erosion: proceedings of the 7th international conference on scour and erosion <http://hdl.handle.net/1854/LU-5786527>.
- Vandenboer, K., van Beek, V., & Bezuijen, A. (2017). *Pipe depth measurement in small-scale backward erosion piping experiments*, <http://resolver.tudelft.nl/uuid:c01741bd-17b6-467f-95b5-3e65cb1dc950>
- Veer, G. (2006). *Geochemical soil survey of the Netherlands. Atlas of major and trace elements in topsoil and parent material; assessment of natural and anthropogenic enrichment factors*: Utrecht University.
- Vergouwe, R. (2014). VNK2 Rijkswaterstaat,
- Vliz. (2006). Vlaams instituut voor de zee. Retrieved from http://www.vliz.be/cijfers_beleid/zeecijfers/main.php?id=6&sid=10&ssid=19
- Volkenborn, N., Hedtkamp, S., Van Beusekom, J., & Reise, K. (2007). *Effects of bioturbation and bioirrigation by lugworms (Arenicola marina) on physical and chemical sediment properties and implications for intertidal habitat succession*, vol. 74, <https://doi.org/10.1016/j.ecss.2007.05.001>
- Wang. (2014). *Simulation of pipe progression in a levee foundation with coupled seepage and pipe flow domains* Tsinghua University, Beijing, <https://doi.org/10.1016/j.sandf.2014.09.003>
- White, C. (1940). *The equilibrium of grains on the bed of a stream*, vol. 174, <https://doi.org/10.1098/rspa.1940.0023>
- Widdows, J., Blauw, A., Heip, C., Herman, P., Lucas, C., Middelburg, J., Schmidt, S., Brinsley, M., Twisk, F., & Verbeek, H. (2004). *Role of physical and biological processes in sediment dynamics of a tidal flat in Westerschelde Estuary, SW Netherlands*, vol. 274, <https://doi.org/10.3354/meps274041>
- Wiersma, A., & Hijma, M. (2018). *Korrelgroottes en heterogeniteit van rivierafzettingen in het licht van piping* Deltares,
- Wooldridge, L., Worden, R., Griffiths, J., Thompson, A., & Chung, P. (2017). *Biofilm origin of clay-coated sand grains*, vol. 45, <https://doi.org/10.1130/G39161.1>
- Wooldridge, L., Worden, R., Griffiths, J., Utley, J., & Thompson, A. (2018). *The origin of clay-coated sand grains and sediment heterogeneity in tidal flats*, vol. 373, <https://doi.org/10.1016/j.sedgeo.2018.06.004>
- Yokoi, H. (1968). *Relationship between soil cohesion and shear strength*, vol. 14, <https://doi.org/10.1080/00380768.1968.10432750>
- Zee, R. A. v. d. (2011). *Influence of sand characteristics on the piping process*. (Master Thesis). Delft University of Technology, Delft. <http://resolver.tudelft.nl/uuid:bfbcaf-502f-483a-bce0-3912c2800026>

Annexes

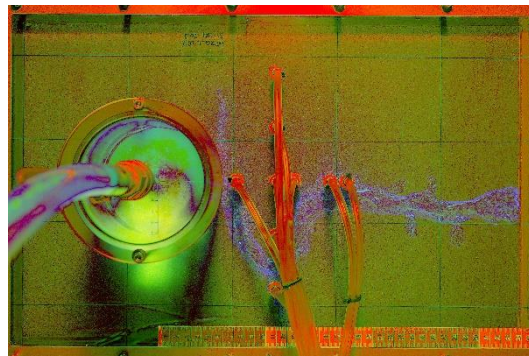
Annex I. Soil characteristics SSE

Name	RD [-]	k [m/d]	U [-]	d ₇₀ [μm]	n [-]	Fines <63 μm [w%]	Fines <16 μm [w%]	Fines <2 μm [w%]	SF D-Geo Flow* [-]	SF Sell- meijer* [-]
G207	81	1.38	1.7	160	0.36	4.8	3.4	2.1	2.1	1.7
G208	80	3.02	1.7	160	0.36	4.3	3.2	1.9	1.9	1.6
G209	79	1.38	1.7	160	0.36	5.6	4.4	2.5	1.5	1.2
G210	78	0.43	1.6	160	0.36	4.9	3.7	2.2	5.7	3.8
G211	83	0.86	1.6	160	0.36	4.9	3.7	2.2	1.6	1.1
F213	80	0.29	45.5	110	0.38	28.5	16.2	11.2	7.1	6.0
F214	75	0.38	2.4	130	0.41	19	5.5	1	2.5	2.1
F215	76	0.53	2.4	130	0.42	19	5.5	1	2.3	1.9
B+1%K	87	1.47	1.6	171	0.38	1.5	1.5	0.2	1.1	0.9
B+3%K	86	0.17	1.7	171	0.37	8.7	7.8	2.2	2.5	1.9
B132	65	8.04	1.54	154	0.38	3	-	-	0.7	0.6
B142	91	5.36	1.54	154	0.35	3	-	-	0.7	0.6
S170	89	6.57	2.25	300	0.37	7	-	-	2.7	2.1
E169	94	27.65	1.6	431	0.32	0	-	-	0.9	0.7
O163	94	11.23	2.06	307	0.32	2	-	-	1.6	1.7
O140	65	17.28	2.06	307	0.35	2	-	-	1.0	0.9
W130	65	44.06	1.58	400	0.38	1	-	-	1.3	1.2
W131	65	46.66	1.58	400	0.38	1	-	-	1.1	1.0
I166	100	3.97	2.43	223	0.33	7	-	-	1.5	1.2
I168	89	2.33	3.17	203	0.33	16	-	-	1.3	1.0

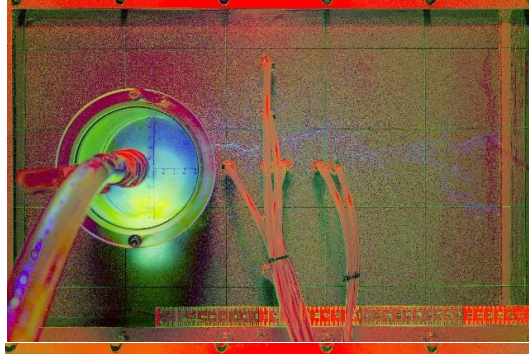
*Corrected for the 3D-effect by multiplying by 1.5

Annex II. Photos SSE

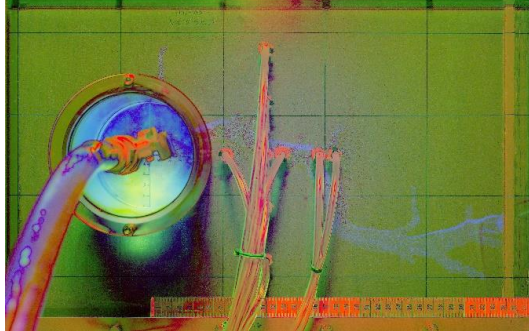
G207



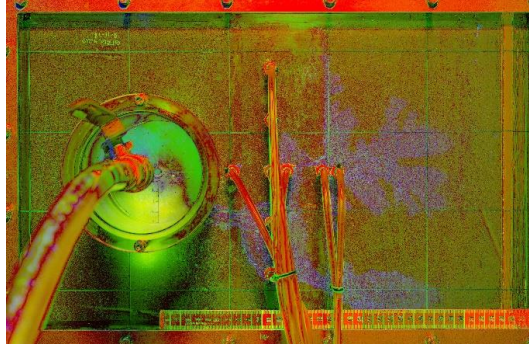
G208



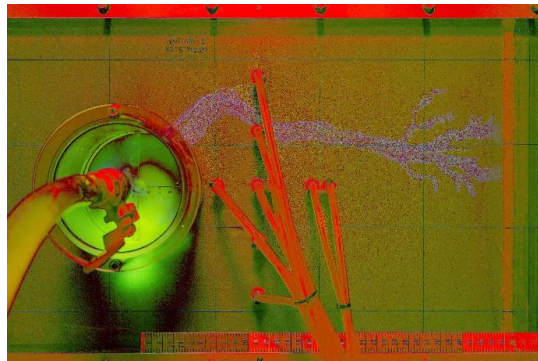
G209



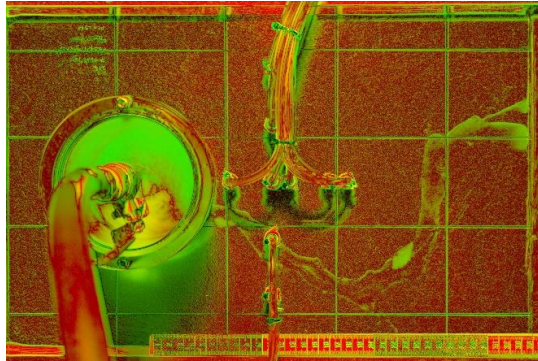
G210



G211



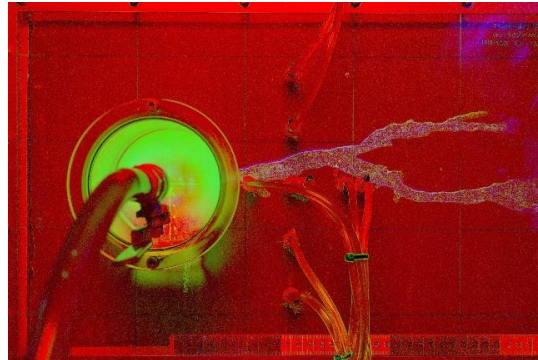
F214



F215



Baskarp +1% Kaolinite

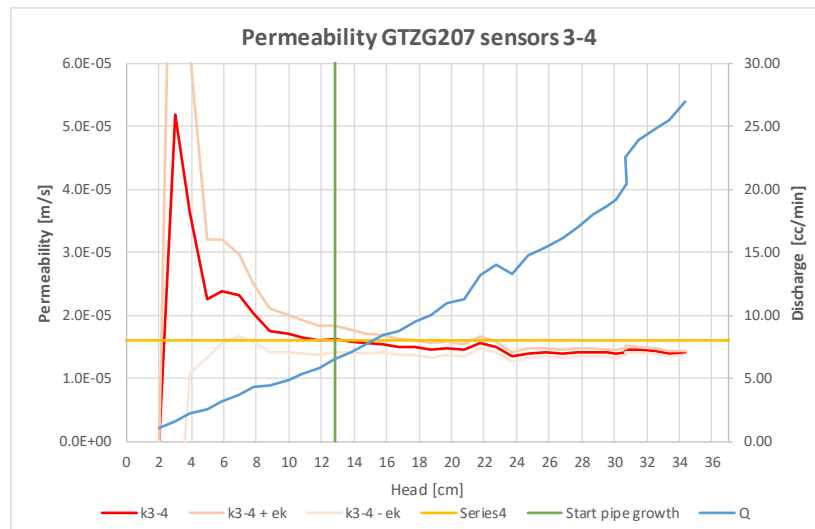


Baskarp +3% Kaolinite

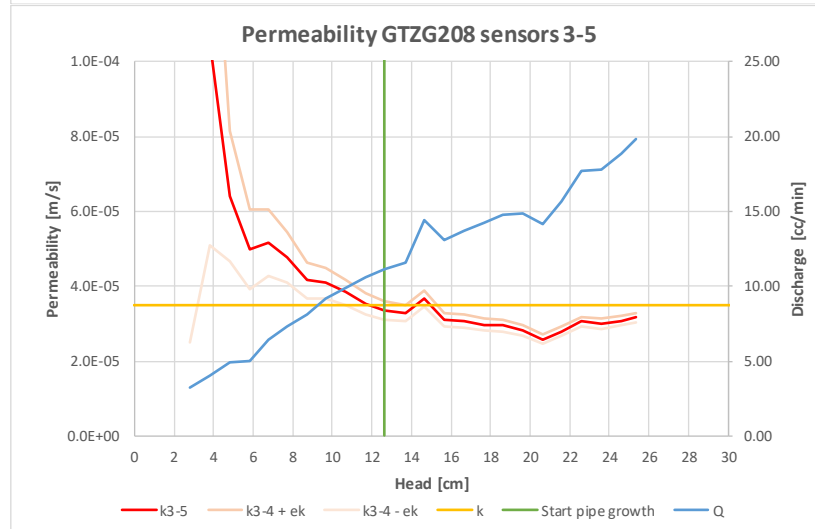


Annex III. Permeability SSE

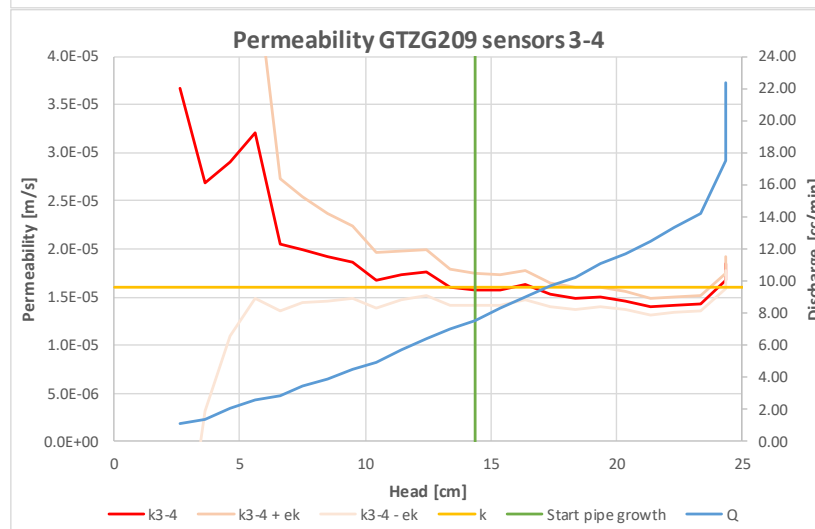
G207



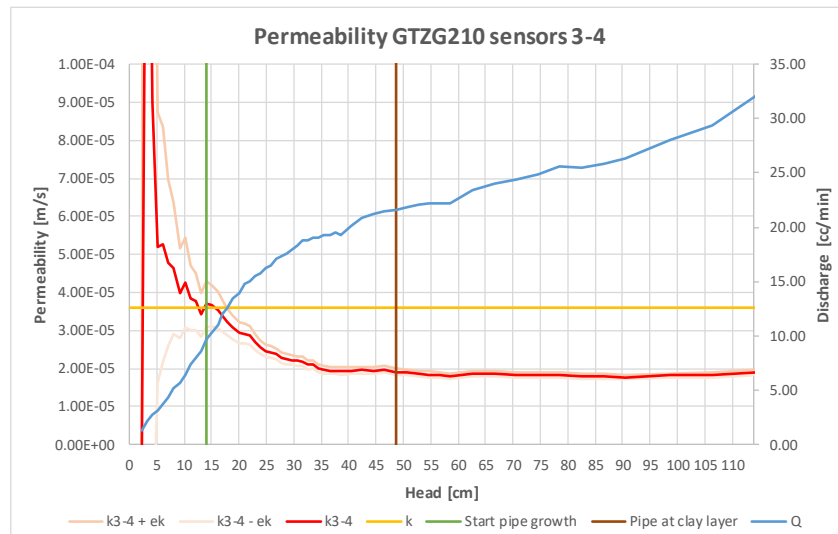
G208



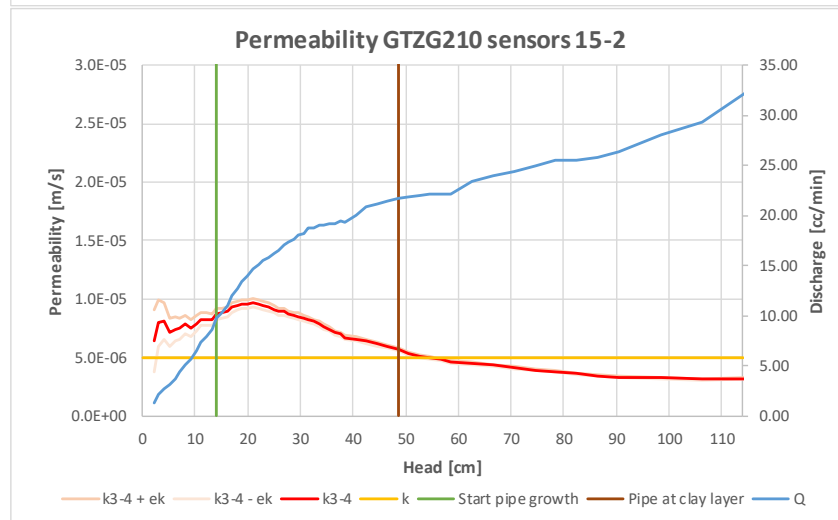
G209



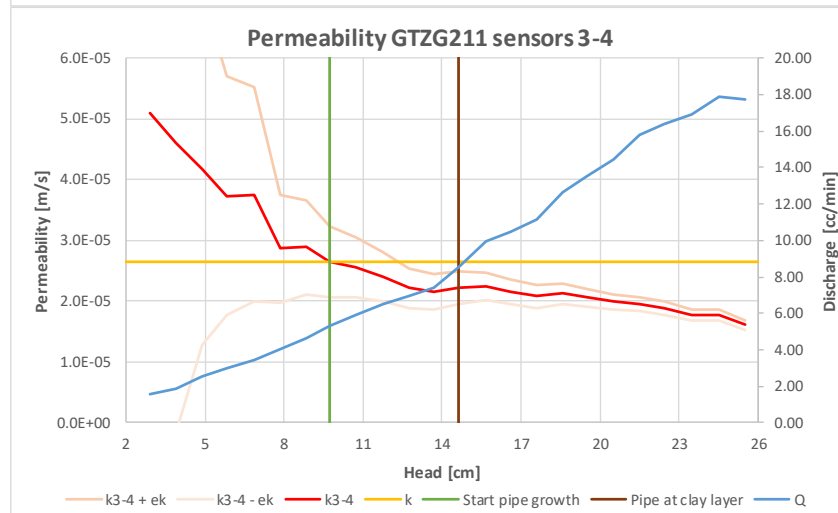
G210



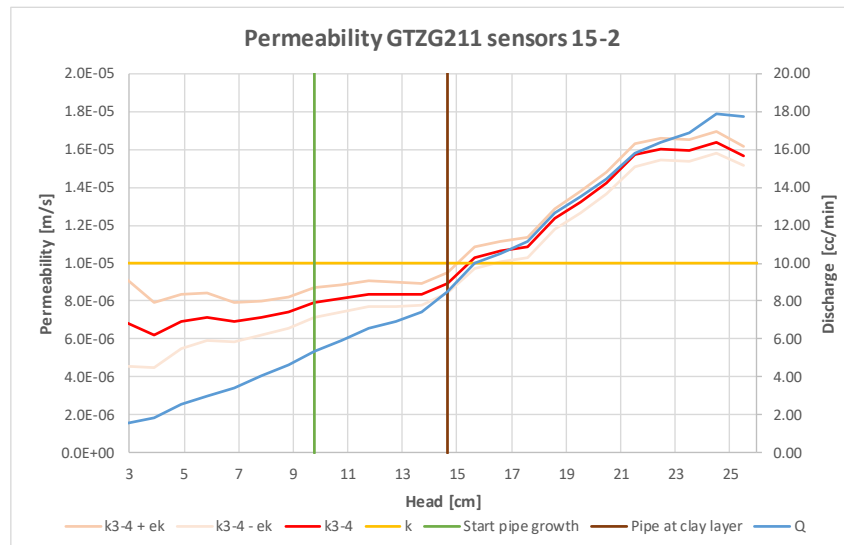
G210 - Overall



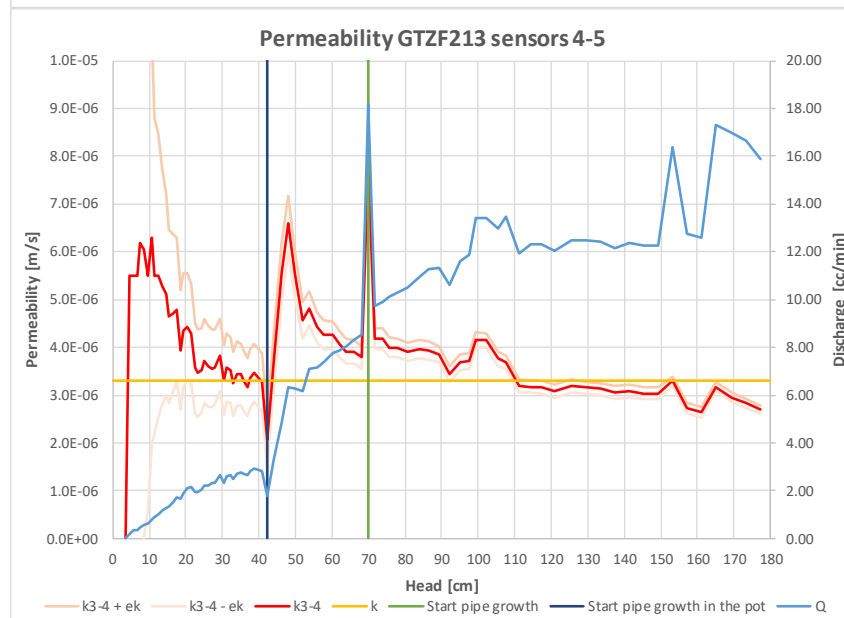
G211



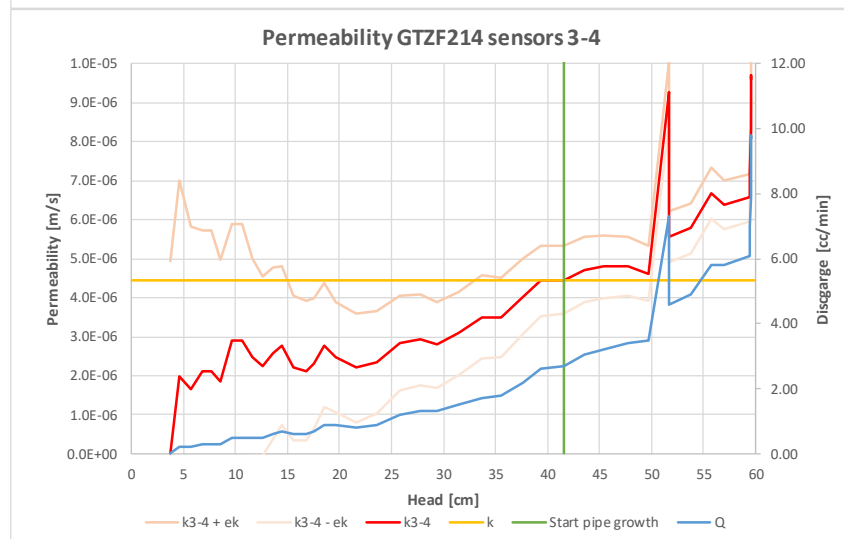
G211 - Overall



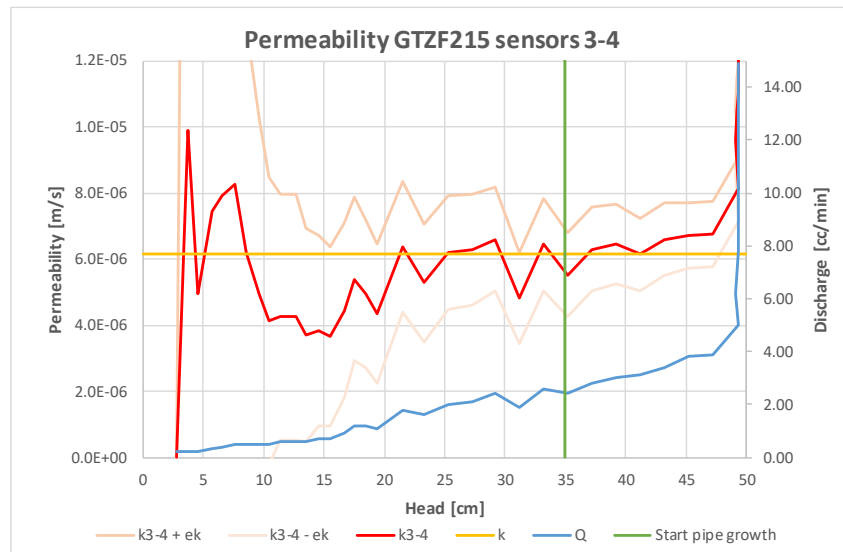
F213



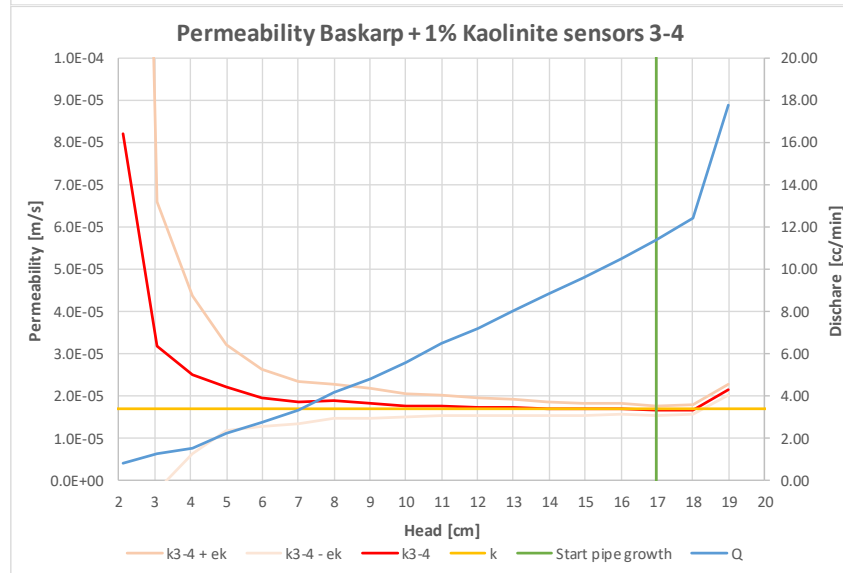
F214



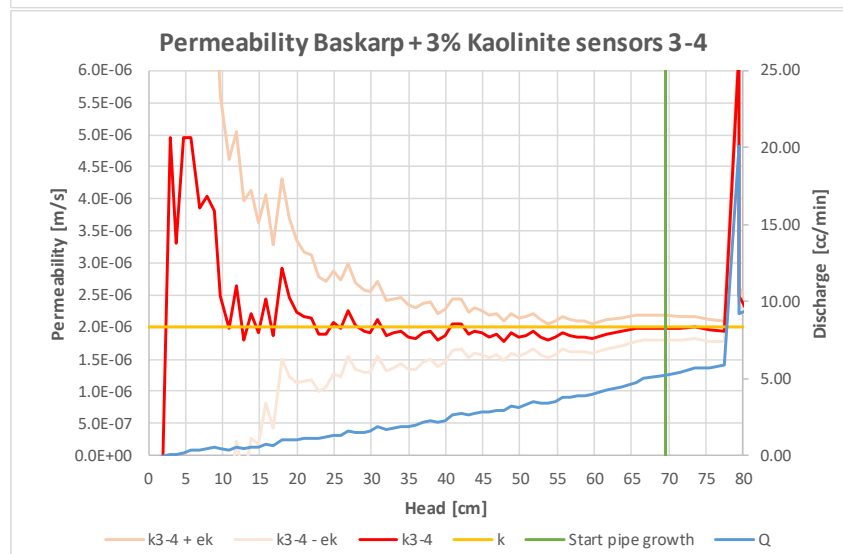
F215



B+1%K

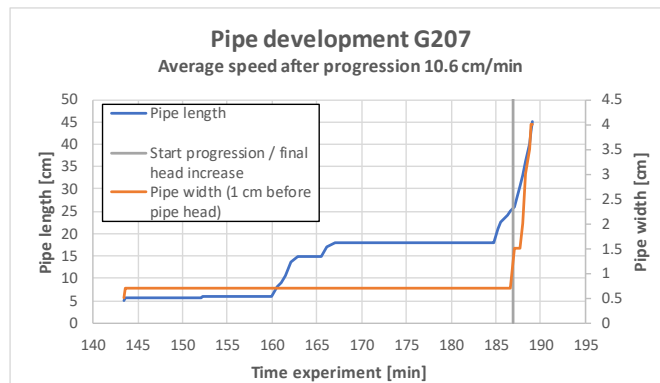


B+3%K

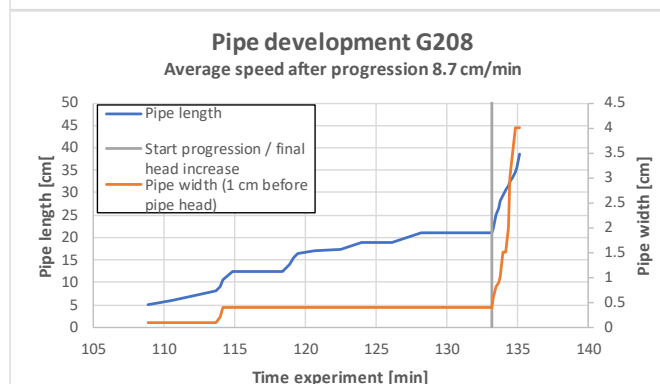


Annex IV. Pipe development SSE

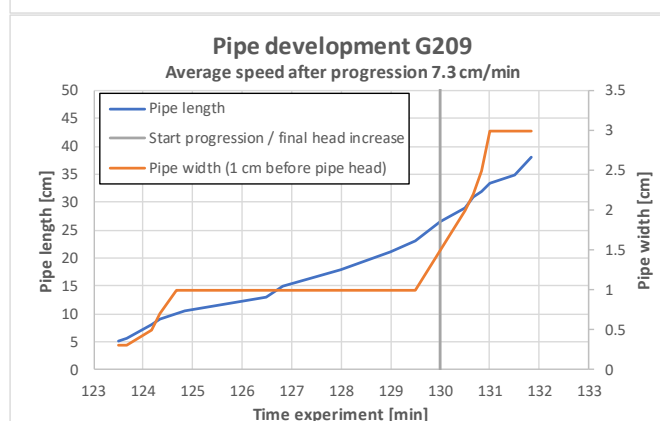
G207



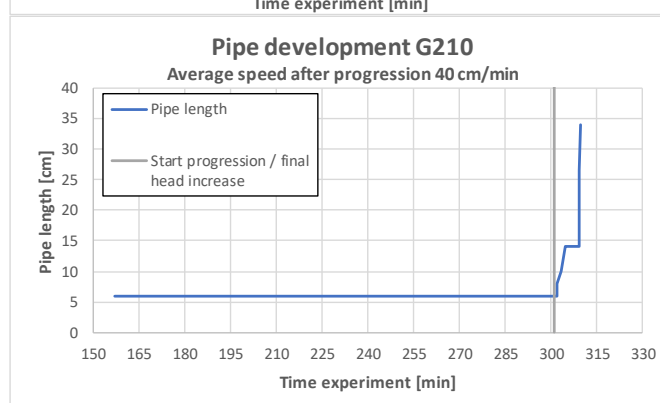
G208



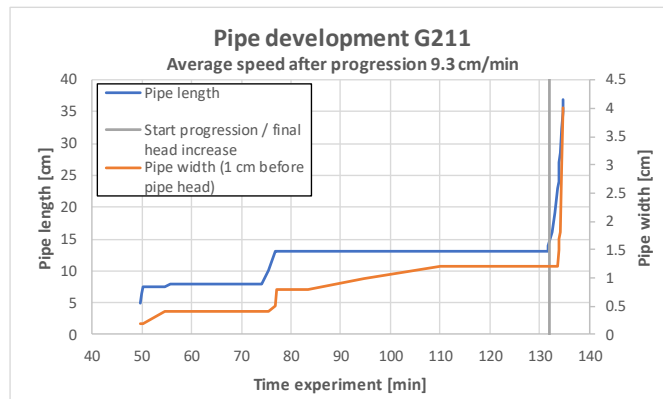
G209



G210



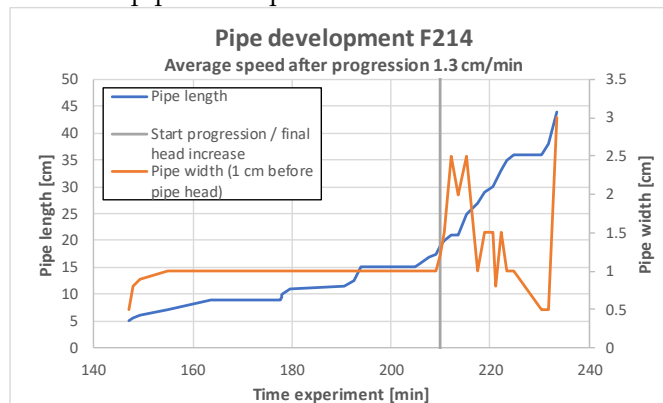
G211



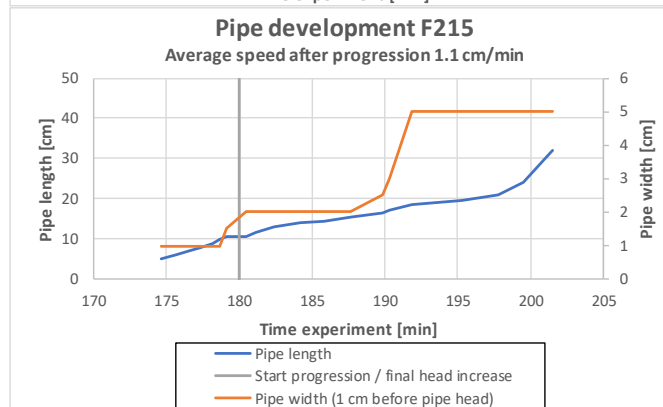
F213

No visual pipe developed

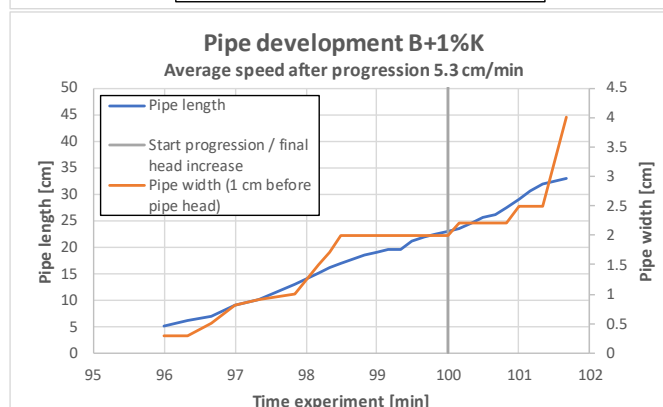
F214



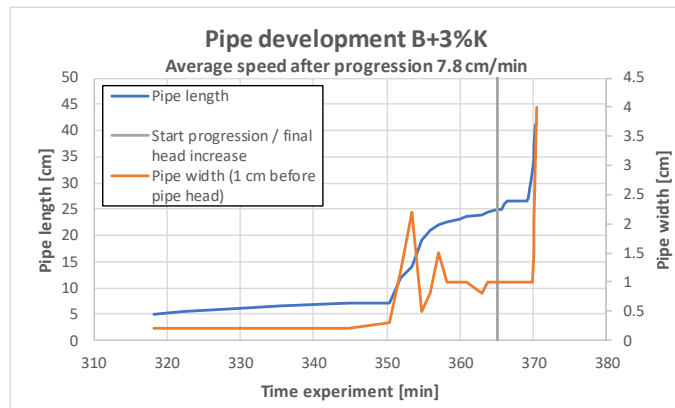
F215



B+1%K



B+3%K



Annex V. Piping models

.a. Sellmeijer

Assumptions for the Sellmeijer model

- 2D model
- Analysis of 3 processes:
 - Groundwater flow (Darcy and continuity)
 - Water flow in the pipe (Poiseuille)
 - Force balance granules in the pipe (White)
- Balance at grain level (criteria for erosion):
 - Drag force
 - Weight of the grain
- Critical point: ΔH_c .
- The potential in the pipe is the same as the potential around the pipe (unlike the SD-model)
- The dike material is impermeable
- The pipe is very wide (horizontal plates), i.e. 2D
- Laminar flow
- Homogeneous sand layer under an impermeable cover layer
- Progressive erosion when the pipe length is half the total seepage length (l_c)
- Fixed exit point

Refined Sellmeijer model:

$$F_{resistance} = \frac{\gamma'_p}{\gamma_w} \{ \eta \tan(\vartheta) \} \left(\frac{RD}{RD_m} \right)^{0.35} \left(\frac{U}{U_m} \right)^{0.13} \left(\frac{KAS}{KAS_m} \right)^{-0.02} \quad Eq.29$$

$$F_{scale} = \left(\frac{d_{70}}{\kappa_{h,avg} L} \right)^{1/3} \left(\frac{d_{70}}{d_{70m}} \right)^{0.4} \quad Eq.30$$

$$F_{geometry} = 0.91 \cdot \left(\frac{D}{L} \right)^{\left(\frac{0.28}{L} \right)^{2.8} - 1} + 0.04 \quad Eq.31$$

$$\text{with: } \kappa_{h,avg} = \sum_{m=1}^n \frac{\kappa_{h,avg} D_m}{D_{tot}}$$

.b. Shields-Darcy

Like the Sellmeijer model, the Shields-Darcy (SD) model describes the critical head difference over the flood defense by analysing: groundwater flow to the pipe, flow through the pipe and erosion criteria for the start of movement of particles in the pipe (Van Beek & Hoffmans, 2017). The subsoil is schematized with resistances against flow per layer depending on the progression of the pipe. The model approximates the flow towards the pipe in 2D in a homogeneous isotropic sand layer. The pipe consists of a semicircle and the Shields approach for laminar flow is used to indicate the initiation of erosion.

The growth of a channel under a dike is clearly traceable in the change of water pressure at the tip of the pipe. A reduction in water pressure indicates channel formation. Upstream of the piping channel, on the left side in Figure 80, where the pipe has not yet developed, the gradient is higher than at the downstream side. The permeability of the sand goes up in the channel due to the removal of grains, by Darcy's law, a lower head gradient is needed to transport the water. On the upstream side of that channel, the sand is still undisturbed, the water will start to flow towards the location with the lower head, the pipe (Förster et al., 2012).

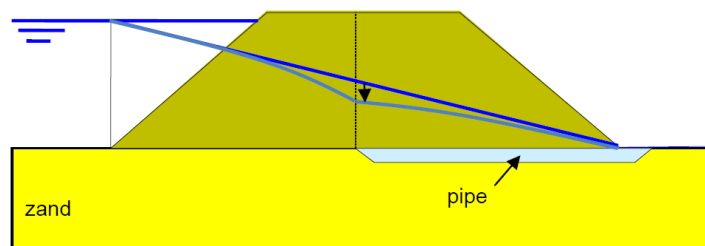


Figure 80 - Head drop during pipe progression (Förster et al., 2012)

The reason why the SD model is not widely used is that the flow is highly simplified and that is not what is needed in the future. It is likely that future models, model the subsurface and the flow more precisely. In 2017, Van Beek and Hoffmans gave a future perspective on the modelling of BEP. Their vision was (Van Beek & Hoffmans, 2017): "Future developments should aim for an improved piping model, which include aspects of both the Sellmeijer and SD model, such as the Shields approach for prediction of the head loss in the pipe, the pipe flow through shallow and wide pipes and the numerical calculation of groundwater flow towards the pipe, combined with new insights on a local, scale-independent criterion for progression at the pipe tip. In addition, better subsurface characterization and collection of field observations are essential for model validation and safety assessment."

Hoffmans (2014) schematized the subsoil as displayed in Figure 81.

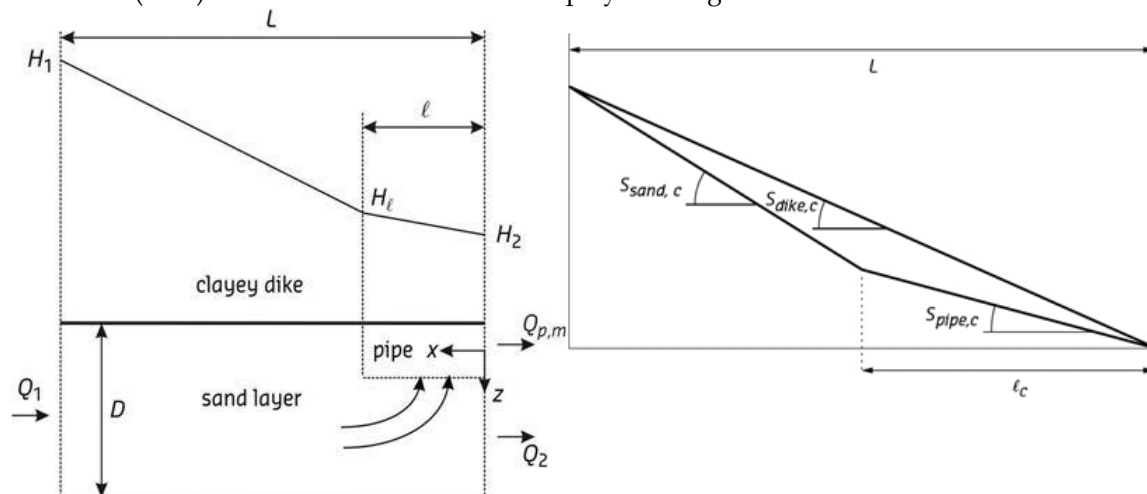


Figure 81 - Simplification of the head difference in the sand layer during pipe formation (Hoffmans, 2014)

In this approach, the sand layer consists of two zones. Zone A is directly under the dike and zone B is the lower part of the aquifer, assuming that zone B does not affect piping (Figure 82). All the water that enters zone A will flow to the pipe. The thickness of both layers is not known in advance. The basis of this approach is the resistance of the sand layer and the resistance of the pipe to flow. The influence of the development of the pipe on the rise in height has been considered and it is clear to what depth the sand layer contributes to the flow to the pipe. This results in a reduction in scale factor.

The subsoil is schematized with resistances to flow per part. Zone A and B below and above, a section of the pipe with its own resistance ($\Omega_{p,h}$), a section that flows through zone A and later flows vertically to the pipe with resistance ($\Omega_{s,v}$) and finally the flow through zone B which follows the resistance of the aquifers under the full dike (Ω_s) (Figure 82) (Hoffmans, 2014; Van Beek & Hoffmans, 2017).

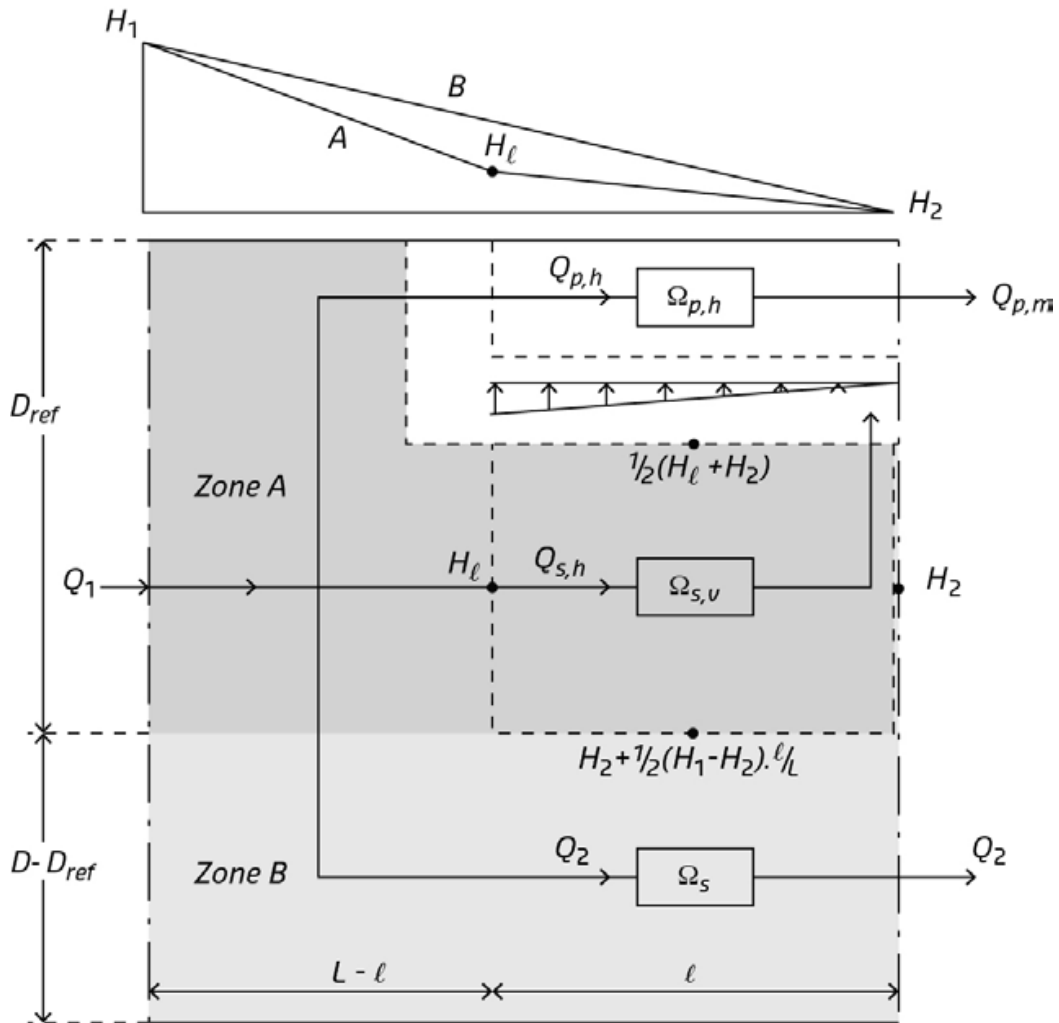


Figure 82 - Schematisation of the subsurface, head and pipe formation in the SD model (Van Beek & Hoffmans, 2017)

The critical head difference over the dike is defined as:

$$\frac{H_c}{L} = S_{pipe,c} + \left(1 - \frac{l_c}{L}\right) (S_{sand,c} - S_{pipe,c}) \quad Eq.32$$

This formula describes the total decline when two distinct gradients (with and without pipe) are considered. Three unknown parameters have been solved: l_c , $S_{sand,c}$ and $S_{pipe,c}$ (see list of symbols).

Critical resistance of the pipe ($S_{pipe,c}$)

$$S_{pipe,c} = \frac{\sqrt{g} (\Psi_{lam,c} (\frac{\rho_s}{\rho} - 1) d_{15})}{v \sqrt{\alpha_{Re,l}}} \quad Eq.33$$

$$2Re_{m,c} \approx \frac{d_{50}}{l_{Re}} \quad Eq.34$$

$$\Psi_{lam,c} = 0.2(D_*)^{-1/3} \quad Eq.35$$

$$D_* = d_{50} \left(\frac{\Delta g}{\nu^2} \right)^{1/3} \text{ with } d_{50} \text{ in range } 0,1 \text{ mm to } 0,5 \text{ mm} \quad \text{Eq.36}$$

The Shields parameter is determined from laminar flow experiments by Govers (1987), Pilotti and Menduni (2001) and Loiseleux et al. (2005) (Hoffmans, 2014). The grainsize was chosen as d_{50} because research by Van Beek shows that the resistance to washing out of small grains is largely determined by the larger grains that form the skeleton (Van Beek & Hoffmans, 2017).

Critical pipe length (l_c)

The critical pipe length is defined as:

$$\frac{l_c}{L} = \exp \left(- \left(\frac{\alpha_f D}{L} \right)^2 S_{pipe,c} \right) \quad \text{Eq.37}$$

Critical resistance of upstream sand ($S_{sand,c}$)

$$S_{sand,c} = \left(1 + \frac{\Omega_s}{\Omega_{p,c}} \right) S_{pipe,c} = S_{pipe,c} + Q_{p,m,c} \Omega_s = S_{pipe,c} + \frac{q_{p,m,c}}{DK} \quad \text{Eq.38}$$

$$\text{with: } q_{p,m,c} = 2 \text{Re}_{m,c} \nu \quad \text{Eq.39}$$

In the end, three unknown coefficients remain: the length scale parameter (l_{Re}), the groundwater coefficient (α_f) and the Reynolds coefficient ($\alpha_{Re,1}$). Van Beek and Hoffmans (2017) used all available Dutch data to calibrate and validate these three parameters and found as result: $l_{Re} = 18E-6$ [m], $\alpha_f = 5$ [-] and $\alpha_{Re,1} = 6$ [-]. An important notion here is that the outcome of the SD model is unstable for thick sand layers ($D/L > 0.5$), and vice versa where $L < 2D$.

The SD model is much less sensitive to variations in the thickness of the aquifer because a reference thickness (D_{ref}) can be determined. It is assumed that all the water that flows out of the pipe is the water that flows into zone A, it can be stated on basis of continuity that D_{ref} (Van Beek & Hoffmans, 2017):

$$D_{ref} = \frac{Q_{p,m}}{BKS_{sand}} = \frac{q_{p,m}}{KS_{sand}} = D \left(1 - \frac{S_{pipe}}{S_{sand}} \right) \quad \text{Eq.40}$$

Assumptions for the Shields-Darcy model:

- 2D model
- Criterion for erosion: $S_{pipe} > S_{pipe,c}$
- 1D horizontal groundwater flow described with Darcy
- Start erosion described with Shields
- Unstable for thick sand layers ($D / L > 0.5$), or vice versa the area where $L < 2 \cdot D$
- Laminar flow
- Homogeneous isotropic sand layer
- Cross section of the pipe is a circle and the flow cross-section varies with time. Referred to as hydraulic radius (R)
- Critical point: $l > l_c$
- Water through zone A exits through the pipe, making it possible to determine D_{ref}
- Gradient upstream of the pipe is constant
- Lower head gradient in the pipe than upstream
- The head in the pipe decreases linearly in the direction of flow

.c. Numerical model to simulate the pipe progression

In 2014, Wang et al. produced a numerical model in which the erosion length can be calculated over a certain time. The assumption here is that due to the groundwater flow the small sand particles first erode, so that the porosity increases, and the soil becomes less strong. This progresses to a certain extent ($n_c \approx 0.7$) in which the small particles are transported, which has an influence on the flow (Wang, 2014). The formula for the increase of the length of the pipe in a given time is given in Eq. Eq.41.

$$\Delta L = \frac{C_3(u - u_c)}{P_f(1 - n)} \cdot \Delta t \quad \text{Eq.41}$$

With u by Darcy:

$$u = \frac{k}{n} \frac{d\phi}{dx}, \quad u_c = \frac{k_c}{n_c} \frac{d\phi}{dx} \quad \text{Eq.42}$$

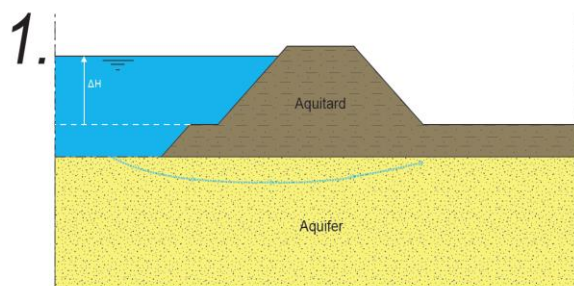
and

$$k_c = 1219.9 \cdot d_{10}^{1.565} \frac{n_c^{2.3475}}{(1 - n_c)^{1.565}}, \quad k = 1219.9 \cdot d_{10}^{1.565} \frac{n^{2.3475}}{(1 - n)^{1.565}} \quad \text{Eq.43}$$

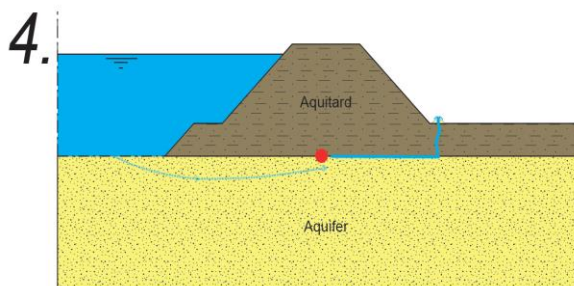
Assumptions for the numerical model by Wang et al. (Wang, 2014)

- 2D model
- Analysis of 3 processes:
 - Groundwater flow (Darcy 2D)
 - Force balance at grain level (Howard and Mclane (1988); Lambe and Whitman (1979))
 - Turbulent pipe flow
- Balance at grain level (As well as in Sellmeijer 4 forces):
 - Flow force
 - Towing force
 - Weight of the grain
- Local relocation of the potential determines the speed in the pipe
- Critical point: none
- Exit point is fixed
- Steady pipe diameter, the same cross-section in time and place (so only erosion at the tip of the pipe)
- Turbulent flow
- The path of the pipe is determined by the path of the least resistance, so it can also occur via sheet pile walls etc. .
- Heterogenic sand layer under a less permeable cover layer

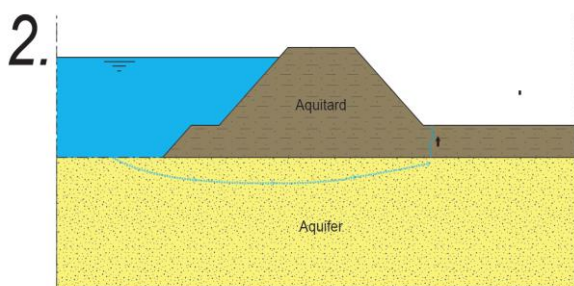
Annex VI. Schematic of the piping process



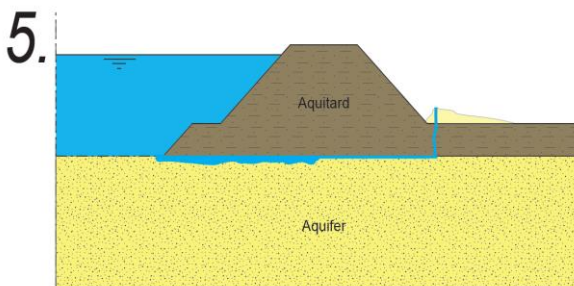
Significant hydraulic gradient induce seepage flow through aquifer.



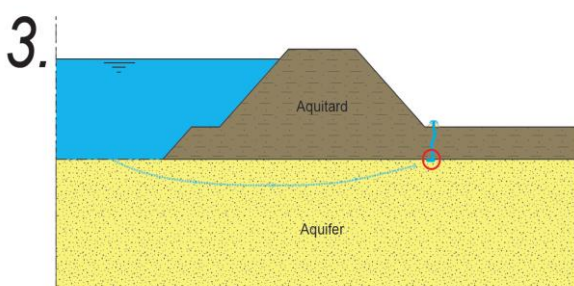
Backward erosion (piping)



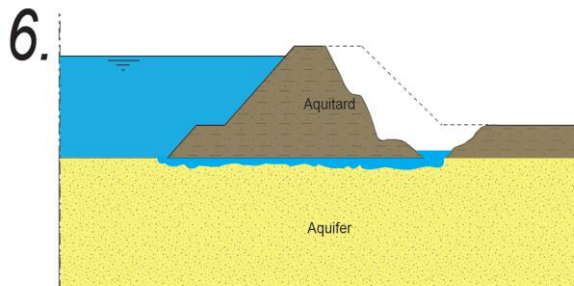
Hydraulic fracture or uplift



Widening of the pipe



Heave and start backward erosion



Dike failure and eventually dike breach

Retrieved from (Stoop, 2018)

Annex VII. SOS probability tidal sand

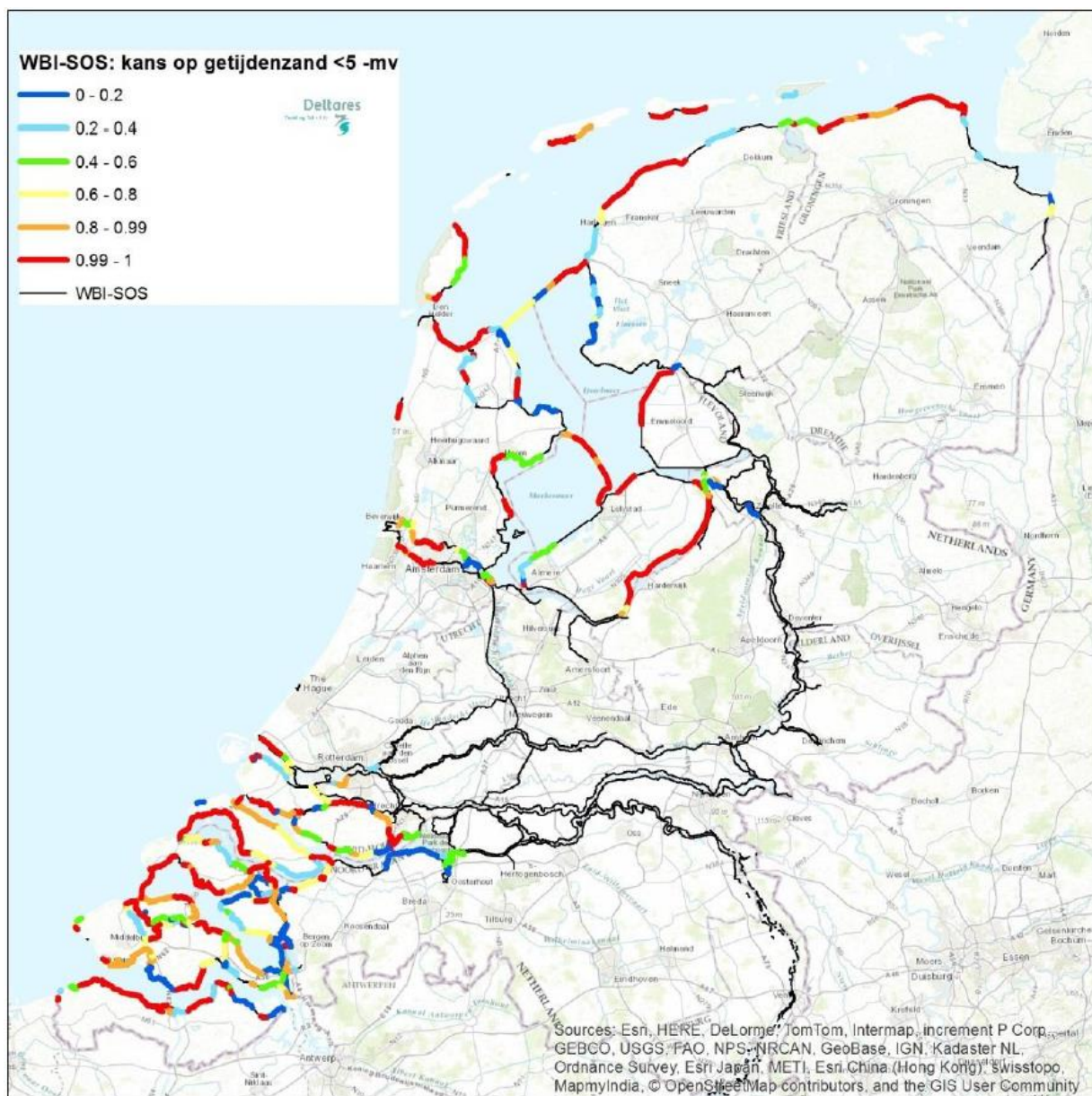


Figure 83 - SOS probability of occurrence of tidal sand in the top 5 m of subsoil in the Netherlands (Hijma & Oost, 2019)

Annex VIII. 3D modelling SSE

The small-scale experiments (SSE) are modelled in 3D, by use of the model DgFlow. This is done because of the 3D character that the piping process has, as mentioned in (3.1.3.g). When the model is wider, the supply of water goes up (Figure 84) and local gradients become higher at the outflow. This results in faster erosion, leading to lower critical hydraulic gradients. The influence of this effect is investigated, to be able to better quantify the influence in tidal sand. The goal is to retrieve a factor between the critical heads in the 2D and the 3D calculations.

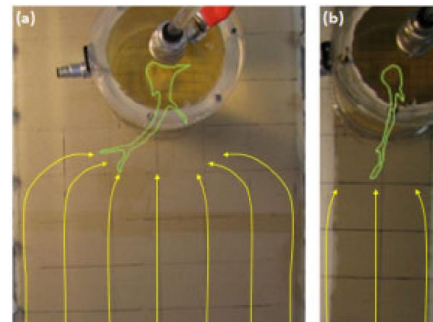


Figure 84 - Visualisation of the difference in flow lines for models (a) 30 cm wide and (b) 10 cm wide (Vandenboer et al., 2014)

DgFlow

DgFlow simulates the interaction of groundwater flow and the development of piping channels underneath a dike. DgFlow is a finite element model in which the groundwater flow is coupled to the pipe flow by representing the pipe as line elements. Since line elements have no width, the shear stress which this flow exerts on the walls of the pipe is incorporated as a width-to-depth ratio (Van Beek et al., 2019; Van Esch, 2015). The numerical simulation program is incorporated in GiD, a pre- and post-processor. In this processor, the 3D model is drawn.

Input parameters

The base input parameters in DgFlow comprise of the boundary conditions, the MPicard number, grainsize and permeability. The boundary conditions are essentially the same as in the 2D D-Geo Flow calculations. A head increase of 1 cm every 5 minutes and a calculation and output step every minute. The MPicard number (as explained in 4.2.2) is kept at 500 to reduce the calculation time, which is a lot longer in 3D calculations than in 2D calculations. The grainsize and permeability can be found in Annex I. Besides these input parameters, 3D DgFlow requires some extra input, which is evaluated below.

Width-to-depth ratio

The width to depth ratio (w/a -ratio), which determines the amount of shear stress exerted on the pipe walls, is studied by Van Beek et al. (2019). They compared experiments to 2D Sellmeijer calculations, another piping model by Robbins and Griffiths (2018) and calculations with DgFlow with w/a -ratios: 4, 8, 12 and 20. From the experiments conducted on tidal sand, the pipe width is determined from photos that were taken every 10 seconds. When the pipe started to grow, the width of the pipe is measured 1 cm before the pipe tip and is multiplied by the time that the width stayed the same (see Annex IV). In this way, a weighted width of the pipe is determined. The depth of the pipe is assumed to be 1 mm (see 3.1.3.e). The weighted w/a -ratios are given in Table 15.

Table 15 - Ratios w/a tidal sand experiments

G207	G208	G209	G210	G211	F213	F214	F215	B+1% K	B+3% K
8	5	12	Pipe very wide for a long time due to clay layers	8	No visual pipe developed	11	30	16	5

Ideally, all 5 values are used: 4, 8, 12, 20 and the measured value in the experiments (Table 15). The ratios 4, 8, 12 and 20 come from the validation of the program (Van Beek et al., 2019). That is the range of values which are expected based on experiments. Due to time constraints, only $w/a = 8$ is used. This is relatively close to the observed values in the SSE and in 3.1.3.e it is mentioned that for a d_{50} of 0.13 mm, the w/a -ratio was 7-8. For experiment G209, calculations are performed to sense the influence differences in the w/a -ratio. The difference in critical hydraulic head for w/a -ratio's 4, 12 and 20, compared to 8 are -36%, +82% and +123% respectively. This leads to the conclusion that the dependency on the w/a -ratio is very larger.

Initial pipe depth

The initial pipe depth is related to the height by which the water level is raised per calculation step. If the water level is raised with 1 cm every 5 minutes, the initial pipe depth is 1 cm / 5 is 2 mm. Since this parameter has an upper limit 0.1 mm, this value is used. The uncertainty in this parameter is not known.

Model factor

The Sellmeijer model is calibrated by use of MSeep on a large dataset in the early stages of the development, which resulted in a model factor of 0.91 (3.1.2.a). In DgFlow, equations are solved differently. MSeep needed an extra assumption at the tip of the pipe and this difference leads to different outcomes. That is why a slightly different model factor of 0.89 is used as a calibration factor between DgFlow and experimental results.

Theta

The time-weighting coefficient theta is a numerical input parameter which determines the numerical scheme to be explicit (1) or implicit (0). Explicit schemes evaluate the solution based on known quantities of the previous timestep and are conditionally stable. Implicit schemes require more computational effort because an iterative step is required to compute a solution based on the next timestep. Implicit schemes are unconditionally stable, meaning that the solution remains stable with increasing timesteps. Only the explicit scheme is used due to time constraints, it is known that the implicit scheme gives more accurate results. More calculations must be performed to know what the difference in numerical error between the models does to the outcome.

Porosity

Porosity is only of importance when unsaturated or time-dependent flow is considered. Since the flow in the pipe is always time-independent and the permeability is supplied to the program, the porosity is not of importance.

Material model saturation

The material model saturation is set to saturated because the unsaturated flow is not yet incorporated in DgFlow.

Model configuration

The model configuration is a recreation of the sand box used in the SSE. The largest difference is that the model is cut in half in the direction of the pipe (Figure 85). The model being cut in half has the following two reasons: 1) the calculation time is much lower and has almost no effect on the critical head difference. And 2) the modelling of the pipe can now be done on the line-element on the corner of the half box. An important notion is that the width-to-dept ratio, supplied to DgFlow, is also half the real value because the model is cut in the middle of the pipe. In Figure 85, the model is visualized. The dark 6 cells (in the right figure) is the outflow. Water flows in through the left side of the box (y-z plane). The pipe is situated at the top of the model in x-direction.

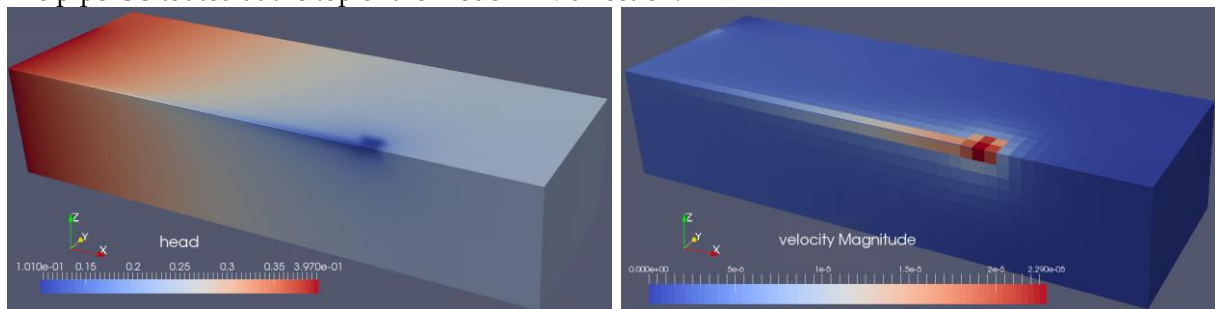


Figure 85 - Visualisation of the results from DgFlow with a hole-type outflow, presenting the head and water velocity at the final calculation step visualized with Paraview

In the first calculations, another model was used. In that model the outflow hole was stretched over the total width. Later it was realized that the outflow being small as in the figure above, results in much

lower critical gradients and represents the model much better because when the outflow is stretched over the width, the model is essentially 2D. Both the results of the calculation are performed.

Results

The critical head differences calculated with DgFlow are given in Table 16.

Table 16 - Results SSE on tidal sand and fluvial sand, calculations with 3D DgFlow

Exp.#	H _{c,measured} [cm]	H _{c,DgFlow} [cm]	
		Line outflow	Hole outflow
G207	36	10	8
G208	26	6	8
G209	25	10	8
G210 - 2 clay layers	116	-	-
G211 - 1 clay layer	26	-	-
F213	180	37	7
F214	60	30	7
F215	50	22	7
Baskarp + 1%K	19	10	8
Baskarp + 3%K	81	71	8

Discussion

The modelling in 3D took much time and unfortunately has not led to any changes in the conclusions of this thesis. As presented in Table 16, the results with the model with the hole type of outflow, are not even close to the obtained values in the experiments. The obtained values do not resemble the changes in permeability, which are very important. The values are very close and unfortunately there was no time to investigate the cause. It has probably to do with the width to depth ratio of the pipe.

The results in the model with a line type of outflow do much better represent the changes in permeability. Since this model is too close to a 2D model, the values cannot be used as the results of a 3D situation.

Conclusion

No answer could be found in the available amount of time to the problems mentioned in the discussion. The 3D-effect, which was hoped to be found from these calculations, cannot be based on the found results. This is because the results are not reliable enough, based on the expected results from 2D calculations and the expected value of the 3D-effect from literature. In addition to that, the unknown tidal sand strength also causes uncertainty in the results. Since also experiments on fluvial sand were available, which are conducted by Van Beek (2015), these experiments are used to find the influence of the 3D-effect in this experimental set up (see 4.3.1).